DEEP ULTRAVIOLET RESONANCE RAMAN SPECTROSCOPY OF MEMBRANE PROTEINS

A Dissertation

Presented to

The Faculty of the Graduate School

At the University of Missouri

In Partial Fulfillment

Of the Requirements for the Degree

Doctor of Philosophy

By

CHRISTOPHER HALSEY

Dr. Jason Cooley, Dissertation Supervisor

DECEMBER 2012

The undersigned, appointed by the dean of the Graduate School,

have examined the dissertation entitled

DEEP ULTRAVIOLET RESONANCE RAMAN SPECTROSCOPY OF MEMBRANE PROTEINS

Presented by Christopher Halsey

A candidate for the degree of

Doctor of Philosophy

And hereby certify that, in their opinion, it is worthy of acceptance.

_____

Dr. Jason Cooley

_____

Dr. Carol Deakyne

_____

Dr. Kent Gates

_____

Dr. Michael Henzl

This work is dedicated to my magnificent wife, Julia. I am eternally grateful for her encouragement and support, even while I was collecting data late at night instead of coming home.

ACKNOWLEDGEMENTS

My most heartfelt thanks go to my graduate advisor, Dr. Jason Cooley, for his patience and guidance over these past five years as I went from knowing absolutely nothing to knowing what seems but a fraction more. While in his lab, I have had the foundational opportunity to see meaningful scientific questions posed, cleverly investigated, and finally published to benefit of the scientific community. I take all of this with me as I seek to create a similar experience for undergraduate researchers under my guidance. A personal appreciation of the biophysical research community now exists that I could not conceive of before beginning my studies at the University of Missouri. Much of this is also due to Dr. Renee JiJi's advice and direction in deep-UV Raman instrumentation, data interpretation, critiques of manuscripts and presentations, and beyond.

I thank the members of my graduate dissertation committee, Drs. Kent Gates, Carol Deakyne, and Mike Henzl, for their guidance and helpful criticisms as this research unfolded. I want to express my appreciation to the Department of Chemistry at the University of Missouri, which has provided the financial and material means to conduct this research in a friendly, collaborative atmosphere.

I must especially acknowledge the efforts of Bill Vellema, whom I have consulted regularly throughout this research when things simply went wrong. His expertise of electronics, plumbing, general instrumentation, and common sense have kept my research projects afloat more times than I care to admit.

I thank my fellow group members from the Cooley and JiJi labs past and present: Mia Brown, Dr. Carol Roach, Dr. John Simpson, Dr. Mingjuan Wang, Emily Schmidt, Jian Xiong, Olayinka Oshokoya, Michael Eagleburger, and Eddie Pittman. Some have been role models, some patient learners, and some co-authors. All have commiserated the setbacks and long group meetings. They have also been the ones to celebrate the successes with me along the way.

Finally, I thank those teachers that brought me to the University of Missouri to begin with. First: my mother Julie who knew I was going to end up a teacher early on and encouraged my varied academic interests. Later in high school, Doc Kramme helped seal my decision to apply to undergraduate chemistry programs. At Truman State University, Dr. David McCurdy focused my attention to analytical chemistry and the desire to pursue graduate work.

TABLE OF CONTENTS

LIST OF FIGURES

LIST OF TABLES

LIST OF ABBREVIATIONS

2Fe-2S	Rieske two-iron two-sulfur cluster
β-DM	β-dodecyl maltoside
λ_{ex}	Excitation wavelength (nm)
Am	Amide
BChl	Bacteriochlorophyll
C_α	Alpha carbon of the amino acid backbone where the side chain is bonded
CD	Circular dichroism
Cyt bc_1	Cytochrome bc_1, ubihydroquinone:cytochrome c oxidoreductase
Cyt *c*	Cytochrome *c*
DEAE	Diethylaminoethyl
DMPC	Dimyristoyl phosphatidylcholine
DUVRR	Deep-UV resonance Raman
FTIR	Fourier transform infrared spectroscopy
MPYE	Mineral-enriched peptone yeast extract
NE lipids	Non-extruded lipids
NMA	n-methyl acetamide
NMR	Nuclear magnetic resonance
Rcaps	*Rhodobacter capsulatus*
SRCD	Synchrotron Radiation Circular Dichroism
SUV	Small unilamellar vesicle

TM	Transmembrane
UQ	Ubiquinone
UVRR	UV resonance Raman
Val	Valinomycin
Val-K	Valinomycin-potassium complex

ABSTRACT

Despite the various protein structure determination methods in use, a need still exists for adequate resolution of membrane protein structure while remaining rapid and inexpensive. Deep-UV resonance Raman (DUVRR) spectroscopy addresses this need and also offers a high sensitivity to the protein backbone such that membrane proteins require no further modification from their native state in the lipid bilayer. DUVRR spectroscopy is a mature technique for secondary structure determination of aqueous proteins but had not been seriously explored as a means of structure determination for membrane proteins. Early progress in characterizing the secondary structure of the lipid-solvated cytochrome bc_1 complex led to exploring other membrane proteins mostly based on the α-helix motif. DUVRR is not limited to proper membrane proteins, but also interrogates lipophilic protein-like structures such as the depsipeptide valinomycin. We find DUVRR spectroscopy characterizes membrane protein structure as well as aqueous protein structure. Additionally, it can describe the degree to which the protein backbone is embedded into the membrane. This largely is explained by the absence of hydrogen bonding from water to the amide backbone and its effect on the carbonyl stretching mode in DUVRR spectra. These findings are promising and indicate a need for further investigation of the variety of secondary structures formed in the lipid bilayer.

Chapter 1: Structure Determination of Membrane Proteins

1.1 Overview

X-ray diffraction and nuclear magnetic resonance (NMR) have emerged as the primary means of structure determination (tertiary structure, specifically)[1]. In the absence of a resolved structure, methods that identify secondary structure elements often provide sufficient satisfactory structural information and are better able to comment on protein function. Circular dichroism (CD) is often the method of choice for secondary structure determination and is widely employed[2]. Secondary and tertiary structure elements are described in detail below. Membrane proteins are integrally associated with detergent, lipid, or some other amphiphilic structure and pose unique challenges to structure-determination methods. Despite accounting for 20-30% of expressed proteins, deposited tertiary structures of membrane proteins account for less than 1% of total structures in the protein data bank[3]. A recent review describes the progress in determining membrane protein structures as exponential in growth[4]. Each method used to determine protein structure has certain limitations on sample preparation, analysis time, and/or resolution.

1.2 Protein Structure Terminology

Structure can refer to any of the four structural hierarchies: primary, secondary, tertiary, or quaternary. However, it is helpful to limit the discussion here to secondary (low resolution) and tertiary (high resolution) structure. Quaternary structure features are excluded here because they apply to proteins with more than one domain and rely heavily on previously characterized tertiary structures.

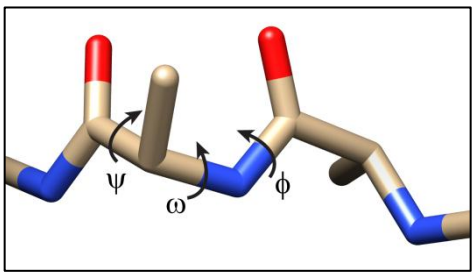

Figure 1-1. The ϕ, ψ, and ω torsional angles along the protein backbone.

1.2.1 Secondary Structure

Secondary structure characterization of a protein primarily describes the hydrogen bonding patterns. Secondarily, it describes the individual dihedral angles of the protein backbone along which three torsional angles can be defined: the ϕ, ψ, and ω (Figure 1-1). Given the planar character of the amide bond, the ω (along the C_α-C-N-C_α bonds) either adopts the more stable trans configuration of 180° or the cis configuration of 0°. The ϕ (along the C-N-C_α-C bonds) and ψ (along the N-C_α-C-N) angles have more flexibility. Characteristic hydrogen bonding arrangements can occur between the carbonyl oxygen and amide nitrogen anywhere from one to five residues away. A standard nomenclature and description of these characteristics was published simultaneously in three journals[5]. Reviews[6] published later have served as standards for defining specific secondary structure types, which are discussed below. These standards, unfortunately, are not always rigorously followed depending on the sensitivity of the method used and its ability to distinguish between subtle differences amongst individual structures.

1.2.1.1 Helices

Most helical structures feature a hydrogen bond 3 to 5 residues away from the carbonyl oxygen to the amide hydrogen which causes the backbone to trace a helical path along an axis. The most common and stable helical form is the right-handed alpha-helix. It was also the first structure to be predicted[7]. For every turn along the helical axis there are 3.6 residues that span 1.5 Å along the axis. The 13 atoms (hydrogen included) involved in the closed loop of the hydrogen bond identify the alpha helix as a 3.6_{13} helix. The ϕ and Ψ angles center around -60° and -45°, respectively. Other helical structures

have been identified or theorized that range from a tighter 3_{10} helix (2nd most common) to the wider π helix (4.3_{16} helix).

1.2.1.2 Beta Sheet

Beta sheet structures are generally more extended than alpha helices. The backbone carbonyls and amides alternate their orientation along this extended conformation which gives rise to two hydrogen bonding schemes between individual strands: the parallel and anti-parallel[8]. As the protein continues from the N to C terminus, parallel strands propagate in the same direction while anti-parallel strands alternate their direction as the beta sheet continues. The C_α does not lie in the plane defined by the extended backbone. Instead, it alternately lies above and below the plane which gives the designation for the pleated beta sheet. Hydrogen bonding in anti-parallel beta sheets is perpendicular to the strand. Parallel strands offset the carbonyl oxygen and amide nitrogen and its hydrogen bonds are more regularly spaced than those in anti-parallel strands. Parallel beta strands, although less stable, also tend to have a closer distribution around -119° and 113° for the ϕ and ψ angles, respectively[6a]. The dihedral angles of anti-parallel strands are more widely scattered about -139° and 135°. The plane of the sheet will twist as additional strands are added[9].

1.2.1.3 Turns

Turns in a protein, where the protein reverses its general direction, are non-repetitive and occur over only a few (2-5) residues but are abundant in protein structures. Their conformational flexibility is much greater than helices and beta sheets. The amino acid's position in the turn becomes more important in determining the allowed dihedral angles. Five general types of turns (α, β, γ, δ, and π) have been characterized and derive their name from how far away the hydrogen bonding residue pair lies. β turns occur most often in protein structures and feature a hydrogen bond three residues away. α turns

are also observed, featuring a hydrogen bond four residues away (similar to the alpha helix). Even within the β turn class, there is much variation[10].

1.2.1.4 Disordered

The final category in protein secondary structure is the disordered or unfolded conformation, in which each amino acid randomly samples all sterically-allowed ϕ and ψ angles[6a, 11]. Historically this has also been called random coil. Recent evidence[12] suggests that these seemingly disordered proteins do have local regions of order that adopt turn-like conformations or those of polyproline-II (PPII, a left-handed 3_1-helix formed by trans-L-polyproline)[13]. High resolution structural determination methods often cannot resolve disordered regions because of the large spatial sampling of disordered residues.

1.2.2 Tertiary Structure

Knowledge of the tertiary structure of a protein requires the determination of the three-dimensional coordinates of the individual atoms. If atomic coordinates are known through X-ray diffraction or NMR spectroscopy, then the secondary structures can also be inferred from it. Tertiary structures embedded in a membrane or detergent are often different than those exposed to solvent. A structural comparison[14] between alpha helices in water-soluble globular proteins and membrane-bound proteins shows a significant shift of 4.5° and -5.4° in the ϕ and ψ angles. Packing angles between alpha helices are altered to 20° compared to -35° in soluble proteins[15]. Membrane-bound helices also sampled a wider range of ϕ and ψ angles. This may be caused, however, by the overall poorer resolution of deposited crystal structures of membrane proteins. Overall, the steric limitations of the lipid bilayer have imposed fewer structural motifs for membrane proteins, namely single alpha helices (albeit somewhat altered), bundles of alpha helices, or beta barrels. The lipid bilayer imposes these folds and hydrogen bonds as a means to reduce its free energy in the membrane. Several reviews[4, 16] have now

been published detailing these structures further, including well-defined classes such as the seven helix bundle of G-protein-coupled receptors[17].

1.3 Sample Preparation Challenges of Membrane Proteins

The challenge of structural analysis of a membrane protein sometimes lies in its expression and purification. Adequate expression of a membrane proteins in engineered bacterial systems has been problematic[18]. Natural expression levels of membrane proteins do not yield practical quantities of desired product, therefore overexpression is often induced by molecular genetics. Cell toxicity is a concern at these high levels of expression so the cells either die or sequester the protein in inclusion bodies, requiring a urea-denaturing step. The protein must then be able to reversibly fold in a given detergent/lipid system. Well-established chromatography methods have made isolation of the membrane protein into artificial membranes or detergents the method of choice when preparing for subsequent structural analysis[19]. Once the membrane protein has been sufficiently purified in a suitable environment, technique-specific challenges still remain which are discussed in the next section.

1.4 Protein Absorbance at Different Wavelengths and Associated Challenges

Structural analysis of membrane proteins is made difficult any time the lipid environment interferes with the structural stability of the protein or interferes, i.e. via scattering or absorption, with a given choice of wavelength. Ideally, a membrane protein's structure could be interrogated in its native cellular environment but other surrounding proteins interfere with any current technique in use. Therefore the membrane protein must be purified and/or selectively labeled isotopically, fluorescently, or with a paramagnetic probe. These efforts provide limited structural information or are time-consuming to accomplish. Most of the electromagnetic spectrum has been used in the structural analysis of membrane proteins. Various methods using these different wavelengths are detailed below with the exception of Raman spectroscopy which is not wavelength-specific and is discussed in more

detail in the next chapter. Naturally, combining these structural efforts is perhaps the best option to overcome individual techniques' limitations[20].

1.4.1 Radio

NMR uses radio frequency pulses in the presence of a magnetic field to determine chemical shifts of multiple NMR-active nuclei. Proteins subject to NMR analysis are typically C^{13} and N^{15} labeled for maximum sensitivity while the surrounding solvent and lipid molecules are deuterated, which can be cost-limiting. For NMR analyses, protein size (40 kDa[21] or less) and correlation times (too long for high resolution) are the limiting factors[22]. To date, 88 unique membrane protein structures have been deposited in the protein data bank (PDB) using NMR[23]. Helpful reviews about structure determination by NMR specifically for membrane proteins have recently been published by Jamin[24] and Kang[25].

1.4.2 Microwave

Electron paramagnetic resonance (EPR) uses microwave frequency in the presence of a continuous wave or pulsed microwave frequency to determine the nearby nuclear and electronic influence on unpaired electrons in paramagnetic metals, free radicals, and spin labels. In site-directed spin labeling, spin labels are covalently linked to cysteines which can be engineered in nearly any location in the protein[26]. Distances between spin labels can be determined to find appropriate distance restraints in a membrane protein from 8 to 80 Å regardless of the size of the protein[27]. Advanced pulsed methods have yielded the most recent success with membrane proteins using pulsed electron double resonance (PELDOR) and more specifically, double electron-electron resonance (DEER)[28].

1.4.3 Infrared

Absorbance of infrared light stimulates vibrational transitions in a molecule with an intensity proportional to the polarity of the bond[29]. For proteins, the abundance of structural information comes from the composite vibrations from the protein backbone, called amide modes, and specifically the

amide I mode from 1600-1700 cm^{-1}. Without sample deuteration a large H-O-H bend must be subtracted, which is the case for soluble and membrane proteins alike[30]. All molecules in a system (including lipids) will contribute to the IR spectrum. Fortunately lipid group vibrations are usually resolved from protein vibrational modes[31]. Secondary structure using fits to IR spectra has at times been overdetermined and should be carefully done[32]. Structural determination in membrane proteins has been most successfully achieved with attenuated total reflectance (ATR). This requires guiding an IR beam through a crystal with a high index of refraction such that the beam is totally reflected within the crystal[29]. At each surface of reflection, an evanescent wave is created of the same IR wavelength that penetrates a very thin portion (of the same order as the IR wavelength) of the surface where membranes can be deposited with proteins of interest. Polarized IR light with oriented membranes can be used to determine protein orientation in the membrane[33].

1.4.4 Visible

While the protein backbone does not absorb in the visible region, its cofactors such as carotenoids, heme, and chlorophyll all have discrete visible absorbance bands which can be used to derive structural information. Carotenoids absorb in the blue, heme has type-specific Soret band absorbance in the blue and yellow-green, and chlorophylls absorb in the red. Pump-probe techniques are of great use here and will excite the chromophore to probe nearby effects as energy is transferred to its surroundings. Carotenoids have also been the subject of resonance Raman studies of bacteriorhodopisin[34], a pigment in *Halobacterium halobium*[35], and plant tissue[36]. Hemes in particular coordinate amino acids at the axial positions and are directly influenced by protein structure. Resonance Raman spectroscopy ($\lambda_{excitation}$ = 243 nm, in the Soret band), especially in the time domain, can reveal much about the heme environment during transient processes[37]. Recent reviews have been published with chlorophyll as a structural probe of light harvesting complexes[38] and photosystem II[39].

1.4.5 Ultraviolet

The protein backbone and aromatic side chains both have characteristic ultraviolet (UV) absorbance. Alpha helical, beta sheet, and random coil structures even have unique deep-UV absorbance which can only be measured if oxygen can be thoroughly removed from the system[40]. Tryptophan, which has an energetic preference for the lipid-water interface of membrane proteins[41] and stabilizes their structure[42], has the highest extinction coefficient of the aromatic residues and is routinely used to determine the water-accessibility of the indole group using fluorescence[43]. Structural determination with UV light is most commonly done with circular dichroism, which measures the difference in absorbance between right and left-circularly polarized light. The chiral nature of proteins have made them ideal for this technique. However, lipid-containing samples will scatter UV light and prevent absorption by the protein. For membrane proteins, it is desirable to use detergent micelles or extruded liposome samples which tend to have the most homogeneous size distributions and high protein to lipid ratios. Even then, common membrane components like cholesterol give membranes an undesirable opacity. Synchrotron radiation sources have a much higher light flux which enables CD measurements to be taken deeper in the UV down to the vacuum region (i.e. 160 nm)[44]. Furthermore, secondary structure determination cannot rely on soluble protein reference spectral databases given the change in the dielectric constant in the membrane which is known to cause non-uniform wavelength shifts[45]. For Beer's law to be ideally met, the membrane proteins must be randomly distributed throughout the solution which is not possible because of localization within the lipid entity unless there is nearly a 1:1 ratio between protein and liposome/micelle. The dilution of the protein and the high lipid content requires intense synchrotron radiation (e.g. opsin[46]). Similar studies[47] are now being done that can begin to differentiate contributions from the transmembrane and extramembrane segments of membrane proteins.

1.4.6 X-ray

X-ray crystallography (XRC) has resulted in the majority of deposited membrane protein structures (around 250 to date[48]). Unfortunately, XRC requires a proper detergent system to induce crystallization[49]. This requires a wide array of screening solutions to test for proper crystallization conditions and still yields lower resolution structures on average. Cryo-electron microscopy, a related technique that uses an electron beam, has sufficiently matured to determine structures at less than 2 Å resolution but has the same challenges of sample crystallization[50]. Seven membrane protein structure deposits have been made to date in the protein data bank using this technique[51].

1.4.7 Need for a New Technique

Amongst the strategies discussed above, the most accurate and high resolution techniques (XRC and NMR) are also the most time- and money-consuming. Cheaper and faster methods are limited to low resolution. There is a need to balance these two alternatives to maintain low cost and a higher structural resolution. Other desirable qualities include: not being limited by protein size, requiring very little sample, being amenable to the presence of lipid or detergent and free from non-native labeling. No technique described so far can claim all of these qualities. In the next chapter, the case is made for deep-UV resonance Raman spectroscopy as a emergent means of membrane protein structural analysis.

1.5 Bibliography

1. RCSB PDB Statistics. http://www.pdb.org/pdb/static.do?p=general_information/pdb_statistics/index.html (accessed June 25th, 2012).

2. Whitmore, L.; Wallace, B. A., Protein Secondary Structure Analyses from Circular Dichroism Spectroscopy: Methods and Reference Databases. *Biopolymers* **2008,** *89* (5), 392-400.

3. Wallin, E.; Von Heijne, G., Genome-Wide Analysis of Integral Membrane Proteins from Eubacterial, Archaean, and Eukaryotic Organisms. *Protein Science* **1998,** *7*, 1029-1038.

4. White, S. H., Biophysical Dissection of Membrane Proteins. *Nature* **2009,** *459* (7245), 344-346.

5. (a) Edsall, J. T.; Flory, P. J.; Kendrew, J. C.; Liquori, A. M.; Némethy, G.; Ramachandran, G. N.; Scheraga, H. A., A Proposal of Standard Conventions and Nomenclature for the Description of Polypeptide Conformations. *Biopolymers* **1966,** *4*, 121-130; (b) Edsall, J. T.; Flory, P. J.; Kendrew, J. C.; Liquori, A. M.; Némethy, G.; Ramachandran, G. N.; Scheraga, H. A., A Proposal of Standard Conventions and Nomenclature for the Description of Polypeptide Conformations. *Journal of Biological Chemistry* **1966,** *241* (4), 1004-1008; (c) Edsall, J. T.; Flory, P. J.; Kendrew, J. C.; Liquori, A. M.; Némethy, G.; Ramachandran, G. N.; Scheraga, H. A., A Proposal of Standard Conventions and Nomenclature for the Description of Polypeptide Conformations. *Journal of Molecular Biology* **1966,** *15*, 399-407.

6. (a) Ramachandran, G. N.; Sasisekharan, V., Conformation of Polypeptides and Proteins. *Advances in Protein Chemistry* **1968,** *23*, 283-438; (b) Richardson, J. S., The Anatomy and Taxonomy of Protein Structure. *Advances in Protein Chemistry* **1981,** *34*, 167-339; (c) Rose, G. D.; Gierasch, L. M.; Smith, J. A., Turns in Peptides and Proteins. *Advances in Protein Chemistry* **1985,** *37*, 1-109; (d) Kabsch, W.; Sander, C., Dictionary of Protein Secondary Structure: Pattern Recognition of Hydrogen-Bonded and Geometrical Features. *Biopolymers* **1983,** *22*, 2577-2637.

7. Pauling, L.; Corey, R. B.; Branson, H. R., The Structure of Proteins: Two Hydrogen-Bonded Helical Configurations of the Polypeptide Chain. *Proceedings of the Natiocal Academy of Sciences of the United States of America* **1951,** *37*, 205-211.

8. Pauling, L.; Corey, R. B., Configurations of Polypeptide Chains with Favored Orientations Around Single Bonds: Two New Pleated Sheets. *Proceedings of the Natiocal Academy of Sciences of the United States of America* **1951,** *37*, 729-740.

9. Chothia, C., Conformation of Twisted β-pleated Sheets In Proteins. *Journal of Molecular Biology* **1973,** *75*, 295-302.

10. Hutchinson, E. G.; Thornton, J. M., A Revised Set of Potentials for β-turn Formation in Proteins. *Protein Science* **1994,** *3*, 2207-2216.

11. Brant, D. A.; Flory, P. J., The Configuration of Random Polypeptide Chains. II. Theory. *Journal of the American Chemical Society* **1965,** *87*, 2791-2800.

12. Schweitzer-Stenner, R., Conformational Propensities and Residual Structures in Unfolded Peptides and Proteins. *Molecular BioSystems* **2012,** *8*, 122-133.

13. Cowan, P. M.; McGavin, S., Stucture of Poly-L-Proline. *Nature* **1955,** *176*, 501-503.

14. Hildebrand, P. W.; Preissner, R.; Frömmel, C., Structural Features of Transmembrane Helices. *FEBS Letters* **2004,** *559*, 145-151.

15. Bowie, J. U., Helix Packing in Membrane Proteins. *Journal of Molecular Biology* **1997,** *272*, 780-789.

16. (a) White, S. H.; Wimley, W. C., Membrane Protein Folding and Stability: Physical Principles. *Annual Review of Biophysics and Biomolecular Structure* **1999,** *28*, 319-365; (b) von Heijne, G., Principles of Membrane Protein Assembly and Structure. *Progress in Biophysics and Molecular Biology* **1996,** *66*, 113-139; (c) von Heijne, G., Recent Advances in the Understanding of Membrane Protein Assembly and

Structure. *Quarterly Reviews of Biophysics* **1999,** *32* (4), 285-307; (d) Popot, J.-L.; Engelman, D. M., Helical Membrane Protein Folding, Stability, and Evolution. *Annual Review of Biochemistry* **2000,** *69*, 881-922; (e) Schulz, G. E., β-Barrel Membrane Proteins. *Current Opinion in Structural Biology* **2000,** *10* (4), 443-447; (f) Koebnik, R.; Locher, K. P.; Van Gelder, P., Structure and Function of Bacterial Outer Membrane Proteins: Barrels in a Nutshell. *Molecular Microbiology* **2000,** *37* (2), 239-253.

17. (a) Ubarretxena-Belandia, I.; Engelman, D. M., Helical Membrane Proteins: Diversity of Functions in the Context of Simple Architecture. *Current Opinion in Structural Biology* **2001,** *11* (3), 370-376; (b) Hanson, M. A.; Stevens, R. C., Discovery of New GPCR Biology: One Receptor Structure at a Time. *Structure* **2009,** *17*, 8-14.

18. (a) Granseth, E.; Seppälä, S.; Rapp, M.; Daley, D. O.; Von Heijne, G., Membrane Protein Structural Biology - How Far Can the Bugs Take Us? *Molecular Membrane Biology* **2007,** *24*, 329-332; (b) Junge, F.; Schneider, B.; Reckel, S.; Schwarz, D.; Dötsch, V.; Bernhard, F., Large-Scale Production of Functional Membrane Proteins. *Cellular and Molecular Life Sciences* **2008,** *65*, 1729-1755.

19. (a) Duquesne, K.; Sturgis, J. N., Membrane Protein Solubilization. *Methods in Molecular Biology* **2010,** *601*, 205-217; (b) Rigaud, J.-L.; Mosser, G.; Lacapere, J.-J.; Olofsson, A.; Levy, D.; Ranck, J.-L., Bio-Beads: An Efficient Strategy for Two-Dimensional Crystallization of Membrane Proteins. *Journal of Structural Biology* **1997,** *118*, 226-235; (c) Lin, S.-H.; Guidotti, G., Purification of Membrane Proteins. *Methods in Enzymology* **2009,** *463*, 619-629.

20. Cowieson, N. P.; Kobe, B.; Martin, J. L., United We Stand: Combining Structural Methods. *Current Opinion in Structural Biology* **2008,** *18*, 617-622.

21. Van Horn, W. D.; Kim, H. J.; Ellis, C. D.; Hadziselimovic, A.; Sulistijo, E. S.; Karra, M. D.; Tian, C.; Sönnichsen, F. D.; Sanders, C. R., Solution Nuclear Magnetic Resonance Structure of Membrane-Integral Diacylglycerol Kinase. *Science* **2009,** *324*, 1726-1729.

22. Arora, A.; Tamm, L. K., Biophysical Approaches to Membrane Protein Structure Determination. *Current Opinion in Structural Biology* **2001,** *11*, 540-547.

23. Warschawski, D. E. Membrane Proteins of Known Structure Determined by NMR. www.drorlist.com/nmr/MPNMR.html (accessed June 21, 2012).

24. Montaville, P.; Jamin, N., Determination of Membrane Protein Structures Using Solution and Solid-State NMR. *Methods in Molecular Biology* **2010,** *654*, 261-282.

25. Kang, C.; Li, Q., Solution NMR Study of Integral Membrane Proteins. *Current Opinion in Structural Biology* **2011,** *15*, 560-569.

26. (a) Hubbell, W. L.; Cafiso, D. S.; Altenbach, C., Identifying Conformational Changes with Site-Directed Spin Labeling. *Nature Structural Biology* **2000,** *7*, 735-739; (b) Czogalla, A.; Pieciul, A.; Jezierski, A.; Sikorski, A. F., Attaching a Spin to a Protein - Site-Directed Spin Labeling in Structural Biology. *Acta Biochimica Polonica* **2007,** *54*, 235-244.

27. Mchaourab, H. S.; Stted, P. R.; Kazmier, K., Toward the Fourth Dimension of Membrane Protein Structure: Insight into Dynamics from Spin-Labelin EPR Spectroscopy. *Structure* **2011,** *19*, 1549-1561.

28. Jeschke, G.; Polyhach, Y., Distance Measurements on Spin-Labelled Biomacromolecules By Pulsed Electron Paramagnetic Resonance. *Physical Chemistry Chemical Physics* **2007,** *9*, 1895-1910.

29. Barth, A., Infrared Spectrscopy of Proteins. *Biochimica et Biophysica Acta* **2007,** *1767*, 1073-1101.

30. Arrondo, J. L. R.; Goñi, F. M., Structure and Dynamics of Membrane Proteins as Studied by Infrared Spectroscopy. *Progress in Biophysics and Molecular Biology* **1999,** *72*, 367-405.

31. Tamm, L. K.; Tatulian, S. A., Infrared Spectroscopy of Proteins and Peptides in Lipid Bilayers. *Quarterly Reviews of Biophysics* **1997,** *30* (4), 365-429.

32. Jackson, M.; Mantsch, H. H., The Use and Misuse of FTIR Spectroscopy in the Determination of Protein Structure. *Critical Reviews in Biochemistry and Molecular Biology* **1995,** *30* (2), 95-120.

33. Vigano, C.; Manciu, L.; Buyse, F.; Goormaghtigh, E.; Ruysschaert, J.-M., Attenuated Total Reflection IR Spectroscopy as a Tool to Investigate the Structure, Orientation and Tertiary Structure Changes in Peptides and Membrane Proteins. *Biopolymers (Peptide Science)* **2000,** *55*, 373-380.

34. Campion, A.; Terner, J.; El-Sayed, M. A., Time-Resolved Resonance Raman Spectroscopy of Bacteriorhodopsin. *Nature* **1977,** *265*, 659-661.

35. Mendelsohn, R., Resonance Raman Spectroscopy of the Photoreceptor-Like Pigment of *Halobacterium halobium*. *Nature* **1973,** *243*, 22-24.

36. Gill, D.; Kilponen, R.; Rimai, L., Resonance Raman Scattering of Laser Radiation by Vibrational Modes of Carotenoid Pigment Molecules in Intact Plant Tissues. *Nature* **1970,** *227*, 743-744.

37. Kitagawa, T., Structures of Reaction Intermediates of Bovine Cytochrome c Oxidase Probed by Time-Resolved Vibrational Spectroscopy. *Journal of Inorganic Biochemistry* **2000,** *82*, 9-18.

38. Lokstein, H.; Krikunova, M.; Teuchner, K.; Voigt, B., Elucidation of Structure-Function Relationships in Photosynthetic Light-Harvesting Antenna Complexes by Non-Linear Polarization Spectroscopy in the Frequency Domain (NLPF). *Journal of Plant Physiology* **2011,** *168*, 1488-1496.

39. Renger, T.; Schlodder, E., Optical Properties, Excitation Energy and Primary Charge Transfer in Photosystem II: Theory Meets Experiment. *Journal of Photochemistry and Photobiology B: Biology* **2011,** *104*, 126-141.

40. Rosenheck, K.; Doty, P., The Far Ultraviolet Absorption Spectra of Polypeptide and Protein Solutions and Their Dependence on Conformation. *Proceedings of the Natiocal Academy of Sciences of the United States of America* **1961,** *47*, 1775-1785.

41. Yau, W.-M.; Wimley, W. C.; Gawrisch, K.; White, S. H., The Preference of Tryptophan for Membrane Interfaces. *Biochemistry* **1998,** *37*, 14713-14718.

42. Hong, H.; Park, S.; Flores Jiménez, R. H.; Rinehart, D.; Tamm, L. K., Role of Aromatic Side Chains in the Folding and Thermodynamic Stability of Integral Membrane Proteins. *Journal of the American Chemical Society* **2007,** *2007*, 8320-8327.

43. Ladokhin, A. S.; Jayasinghe, S.; White, S. H., How to Measure and Analyze Tryptophan Fluorescence in Membranes Properly, and Why Bother? *Analytical Biochemistry* **2000,** *285*, 235-245.

44. Wallace, B. A., Protein Characterization by Synchrotron Radiation Circular Dichroism Spectroscopy. *Quarterly Reviews of Biophysics* **2009,** *42* (4), 317-370.

45. Wallace, B. A.; Lees, J. G.; Orry, A. J. W.; Lobley, A.; Janes, R. W., Analysis of Circular Dichroism Spectra of Membrane Proteins. *Protein Science* **2003,** *2003*, 875-884.

46. McKibbin, C.; Farmer, N. A.; Jeans, C.; Reeves, P. J.; Khorana, H. G.; Wallace, B. A.; Edwards, P. C.; Villa, C.; Booth, P. J., Opsin Stability and Folding: Modulation by Phospholipid Bicelles. *Journal of Molecular Biology* **2007,** *374*, 1319-1332.

47. Powl, A. M.; Miles, A. J.; Wallace, B. A., Tranmembrane and Extramembrane Contributions to Membrane Protein Thermal Stability: Studies with the NaChBac Sodium Channel. *Biochimica et Biophysica Acta* **2012,** *1818*, 889-895.

48. White, S. H. Membrane Proteins of Known 3D Structure. http://blanco.biomol.uci.edu/mpstruc/listAll/list (accessed June 26, 2012).

49. Bill, R. M.; Henderson, P. J. F.; Iwata, S.; Kunji, E. R. S.; Michel, H.; Neutze, R.; Newstead, S.; Poolman, B.; Tate, C. G.; Vogel, H., Overcoming Barriers to Membrane Protein Structure Determination. *Nature Biotechnology* **2011,** *29* (4), 335-340.

50. (a) Wisedchaisri, G.; Reichow, S. L.; Gonen, T., Advances in Structural and Functional Analysis of Membrane Proteins by Electron Crystallography. *Structure* **2011,** *19* (10), 1381-1393; (b) Fujiyoshi, Y., Electron Crystallography for Structural and Functional Studies of Membrane Proteins. *Journal of Electron Microscopy* **2011,** *60*, 149-159.

51. Raman, P.; Cherezov, V.; Caffrey, M., The Membrane Protein Data Bank. *Cellular and Molecular Life Sciences* **2006,** *63*, 36-51.

Chapter 2: Deep Ultraviolet Resonance Raman Spectroscopy

2.1 The Raman Effect

The Raman effect describes a two-photon process with a difference in energy between incident and spontaneously emitted monochromatic light. That energy difference corresponds to the energy of one or multiple combined vibrational modes of a molecule[1]. Similar in concept to Compton scattering with X-rays, Raman describes the inelastic scattering of light contrasted to the more common elastic Rayleigh scattering. Light in the infrared, visible, and ultraviolet wavelengths can be used to observe this effect. Raman, named for Sir Chandrasekhara Venkata Raman, is a scattering phenomenon where light transiently interacts and alters the electron cloud to excite from the initial energy state (usually the ground state) to a virtual energy state. The scattered wavelength can have more energy than the incident wavelength if the relaxation occurs from the virtual energy state to one lower than the initial or vice-versa. Because of the Boltzmann distribution, most Raman scattering is an excitation from the ground state, to the virtual state, and back down to the first vibrational energy state. This is also referred to as Stokes scattering (anti-Stokes describes the former case).

Raman scattering is most commonly used as a vibrational spectroscopic technique, but can be composed of rotational energy transitions. Vibrational modes that change the polarizability of the molecule are Raman-active. Given the difference in selection rules compared to IR, Raman is a complementary technique. IR-active vibrational modes cause a change in the dipole moment. Small molecules with centers of inversion have vibrational modes that are either Raman or IR active, not both. Proteins are sufficiently complex that many vibrational modes (or combinations thereof) appear in both Raman and IR but are not necessarily the same intensity; rather, that is determined by how allowed a particular transition is according to quantum mechanical selection rules. The intense H-O-H bend that

interferes with water-based measurements in IR is weak in the Raman spectrum. Therefore, deuteration of samples is typically no longer necessary. Similar to IR, Raman spectra are measured as a function of frequency, $\tilde{\nu}$, in units of wavenumbers (cm^{-1}) which is proportional to energy. A typical spectrum will have increasing wavenumbers from left to right with 0 cm^{-1} defined as the absolute excitation wavelength. Vibrational modes at positive frequencies will contain Stokes scattering and negative frequencies would contain anti-Stokes scattering. The individual intensity of a Raman band is proportional to the magnitude of the Raman shift to the fourth power, the incident laser intensity, and the polarizability of the molecule (defined as the interaction of the electron cloud in an electric field). Generally, molecules with larger electron clouds and more shielded valence electrons are more easily polarized. Fundamentally, Raman spectroscopy is suited to collecting spectra of water-based samples and is sensitive to polarizable molecules like proteins.

2.2 Resonance Enhancement and UV Excitation Considerations

The energy of the virtual state usually is not degenerate with excited electronic states, in which case no vibrational modes are selected over another. Intensity is purely determined by which transitions are most allowed. As the virtual state approaches the energy of an excited electronic state, those chromophores associated with that excited electronic state will experience enhanced intensities (because of increased Raman cross-sections) in a pre-resonance enhanced state. When the virtual state is degenerate, Raman cross-sections are at a maximum and said to be resonance enhanced. Enhancements of the Raman cross-sections[2] can reach factors of 10^2-10^6. In this fashion, one can select for vibrational modes of a given chromophore by tuning the excitation wavelength to correspond to its electronic transition. For example, resonance Raman spectroscopy of hemoproteins (e.g. hemoglobin) could be excited with Soret band energy, near 420 nm. The resulting Raman spectrum would almost completely contain vibrational stretches arising from porphyrin as these are selected for over non-resonance enhanced vibrational modes from water or surrounding protein[3]. Ultraviolet resonance

Raman spectroscopy (UVRR) typically refers to excitation near 230 nm and is reserved for resonance enhancement of aromatic residues given the $\pi^* \leftarrow \pi$ L_a and $B_{a,b}$ transitions that range from 206 to 223 nm[4]. Histidine, while aromatic, is not sufficiently resonance enhanced[5]. Until recently, literature had not often differentiated UVRR from deep-UV resonance Raman (DUVRR), leaving the reader to determine the excitation wavelength and chromophore of interest, be it aromatic residues or the amide backbone. For clarity, these designations are retained for the remainder of this document. Excitation in deep UV (λ < 210 nm) approaches several amide electronic transitions, such as the strong dipole-allowed $\pi_3^* \leftarrow \pi_2$ transition at 188 nm, the weaker symmetry forbidden $\pi_3^* \leftarrow n_o$ transition at 210 nm, and another $\pi_3^* \leftarrow \pi_1$ transition at 165 nm[6]. This wavelength region also pre-resonantly enhances aromatic vibrational modes.

2.2.1 Advantages and Limitations of DUVRR

Traditional weak Raman scattering intensities are overcome with DUVRR, whose spectra nearly exclusively contain amide and aromatic modes. Water is a weak scatterer, not resonantly enhanced, and is easily subtracted from the spectrum either with or without an internal intensity standard present[7]. Four structurally-sensitive amide modes are present which allows for multiple spectroscopic handles of protein conformation, despite some spectral overlap from aromatic modes. Of the spectroscopy-based secondary structure determination efforts of globular proteins, DUVRR is the most accurate technique despite circular dichroism being much more commonly used[8]. Sample volumes can be as small as 500 µL, which is circulated in a flow system to avoid sample damage from prolonged exposure to the laser beam which is limited to a maximum power of 500 µW. Only a few milligrams of protein sample are needed to acquire a suitable spectrum. The beam is incident on a thin film of sample directly because even Suprasil quartz cuvettes absorb too strongly in the deep UV. Specially-coated optics must be used to efficiently direct the beam to the sample. Protein samples do not require labeled molecules as DUVRR is sensitive and selective enough to the native amide backbone. Yet, vibrational bands can be identified by selective isotopic substitution because the vibrational energy (in wavenumbers) is inversely

proportional to the square root of a bond's reduced mass. As excitation wavelengths become much shorter than the visible spectrum, fluorescence emission no longer interferes at the same Raman scattering wavelengths of proteins. Scattering techniques like Raman are not concerned with sample opacity or adherence to Beer's law. Therefore non-transparent lipid-containing samples can still be analyzed. The tunability of the Ti:sapphire IR source makes excitation profiles relatively easy to obtain over a 10 nm range, giving an additional dimension of analysis with Raman excitation profiles. Pulsed lasers have been used in dynamics studies from the picosecond to microsecond time scales[9]. DUVRR, therefore, offers the advantage of selecting for the amide backbone over all other chromophores in solution.

2.2.2 Instrumentation

The basic Raman spectrometer requires a monochromatic light source that is dispersed through a prism, incident upon the sample and backscattered at approximately 135° towards collimating and focusing lenses and into the detector which disperses the main excitation wavelength from the Raman scattering. Only the monochromatic light source, sample chamber, and detector must change to suit the needs of the sample and excitation wavelength[10]. Resonance Raman spectroscopy is in principle limited by the availability of a suitable laser source for the chromophore of interest. In lieu of using a primary laser source at every possible wavelength, more common laser sources can be frequency mixed, frequency doubled, or Raman shifted with hydrogen or deuterium gas. Of the current laser sources used in the literature concerning membrane protein structure determination, three main excitation sources exist for the three main chromophores. Heme, such as is found in the membrane protein cytochrome *c* oxidase, could be probed with Soret band excitation using a Krypton laser[11] (Kr^+, 413.1 nm) amongst others[12]. Aromatic amino acid residues, especially tryptophan and tyrosine, are regularly surveyed by UVRR with a quadruple harmonic of a 920 nm Ti:sapphire (Ti_2O_3 doped Al_2O_3) laser which lases at 230 nm (pumped by a frequency doubled neodymium-doped yttrium lithium fluoride laser, Nd:YLF)[13].

Frequency doubled Argon lasers (Ar^+, 229 nm) are also used[14]. Similar to UVRR, the laser source for deep UV light must be created from a multiple harmonics of a tunable Ti:sapphire laser pumped by a frequency doubled Nd:YLF laser[15]. The Ti:sapphire beam (IR wavelength near 800 nm) is frequency doubled at the second harmonic LBO (lithium triborate) crystal to create blue light. Both the residual, collinear IR and blue light are frequency mixed at the third harmonic BBO (beta barium borate) crystal to produce violet light. This, in turn, is collinear with the residual IR and frequency mixed with another BBO crystal to produce the desired deep UV light from 195 to 206 nm with approximately 0.25 nm resolution. BBO crystals are moisture-sensitive, therefore the harmonics cavity is kept under a positive pressure of nitrogen gas.

The flow cell is pumped by a peristaltic pump to circulate the small (0.5 – 5 mL) sample volume which can be cooled by a water jacket surrounding the sample reservoir from 4° to 35° C, although measurements are typically taken at room temperature. The sample flows down two thin nitinol wires as a thin film of approximately 1 mm width. The focused laser beam is incident on this this film. The atmosphere is nitrogen purged to avoid contributions to the Raman spectrum from molecular oxygen. The Raman scattered light is collimated and focused into a spectrograph which spatially separates the Rayleigh scattering and directs the Stokes scattering on a liquid nitrogen-cooled charge-coupled device (CCD). Spectral resolution is determined by the bin of the CCD.

2.3 UVRR Spectroscopy of Soluble Proteins

Proteins have been studied by DUVRR spectroscopy since the availability of deep UV lasers in the 1980s. Myoglobin was the subject of the first published UVRR spectrum of a protein in 1984[16]. Built on model studies of *N*-methylacetamide for the protein backbone and benzene for the aromatic residues, a comprehensive list of known vibrational modes, along with isotopic labeling and environmental effects, have been collected[6b, c, 17]. A survey of these modes are discussed below. These

analyses have led to many successful secondary structure characterizations of water-soluble proteins, some even at the tertiary and quaternary structure level[18]. It is the combination of analysis of all four modes simultaneously that make DUVRR the most sensitive technique for secondary structure determination[8, 19].

2.3.1 Amide Vibrational Modes

N-methylacetamide (NMA) was first used experimentally to measure the principal vibrations associated with the amide moiety[20]. Four principal vibrational modes, called amide modes, have since been identified and contributing vibrations determined. Listed from high to low energy, they are the amide I, II, S, and III. Structural sensitivities of each are discussed.

2.3.1.1 Amide I

The amide I is predominantly (70%) a carbonyl stretch with some (13%) NH bending contribution in the 1600 to 1700 cm^{-1} region[6c]. Vibrational contributions to each amide mode have been calculated in potential energy distributions (PEDs)[21]. The hydrogen bonding capability of the carbonyl makes the amide I a very structurally-sensitive mode because each secondary structure has a unique hydrogen bonding geometry. Alpha helices have lower amide I modes (1645-1655 cm^{-1}) because of intramolecular hydrogen bonding and hydrogen bonding to water[17]. Amide I modes of beta sheet and disordered peptides overlap each other between 1660-1680 cm^{-1}. In soluble protein spectra, however, the amide I is usually the least intense of the amide modes (unless the protein has a very high helical content). The amide I is more intense in IR spectra and therefore structural determination is almost exclusively done with this mode[22]. Non-resonance enhanced Raman spectra (λ_{ex}= 514.5 nm) also have amide I modes which allow for structural analysis[23].

2.3.1.2 Amide II

The amide II is an out-of-phase combination of C-N stretching and N-H in-plane bending with equal contributions to the potential energy distribution at 41%. It appears between 1500 and 1600 cm^{-1}. Alpha helices have two distinct modes at lower wavenumbers (1520-1555 cm^{-1}) while beta sheet and disordered structures are at higher wavenumbers (1548-1564 cm^{-1})[17]. Resonance enhancement of the amide makes the amide II much more intense than in non-resonance enhanced spectra. Amide II cross-sections were used in one of the earliest structural determination efforts with DUVRR[24]. Its intensity is inversely proportional to helical content in a protein[17]. Deuteration of the amide backbone removes the coupling with the C-N stretch, and the amide II' band is a pure C-N stretch near 1500 cm^{-1} where it is very intense and not significantly overlapped by other bands (N.B. a prime after a vibrational mode denotes deuteration of the NH to ND). Because of this, the amide II and II' are excellent markers for the extent of deuteration of the protein backbone. H-D exchange rates can provide information about the solvent-accessible residues of membrane proteins.

2.3.1.3 Amide S

The amide S, alternatively called the $C_\alpha H$ bending mode in literature, was the last of the amide modes to be identified and therefore not numerical in sequence. The "S" notation was proposed by Spiro for "secondary structure-sensitive"[25]. Finally, the $C_\alpha H$ bending coupled to NH bending was determined to be its source[26]. The amide S appears from 1374-1397 cm^{-1} for disordered structures and 1395-1406 cm^{-1} for beta sheet structures[17]. Like the amide II, its intensity is also inversely proportional to helical content[17]. Fully alpha-helical peptides show no amide S in their Raman spectra because the alpha-helical conformation forces the C_α hydrogen in close proximity to the amide hydrogen which decouples the two vibrations[27].

2.3.1.4 Amide III

The amide III shares the same C-N stretch and N-H in-plane bending modes as the amide II, only these are in phase and appear between 1200 and 1350 cm^{-1}. Alpha helices have an amide III mode at higher wavenumbers (1254-1345 cm^{-1}), beta sheets at the lower end (1220 to 1241 cm^{-1}), and disordered in between (1240-1279 cm^{-1}). Furthermore, three main sub-bands have been identified in the literature, called the amide III_1, III_2, and III_3 bands, in order of high to low energy. The latter is the "classical" amide III mode described in prior literature before the other two components were identified[28]. Most of the recent DUVRR structural analysis literature has focused on the amide III as it is the most sensitive to secondary structure. Amide III frequency is sinusoidally dependent upon the ϕ and ψ dihedral angles of the protein backbone[29], which had been shown earlier[30] with non-resonance Raman spectroscopy. Therefore, ψ angle distributions can be quantified. However, the amide III is often overlapped with aromatic residue vibrations (assuming aromatic residues are present in the primary protein sequence), which are typically subtracted out in fitting analyses of the mode. The amide III is very rich in structural information when there is not significant spectral overlap in this region.

2.3.2 Aromatic Vibrational Modes

Aromatic residues in a protein's primary sequence are both a blessing and a curse. The amide modes are certainly adequate for structural analysis, but aromatic vibrational modes report on hydrogen bonding and environmental polarity and are largely responsible for reporting on tertiary and quaternary contacts in a protein. The challenge, although not insurmountable, lies in the spectral overlap. This is particularly true of the amide III region. Up to eighteen vibrational modes appear in DUVRR spectra for any given aromatic residue. Individual vibrational modes of interest are discussed below.

2.3.2.1 Tyrosine

Tyrosine (Tyr, Y) vibrational modes were named based on their similarity to benzene vibrational modes such as ring breathing (Y1) and ring stretching (Y7a, Y9a, Y9b). The tyrosine Fermi doublet, formally denoted as the Y1/2Y16a mode, is a broad two-component band at 830/850 cm^{-1} from contributions of the Y1 and an overtone of the out-of-plane ring deformation mode (2Y16a)[31]. The doublet appears to be more sensitive to hydrogen bonding of the tyrosine –OH group in non-resonance enhanced spectra than in UVRR spectra[32]. As the hydroxyl group becomes more hydrogen donating, the 850:830 cm^{-1} intensity ratio decreases but multiple effects change the ratio in resonance enhanced spectra and cannot be solely attributed to hydrogen bonding[6b]. Certain tyrosine vibrational modes (e.g. Y7a, Y8a, and Y9a) are sensitive to solvent exposure and exhibit increased cross-sections as water was excluded from the environment[33].

2.3.2.2 Phenylalanine

Phenylalanine (Phe, F) features, amongst other similar benzene vibrational modes as tyrosine, a unique F12 ring breathing mode near 1000 cm^{-1} which is not overlapped by any other aromatic mode (unless a comparable molar concentration of tryptophan is also present). It is associated with a $\pi^{*} \leftarrow \pi$ electronic transition closer to that of an amide mode and therefore is more intense in DUVRR spectra than in UVRR spectra. No shifts in energy are observed for phenylalanine modes as a function of environment, but intensity and cross-section increases have been observed for at least the F12 and ring stretching modes (F8a and F8b) in more non-polar environments in DUVRR and UVRR[32]. Suggested rationales for the enhancement have been proposed to come from shifts in the absorbance maxima[34], local refractive index changes[35], and Raman hypochromism[36].

2.3.2.3 Tryptophan

Tryptophan's (Trp, W) indole ring has many different vibrational modes spectrally resolved from tyrosine and phenylalanine's benzene-type modes. Tryptophan spectra are the most information-rich of

all the aromatic modes, as it has vibrational modes that are sensitive to environment polarity, hydrogen bonding, structural orientation, and cation-π interactions via energy shifts and intensity changes[34, 37]. The ring stretches, W1 and W2, are shifted away from the Phe and Tyr benzene ring stretching modes and can be sometimes resolved in DUVRR spectra because of an additional N-C stretch from the indole ring[38]. Tryptophan DUVRR spectra also contain a Fermi doublet, the W7 mode which is a N-C stretching mode is split by Fermi resonance with combination bands of out-of-plane bending vibrations, the W25+W33 and W28+W29 modes[6b]. The doublet appears at 1340/1360 cm^{-1}. As the indole senses more non-polar environments, the 1360 cm^{-1} band dominates[39]. The W18 mode is suspected to be sensitive to environment polarity in non-resonance Raman spectra as it increases intensity relative to the W16 intensity in more aqueous surroundings[40]. The W17, a benzene-like vibration with indole NH motion at 880 cm^{-1}, was the first hydrogen-bonding sensitive mode known[41]. Shifts to lower wavenumbers indicate a more hydrogen bond donating character, and vice-versa. Three other bands, the W2, W4, and W6, all have shown energy downshifts as a function of increasing hydrogen bonding donating character of the indole NH[42]. The latter modes involve NH in-plane bending and the former involves ring stretching, but is also the least sensitive; it only has a range of 8 cm^{-1}. In UVRR spectra the W8 is more sensitive than the W17 to hydrogen bonding as shown by Kim et al[39]. In the same study, a new marker of hydrogen bonding was discovered, the W10/W9 intensity ratio. Despite the vast potential of these environmental markers, most hydrogen-bonding sensitive modes are usually too weak to assign or overlapped in DUVRR spectra. Tryptophan spectra feature a W3 mode (C_2-C_3 stretching around 1552 cm^{-1}) which has shown structural sensitivity to the dihedral angle along the side chain (defined by the C_α-C_β-C_1-C_2 atoms) over a range of 15 cm^{-1}. Unfortunately, this band overlaps with the amide II mode in protein DUVRR spectra. Many of the tryptophan bands have higher cross-sections as water is excluded from solvent[33]. Solvent accessibility is also reported by H/D exchange of tryptophan indole N-H groups, with a resulting shift in several bands (especially the W1, W6, W7, and W17)[39]. Tryptophan is sensitive to one other

phenomenon, the cation-π interaction, such as those found in tryptophan-containing membrane channel proteins that shuttle cations across the membrane. In UVRR spectra, the ratio of the W18 and W16 modes described as sensitive to hydrogen bonding in non-resonance Raman spectra is shown to be sensitive to cation-π interactions in UVRR spectra[39, 43].

2.3.2.4 Histidine

The imidazole side chain of histidine is more chemically active amongst the aromatic residues because it can dissociate two protons as well as coordinate metal ions, as evidenced by the common presence of histidine in enzymatic catalysis. However, as mentioned previously, histidine is rarely considered in UVRR literature because of relatively low Raman excitation profiles. Peptides of interest usually must be engineered to have no competing spectral contributions from other aromatics. Given the versatility of histidine, the ability to monitor its protonation and coordination states would be of great benefit to understanding, amongst other things, electron transfer as discussed in chapter 3. Recently, the Spiro lab has published a comprehensive article[44] with formal assignments of histidine vibrational modes in its various protonation and coordination states.

2.4 Effects of Dehydrating the Protein Backbone in Membrane Proteins

The wealth of structural information[45] determined by UVRR and DUVRR spectra of proteins has been collected from soluble proteins, which are the basis of reference spectral positions of amide and aromatic modes. Membrane proteins are only now just beginning to be characterized by Raman spectroscopy. The earliest insight[20c] to expected spectral phenomena resulting from dehydrating the backbone was the appearance of an amide I which was only observed in DUVRR spectra taken with acetonitrile, but not aqueous solvent. The amide I was thought to be too broadened in water, possibly because "of a vibrationally heterogeneous distribution of hydrogen-bonding environments not present in acetonitrile" – an explanation later refuted[46]. One early DUVRR characterization[47] of NMA measured

the cross-sections of the amide modes in water and acetonitrile. In water, the amide II and III are most intense, followed by the amide I and S. In acetonitrile, the amide I dominates, followed by the amide III and then the amide II. The excitation maximum is also blue-shifted. In non-aqueous and non-hydrogen bonding environments, the amide carbonyl is the closest to a bonding order of two. As hydrogen bonding donors approach the carbonyl, the double bond weakens. The increased amide I cross-section in acetonitrile was ascribed to a dominant C=O π fragment orbital, compared to the C=O π* fragment in hydrogen bonding solvents. Another DUVRR study[46] published the same year showed similar amide I enhancement in the vapor phase and confirmed expected shifts in energy, suggesting dielectric effects as a contributing factor. The amide I shifted to higher energy and the amide II and III shifted to lower energies upon desolvation while the amide S was unaffected. The exact geometric displacements from the ground to excited states were further characterized[48], showing a C=O bond elongation in the excited state in non-hydrogen bonded solvents. This elongation was even longer in the gas phase, consistent with previous experimental spectra[46]. These results were later corroborated computationally by studying hydration-induced structural changes of NMA in the presence of three water molecules, the typical hydration ratio per amino acid[49]. In acetonitrile, the carbonyl bond length from ground to excited state changes most significantly (when the amide I dominates). While in water, the C-N bond length changes the most from ground to excited state (when the amide II and III dominate). Aside from intensity differences upon backbone dehydration, secondary structure sensitivity has largely been unaddressed. Aromatic residues, discussed above, generally all have higher Raman cross-sections in the membrane in addition to their sensitivity to hydrogen bonding and solvent polarity[33].

2.4.1 Survey of UVRR and DUVRR Spectroscopy of Membrane Proteins to Date

A survey of recent literature enumerates approximately 20 journal articles wherein membrane proteins (including desolvated amyloid fibril cores) are studied with UVRR spectroscopy, beginning in 1996 (12 years after the first UVRR spectrum of a soluble protein). UVRR-based studies predictably focus

on aromatic amino acid residues and their ability to report on environment polarity and hydrogen bonding on various classes of membrane proteins: photosynthetic proteins[50], G-protein coupled receptors (e.g. rhodopsin)[51], cardiac amyloid fibrils[52], a blood pressure regulating protein[53], outer membrane pores[13, 54], a cation channel protein[55], antimicrobial peptides[39, 56], and a small model beta-sheet peptide[57]. This is only a small sampling of the known classes of membrane proteins and the potential of UVRR spectroscopy in this area is predicted to grow significantly.

Only ten published studies specifically used deep-UV excitation to address amide backbone conformation in a dehydrated environment[53, 58]. The first DUVRR peptide study[53a] of angiotensin II in the presence of dodecylphosphocholine (DPC) micelles was conducted at 208 nm excitation, with barely adequate amide mode enhancement to determine structural differences of the peptide backbone in a protein of which only 33% partitions into the micelle. Only changes in the amide III position was noted when comparing soluble to DPC-solubilized angiotensin, ascribed not to desolvation, but an increase in β-turn structure. Later treatments by Asher and coworkers[53b, 58h] used 206.5 nm excitation and noted the same amide III change from water to a DPC micelle, sodium dodecyl sulfate (SDS) micelle, or acetonitrile as a result of secondary structure change. Subsequent DUVRR reports have noted certain departures from classical amide mode positions and intensities, specifically in the amide I intensity as predicted by earlier NMA studies. Lednev and coworkers[58a], who focused on the desolvated cross-β core of amyloid fibrils, demonstrated the first appearance of increased amide I intensities in a full protein. All amide energies were consistent with previously characterized aqueous antiparallel β-sheet proteins, although the amide modes were noted as being much sharper. This indicates a much more homogeneous distribution of dihedral angles. Amyloid fibrils were also the focus of the most recent publication by Asher and coworkers[58g]. Only an amide I increase was seen for the full polyglutamate aggregate compared with disaggregated protein in water, with energy shifts for all three other amide modes due to the structural change from β-sheet to extended polyproline II conformations. Increased resonance

enhancement at 198 nm was also noted versus 204 nm excitation. Overall, increased hydrogen bonding strength in the aggregated protein was suggested as the cause.

The first investigation of a model membrane peptide in a lipid bilayer was reported by Kim and coworkers[57]. AcWL5, a 6-residue tryptophan containing self-associating β-sheet peptide, was probed at 230 and 207.5 nm in the presence of 1,2-dimyristoyl-*sn*-glycero-3-phosphocholine (DMPC) small unilamellar vesicles (SUVs, also referred to as liposomes). Amide mode assignments were consistent with those from soluble protein spectra going from a disordered to a β-sheet, but Raman cross-sections for tryptophan increased in the lipid environment – up to 30 fold.

This was followed by the first full scale investigation of a whole membrane protein: the 300 kDa cytochrome bc_1 isolated from *Rhodobacter capsulatus*[58c]. Cytochrome bc_1, isolated in detergent micelles, had an unambiguously large amide I intensity in the DUVRR spectrum excited at 198 nm. For meaningful comparison, water-soluble cytochrome *c* was measured for its similarity in aromatic and secondary structure content (within 3%), although cytochrome bc_1 is made up of several membrane spanning alpha helices. An important shift in both the amide I intensity and energy were analyzed and desolvation of the amide transmembrane backbone was suggested as the cause. These findings are discussed in detail in chapter 4. In order to tease out individual desolvated secondary structure components, a pure alpha helical model peptide derived from glycophorin was measured at 197 nm excitation in DPC micelles[58d]. It was discovered that desolvation of the backbone by a lipid membrane does not complicate secondary structural characterization. It also reports on the degree of desolvation. See chapter 5 for a detailed account. Efforts are now underway in the Cooley lab to fully understand the spectral consequences for amide vibrational mode intensities and energies of individual secondary structures in a membrane. The application of these findings extends to biologically relevant processes such photosynthesis and the electron transport chain.

Finally, two studies focus on the depsipeptide valinomycin, a potassium-selective carrier, in solvent[58f] and model membranes[58b] which is discussed in detail in chapter 6. Despite valinomycin not having a pure amide backbone and interlaced with ester linkages, meaningful structural dynamics can be gleaned from DUVRR spectra and the change in hydrogen bonding from the complexed to the uncomplexed state. Overall, DUVRR is well equipped to comment on the structure and dynamics of all types of proteins and protein-like molecules in the membrane, unlimited in size or function.

2.5 Bibliography

1. Carey, P. R., *Biochemical Applications of Raman and Resonance Raman Spectroscopies*. Academic Press, Inc.: New York, 1982.

2. Ingle Jr., J. D.; Crouch, S. R., Molecular Scattering Methods. In *Spectrochemical Analysis*, Prentice-Hall, Inc.: Upper Saddle River, NJ, 1988; pp 494-542.

3. Efremov, E.; Ariese, F.; Gooijer, C., Achievements in Resonance Raman Spectroscopy Review of a Technique with a Distinct Analytical Chemistry Potential. *Analytica Chimica Acta* **2008,** *606*, 119-134.

4. (a) Sweeney, J. A.; Asher, S. A., Tryptophan UV Resonance Raman Excitation Profiles. *Journal of Physical Chemistry* **1990,** *94*, 4784-4791; (b) Fodor, S. P. A.; Copeland, R. A.; Grygon, C. A.; Spiro, T. G., Deep-Ultraviolet Raman Excitation Profiles and Vibronic Scattering Mechanisms of Phenylalanine, Tyrosine, and Tryptophan. *Journal of the American Chemical Society* **1989,** *111* (15), 5518-5525.

5. Caswell, D. S.; Spiro, T. G., Ultraviolet Resonance Raman Spectroscopy of Imidazole, Histidine, and Cu(imidazole)$_4^{2+}$: Implications for Protein Studies. *Journal of the American Chemical Society* **1986,** *108*, 6470-6477.

6. (a) JiJi, R. D.; Balakrishnan, G.; Hu, Y.; Spiro, T. G., Intermediacy of Poly(L-Proline) II and β-Strand Conformations in Poly(L-Lysine) β-Sheet Formation Probed by Temperature-Jump/UV Resonance Raman Spectroscopy. *Biochemistry* **2006,** *45*, 34-41; (b) Harada, I.; Takeuchi, H., Raman and Ultraviolet Resonance Raman Spectra of Proteins and Related Compounds. In *Spectroscopy of Biological Systems*, Clark, R. J. H.; Hester, R. E., Eds. John Wiley & Sons: Chichester, 1986; Vol. 13, pp 113-175; (c) Austin, J. C.; Jordan, T.; Spiro, T. G., Ultraviolet Resonance Raman Studies of Proteins and Related Model Compounds. In *Biomolecular Spectroscopy, Part A*, Clark, R. J. H.; Hester, R. E., Eds. John Wiley & Sons: Chichester, 1993; pp 55-127.

7. Simpson, J. V.; Oshokoya, O. O.; Wagner, N.; Liu, J.; JiJi, R. D., Pre-processing of Ultraviolet Resonance Raman Spectra. *Analyst* **2011,** *136*, 1239-1247.

8. Chi, Z.; Chen, X. G.; Holtz, J. S. W.; Asher, S. A., UV Resonance Raman-Selective Amide Vibrational Enhancement: Quantitative Methodology for Determining Protein Secondary Structure. *Biochemistry* **1998,** *37*, 2854-2864.

9. Balakrishnan, G.; Weeks, C. L.; Ibrahim, M.; Soldatova, A. V.; Spiro, T. G., Protein Dynamics from Time Resolved UV Raman Spectroscopy. *Current Opinion in Structural Biology* **2008,** *18*, 623-629.

10. McCreery, R. L., *Raman Spectroscopy for Chemical Analysis*. John Wiley & Sons, Inc.: New York, 2000; Vol. 157.

11. Hildebrandt, P.; Vanhecke, F.; Buse, G.; Soulimane, T.; Maul, A. G., Resonance Raman Study of the Interactions Between Cytochrome *c* Variants and Cytochrome *c* Oxidase. *Biochemistry* **1993,** *32*, 10912-10922.

12. Spiro, T. G., Resonance Raman Spectra of Hemoproteins. *Methods in Enzymology* **1978,** *54*, 233-249.

13. Sanchez, K. M.; Neary, T. J.; Kim, J. E., Ultraviolet Resonance Raman Spectroscopy of Folded and Unfolded States of an Integral Membrane Protein. *Journal of Physical Chemistry B* **2008,** *112*, 9507-9511.

14. Zhao, X.; Chen, R.; Raj, V.; Spiro, T. G., Assignment of the 1511 cm^{-1} UV Resonance Raman Marker Band of Hemoglobin to Tryptophan. *Biopolymers* **2001,** *62* (3), 158-162.

15. Balakrishnan, G.; Hu, Y.; Nielsen, S. B.; Spiro, T. G., Tunable kHz Deep Ultraviolet (193-210 nm) Laser for Raman Applications. *Applied Spectroscopy* **2005,** *59*, 776-781.

16. Johnson, C. R.; Ludwig, M.; O'Donnell, S.; Asher, S. A., UV Resonance Raman Spectroscopy of the Aromatic Amino Acids and Myoglobin. *Journal of the American Chemical Society* **1984,** *106*, 5008-5010.

17. Roach, C. A.; Simpson, J. V.; JiJi, R. D., Evolution of Quantitative Methods in Protein Secondary Structure Determination Via Deep-Ultraviolet Resonance Raman Spectroscopy. *The Analyst* **2012,** *137* (3), 555-562.

18. (a) Wang, D.; Spiro, T. G., Structure Changes in Hemoglobin Upon Deletion of C-Terminal Residues, Monitored by Resonance Raman Spectroscopy. *Biochemistry* **1998,** *37* (28), 9940-9951; (b) Kitagawa, T.; Haruta, N.; Mizutani, Y., Time-Resolved Resonance Raman Study on Ultrafast Structural Relaxation and Vibrational Cooling of Photodissociated Carbonmonoxy Myoglobin. *Biopolymers (Biospectroscopy)* **2002,** *67*, 207-213; (c) Balakrishnan, G.; Case, M. A.; Pevsner, A.; Zhao, X.; Tengroth, C.; McLendon, G. L.; Spiro, T. G., Time-Resolved Absorption and UV Resonance Raman Spectra Reveal Stepwise Formation of T Quaternary Contacts in the Allosteric Pathway of Hemoglobin. *Journal of Molecular Biology* **2004,** *340* (4), 843-856.

19. Simpson, J. V.; Balakrishnan, G.; JiJi, R. D., MCR-ALS Analysis of Two-Way UV Resonance Raman Spectra to Resolve Discrete Protein Secondary Structural Motifs. *The Analyst* **2009,** *134*, 138-147.

20. (a) Harada, I.; Sugawara, Y.; Matsuura, H.; Shimanouchi, T., Preresonance Raman Spectra of Simple Amides Using Ultraviolet Lasers. *Journal of Raman Spectroscopy* **1975,** *4*, 91-98; (b) Mirkin, N. G.; Krimm, S., Ab Initio Vibrational Analysis of Hydrogen-Bonded *trans*- and *cis*-*N*-methylacetamide. *Journal of the American Chemical Society* **1991,** *113* (3), 9742-9747; (c) Mayne, L. C.; Ziegler, L. D.; Hudson, B. S., Ultraviolet Resonance Raman Studies of *N*-Methylacetamide. *Journal of Physical Chemistry* **1985,** *1985* (89), 15; (d) Dudik, J. M.; Johnson, C. R.; Asher, S. A., UV Resonance Raman Studies of Acetone,

Acetamide, and *N*-Methylacetamide: Models for the Peptide Bond. *Journal of Physical Chemistry* **1985,** *89*, 3805-3814.

21. Sugawara, Y.; Hirakawa, A. Y.; Tsuboi, M., In-Plane Force Constants of the Peptide Group: Least-Squares Adjustment Starting from *ab initio* Values of *N*-Methylacetamide. *Journal of Molecular Spectoscopy* **1984,** *108*, 206-214.

22. (a) Ganim, Z.; Chung, H. S.; Smith, A. W.; Deflores, L. P.; Jones, K. C.; Tokmakoff, A., Amide I Two-Dimensional Infrared Spectroscopy of Proteins. *Accounts of Chemical Research* **2008,** *41* (3), 432-441; (b) Barth, A., Infrared Spectrscopy of Proteins. *Biochimica et Biophysica Acta* **2007,** *1767*, 1073-1101.

23. (a) Williams, R. W., Protein Secondary Structure Analysis Using Raman Amide I and Amide III Spectra. *Methods in Enzymology* **1986,** *130*, 311-331; (b) Sane, S. U.; Cramer, S. M.; Przybycien, T. M., A Holistic Approach to Protein Secondary Structure Characterization Using Amide I Band Raman Spectroscopy. *Analytical Biochemistry* **1999,** *272*, 255-272.

24. Copeland, R. A.; Spiro, T. G., Secondary Structure Determination in Proteins from Deep (192-223 nm) Ultraviolet Raman Spectroscopy. *Biochemistry* **1987,** *26* (8), 2134-2139.

25. Wang, Y.; Purrello, R.; Spiro, T. G., UV Photoisomerization of *N*-Methylacetamide and Resonance Raman Enhancement of a New Conformation-Sensitive Amide Mode. *Journal of the American Chemical Society* **1989,** *111*, 8274-8276.

26. Wang, Y.; Purrello, R.; Jordan, T.; Spiro, T. G., UVRR Spectroscopy of the Peptide Bond. 1. Amide S, a Nonhelical Structure Marker, is a $C_\alpha H$ Bending Mode. *Journal of the American Chemical Society* **1991,** *113*, 6359-6368.

27. (a) Jordan, T.; Spiro, T. G., Enhancement of C_α Hydrogen Vibrations in the Resonance Raman Spectra of Amides. *Journal of Raman Spectroscopy* **1994,** *25*, 537-543; (b) Schweitzer-Stenner, R.; Eker, F.; Huang, Q.; Griebenow, K.; Mroz, P. A.; Kozlowski, P. M., Structure Analysis of Dipeptides in Water by Exploring and Utilizing the Structural Sensitivity of Amide III by Polarized Visible Raman, FTIR-Spectroscopy and DFT Based Normal Coordinate Analysis. *Journal of Physical Chemistry B* **2002,** *106*, 4294-4304.

28. Mikhonin, A. V.; Ahmed, Z.; Ianoul, A.; Asher, S. A., Assignments and Conformational Dependencies of the Amide III Peptide Backbone UV Resonance Raman Bands. *Journal of Physical Chemistry B* **2004,** *108*, 19020-19028.

29. (a) Ianoul, A.; Boyden, M. N.; Asher, S. A., Dependence of the Peptide Amide III Vibration on the Φ Dihedral Angle. *Journal of the American Chemical Society* **2001,** *123*, 7433-7434; (b) Asher, S. A.; Ianoul, A.; Mix, G.; Boyden, M. N.; Karnoup, A.; Diem, M.; Schweitzer-Stenner, R., Dihedral ψ Angle Dependence of the Amide III Vibration: A Uniquely Sensitive UV Resonance Raman Secondary Structural Probe. *Journal of the American Chemical Society* **2001,** *123*, 11775-11781; (c) Asher, S. A.; Mikhonin, A. V.; Bykov, S., UV Raman Demonstrates that α-Helical Polyalanine Peptides Melt to Polyproline II Conformations. *Journal of the American Chemical Society* **2004,** *126*, 8433-8440.

30. Lord, R. C., Strategy and Tactics in the Raman Spectroscopy of Biomolecules. *Applied Spectroscopy* **1977,** *31* (3), 187-194.

31. Asher, S. A.; Ludwig, M.; Johnson, C. R., UV Resonance Raman Excitation Profiles of the Aromatic Amino Acids. *Journal of the American Chemical Society* **1986,** *108* (20), 3186-3197.

32. Hildebrandt, P. G.; Copeland, R. A.; Spiro, T. G., Tyrosine Hydrogen-Bonding and Environmental Effects in Proteins Probed by Ultraviolet Resonance Raman Spectroscopy. *Biochemistry* **1988,** *27*, 5426-5433.

33. Chi, Z.; Asher, S. A., UV Raman Determination of the Environment and Solvent Exposure of Tyr and Trop Residues. *The Journal of Physical Chemistry B* **1998,** *102* (47), 9595-9602.

34. Liu, G.-y.; Grygon, C. A.; Spiro, T. G., Ionic Strength Dependence of Cytochrome *c* Structure and Trp-59 H/D Exchange from Ultraviolet Resonance Raman Spectroscopy. *Biochemistry* **1989,** *28*, 5046-5050.

35. Larkin, P. J.; Gustafson, W. G.; Asher, S. A., A New Raman Cross Section Measurement Technique Monitors the Tyrosine Environmental Dependence of the Electromagnetic Field Strength. *Journal of Chemical Physics* **1991,** *94* (8), 5324-5330.

36. (a) Harmon, P. A.; Teraoka, J.; Asher, S. A., UV Resonance Raman Saturation Spectroscopy Measures Protein Aromatic Amino Acid Excited State Relaxation Rates. *Journal of the American Chemical Society* **1990,** *112*, 8789-8799; (b) Kauffman, E. W.; Thamann, T. J.; Havel, H. A., Ultraviolet Resonance Raman and Fluorescence Studies of Acid-Induced Structural Alterations in Porcine, Bovine, and Human Growth Hormone. *Journal of the American Chemical Society* **1989,** *111*, 5449-5456.

37. Efremov, R. G.; Feofanov, A. V.; Nabiev, I. R., Effect of Hydrophobic Environment on the Resonance Raman Spectra of Tryptophan Residues in Proteins. *Journal of Raman Spectroscopy* **1992,** *23*, 69-73.

38. Takeuchi, H.; Harada, I., Normal Coordinate Analysis of the Indole Ring. *Spectrochimica Acta Part A: Molecular Spectroscopy* **1986,** *42* (9), 1069-1078.

39. Schlamadinger, D. E.; Gable, J. E.; Kim, J. E., Hydrogen Bonding and Solvent Polarity Markers in the UV Resonance Raman Spectrum of Tryptophan: Application to Membrane Proteins. *Journal of Physical Chemistry B* **2009,** *113*, 14769-14778.

40. Miura, T.; Takeuchi, H.; Harada, I., Raman Spectroscopic Characterization of Tryptophan Side Chains in Lysozyme Bound to Inhibitors: Role of the Hydrophobic Box in the Enzymatic Function. *Biochemistry* **1991,** *30*, 6074-6080.

41. Miura, T.; Takeuchi, H.; Harada, I., Characterization of Individual Tryptophan Side Chains in Proteins Using Raman Spectroscopy and Hydrogen-Deuterium Exchange Kinetics. *Biochemistry* **1988,** *27* (1), 88-94.

42. Miura, T.; Takeuchi, H.; Harada, I., Tryptophan Raman Bands Sensitive to Hydrogen Bonding and Side-Chain Conformation. *Journal of Raman Spectroscopy* **1989,** *20*, 667-671.

43. Schlamadinger, D. E.; Daschbach, M. M.; Gokel, G. W.; Kim, J. E., UV Resonance Raman Study of Cation-π Interactions in an Indole Crown Ether. *Journal of Raman Spectroscopy* **2011,** *42*, 633-638.

44. Balakrishnan, G.; Jarzecki, A. A.; Wu, Q.; Kozlowski, P. M.; Wang, D.; Spiro, T. G., Mode Recognition in UV Resonance Raman Spectra of Imidazole: Histidine Monitoring in Proteins. *The Journal of Physical Chemistry B* **2012,** *116*, 9387-9395.

45. Oladepo, S. A.; Xiong, K.; Hong, Z.; Asher, S. A.; Handen, J.; Lednev, I. K., UV Resonance Raman Investigations of Peptide and Protein Structure and Dynamics. *Chemical Reviews* **2012,** *112*, 2604-2628.

46. Mayne, L. C.; Hudson, B. S., Resonance Raman Spectroscopy of *N*-Methylacetamide: Overtones and Combinations of the C-N Stretch (Amide II') and Effect of Solvation on the C=O Stretch (Amide I) Intensity. *Journal of Physical Chemistry* **1991,** *95*, 2962-2967.

47. Wang, Y.; Purrello, R.; Georgiou, S.; Spiro, T. G., UVRR Spectroscopy of the Peptide Bond. 2. Carbonyl H-Bond Effects on the Ground and Excited-State Structures of *N*-Methylacetamide. *Journal of the American Chemical Society* **1991,** *113* (17), 6368-6377.

48. Chen, X. G.; Asher, S. A.; Schweitzer-Stenner, R.; Mirkin, N. G.; Krimm, S., UV Raman Determination of the $\pi\pi^*$ Excited State Geometry of *N*-Methylacetamide: Vibrational Enhancement Pattern. *Journal of the American Chemical Society* **1995,** *117*, 2884-2895.

49. (a) Markham, L. M.; Hudson, B. S., *Ab Initio* Analysis of the Effects of Aqueous Solvation on the Resonance Raman Intensities of *N*-methylacetamide. *Journal of Physical Chemistry* **1996,** *100*, 2731-2737; (b) Torii, H.; Tatsumi, T.; Tasumi, M., Effects of Hydration on the Structure, Vibrational Wavenumbers, Vibrational Force Field and Resonance Raman Intensities of *N*-methylacetamide. *Journal of Raman Spectroscopy* **1998,** *29*, 537-546.

50. (a) Barry, B. A.; Chen, J.; Keough, J.; Jenson, D.; Offenbacher, A.; Pagba, C., Proton-Coupled Electron Transfer and Redox-Active Tyrosine: Structure and Function of the Tyrosyl Radicals in Ribonucleotide Reductase and Photosystem II. *The Journal of Physical Chemistry Letters* **2012,** *3*, 543-554; (b) Chen, J.; Barry, B. A., Ultraviolet Resonance Raman Microprobe spectroscopy of Photosystem II. *Photochemistry and Photobiology* **2008,** *84* (3), 815-818; (c) Chen, J.; Bender, S. L.; Keough, J.; Barry, B. A., Tryptophan as a Probe of Photosystem I Electron Transfer Reaction: A UV Resonance Raman Study. *The Journal of Physical Chemistry B* **2009,** *113* (33), 11367-11370; (d) Dreaden, T. M.; Chen, J.; Rexroth, S.; Barry, B. A., N-Formylkynurenine as a Marker of High Light Stress in Photosynthesis. *The Journal of Biological Chemistry* **2011,** *286* (25), 22632-22641.

51. (a) Mizuno, M.; Kamikubo, H.; Kataoka, M.; Mizutani, Y., Changes in the Hydrogen-Bond Network Around the Chromophore of Photoactive Yellow Protein in the Ground and Excited States. *The Journal of Physical Chemistry B* **2011,** *115*, 9306-9310; (b) Mizuno, M.; Shibata, M.; Yamada, J.; Kandori, H.; Mizutani, Y., Picosecond Time-Resolved Ultraviolet Resonance Raman Spectroscopy of Bacteriorhodopsin: Primary Protein Response to the Photoisomerization of Retinal. *Journal of Physical Chemistry B* **2009,** *113*, 12121-12128; (c) Mizuno, M.; Sudo, Y.; Homma, M.; Mizutani, Y., Direct Observation of the Structural Change of Tyr174 in the Primary Reaction of Sensory Rhodopsin II. *Biochemistry* **2011,** *50* (15), 3170-3180; (d) Kim, J. E.; Pan, D.; Mathies, R. A., Picosecond Dynamics of G-Protein Coupled Receptor Activation in Rhodopsin from Time-Resolved UV Resonance Raman Spectroscopy. *Biochemistry* **2003,** *42* (18), 5169-5175.

52. Pieridou, G.; Avgousti-Menelaou, C.; Tamamis, P.; Archontis, G.; Hayes, S. C., UV Resonance Raman Study of TTR(105-115) Structural Evolution as a Function of Temperature. *The Journal of Physical Chemistry B* **2011,** *115* (14), 4088-4098.

53. (a) Cho, N.; Asher, S. A., UV Resonance Raman and Absorption Studies of Angiotensin II Conformation in Lipid Environments. *Biospectroscopy* **1996,** *2*, 71-82; (b) Holtz, J. S. W.; Lednev, I. K.; Asher, S. A., UV Resonance Raman Study of Angiotensin II Conformation in Nonaqueous Environments: Lipid Micelles and Acetonitrile. *Biopolymers (Biospectroscopy)* **2000,** *57* (2), 55-63.

54. (a) Sanchez, K. M.; Kang, G.; Wu, B.; Kim, J. E., Tryptophan-Lipid Interactions in Membrane Protein Folding Probed by Ultraviolet Resonance Raman and Fluorescence Spectroscopy. *Biophysical Journal* **2011,** *100*, 2121-2130; (b) Schlamadinger, D. E.; Shafaat, H. S.; Sanchez, K. M.; Gable, J. E.; Kim, J. E. In *Tryptophan Residues as Membrane Protein Anchors*, XXII International Conference on Raman Spectroscopy, Champion, P. M.; Ziegler, L. D., Eds. American Institute of Physics: 2010; pp 170-171.

55. Macrae, M. X.; Schlamadinger, D. E.; Kim, J. E.; Mayer, M.; Yang, J., Using Charge to Control the Functional Properties of Self-Assembled Nanopores in Membranes. *Small* **2011,** *7* (14), 2016-2020.

56. (a) Gable, J. E.; Schlamadinger, D. E.; Cogen, A. L.; Gallo, R. L.; Kim, J. E., Fluorescence and UV Resonance Raman Study of Peptide-Vesicle Interactions of Human Cathelicidin LL-37 and Its F6W and F17W Mutants. *Biochemistry* **2009,** *48* (47), 11264-11272; (b) Won, A.; Pripotnev, S.; Ruscito, A.; Ianoul, A., Effect of Point Mutations on the Secondary Structure and Membrane Interaction of Antimicrobial Peptide Anoplin. *The Journal of Physical Chemistry B* **2011,** *115* (10), 2371-2379.

57. Shafaat, H. S.; Sanchez, K. M.; Neary, T. J.; Kim, J. E., Ultraviolet Resonance Raman Spectroscopy of a β-Sheet Peptide: A Model for Membrane Protein Folding. *Journal of Raman Spectroscopy* **2009,** *40* (8), 1060-1064.

58. (a) Xu, M.; Shashilov, V.; Lednev, I. K., Probing the Cross-β Core Structure of Amyloid Fibrils by Hydrogen-Deuterium Exchange Deep Ultraviolet Resonance Raman Spectroscopy *Journal of the American Chemical Society* **2007,** *129*, 11002-11003; (b) Halsey, C. M.; Benham, D. A.; JiJi, R. D.; Cooley, J. W., Influence of the Lipid Environment on Valinomycin Structure and Cation Complex Formation. *Spectrochimica Acta Part A: Molecular and Biomolecular Spectroscopy* **2012,** *96*, 200-206; (c) Halsey, C. M.; Oshokoya, O. O.; JiJi, R. D.; Cooley, J. W., Deep-UV Resonance Raman Analysis of the *Rhodobacter capsulatus* Cytochrome bc_1 Complex Reveals a Potential Marker for the Transmembrane Peptide Backbone. *Biochemistry* **2011,** *50* (30), 6531-6538; (d) Halsey, C. M.; Xiong, J.; Oshokoya, O. O.; Johnson, J. A.; Shinde, S.; Beatty, J. T.; Ghirlanda, G.; JiJi, R. D.; Cooley, J. W., Simultaneous Observation of Peptide Backbone Lipid Solvation and α-Helical Structure by Deep-UV Resonance Raman Spectroscopy. *ChemBioChem* **2011,** *12* (14), 2125-2128; (e) Shafaat, H. S.; Sanchez, K. M.; Neary, T. J.; Kim, J. E., Ultraviolet Resonance Raman Spectoscopy of a β-Sheet Peptide: A Model for Membrane Protein Folding. *Journal of Raman Spectroscopy* **2009,** *40* (8), 1060-1064; (f) Ozdemir, A.; Lednev, I. K.; Asher, S. A., UVRR Spectroscopic Studies of Valinomycin Complex Formation in Different Solvents. *Spectrochimica Acta, Part A: Molecular and Biomolecular Spectroscopy* **2005,** *61*, 19-26; (g) Xiong, K.; Punihaole, D.; Asher, S. A., UV Resonance Raman Monitors Polyglutamine Backbone and Side Chain Hydrogen Bonding and Fibrillization. *Biochemistry* **2012**; (h) Holtz, J. S. W.; Bormett, R. W.; Chi, Z.; Cho, N.; Chen, X. G.; Pajcini, V.; Asher, S. A.; Spinelli, L.; Owen, P.; Arrigoni, M., Applications of a New 206.5-nm Continuous-Wave Laser Source: UV Raman Determination of Protein Secondary Structure and CVD Diamond Material Properties. *Applied Spectroscopy* **1996,** *50* (11), 1459-1468.

Chapter 3: Reporting on Iron Oxidation State in Cytochrome bc_1 with Ultraviolet Resonance Raman Spectroscopy

3.1 Introduction

Electron transport is a specialized and important function of membrane proteins. From the primary electron donor to the terminal electron acceptor, membrane proteins and specifically their metal cofactors are the integral means of transport because of their overlapping midpoint potentials. Some membrane proteins, like cytochrome bc_1, couple their electron transport function with the formation of a pH gradient across the lipid bilayer in the electron transport chain. Together, the potential and pH gradient form a proton motive force which is the thermodynamic driving force in the formation of adenosine triphosphate (ATP). Within the electron transport chain, cytochrome bc_1 (hydroquinone:cytochrome *c* oxidoreductase) and its photosynthetic analog cytochrome b_6f are responsible for a bifurcation in the direction of the electron flow[1]. The unique mechanism of electron transport is the subject of ongoing investigation and the initial impetus for studying this membrane protein.

Cytochrome bc_1 from *Rhodobacter capsulatus*, a purple non-sulfur bacterium, is a homodimer expressed in the periplasmic membrane adjacent to photosynthetic reaction centers and other respiratory enzymes. Each monomer is composed of three subunits, each identified by the redox-active cofactor it contains: cytochrome *b* (with a low and high-potential heme *b*), cytochrome c_1 (with a heme c_1 hereafter abbreviated cyt *c*), and the 2Fe-2S cluster (containing two tetrahedral iron centers bridged by two sulfur atoms, also referred to as a traditional Rieske iron sulfur cluster)[2]. Two active sites are known for the monomer and designated by which side of the membrane they lie: the Q_o site binds

reduced ubiquinol near the outer side of the membrane while the Q_i site binds oxidized ubiquinone near the inner face of the periplasmic membrane.

The two-electron ubiquinol oxidation reaction at the Q_o site transports two electrons along two different pathways of diminishing redox potential. The first oxidation of ubiquinol reduces of the 2Fe-2S cluster, which undergoes a domain conformational transition towards the cyt *c* subunit depositing electrons to the heme c_1. A terminal soluble cytochrome *c* cofactor is the final electron acceptor along this path. The second oxidation of ubiquinol reduces the low potential heme b_L, which then transfers the electron to the high potential heme b_H near the Q_i site, where finally ubiquinone is reduced to ubiquinol after two turnovers of the cycle. This mechanism, named the Q cycle, has undergone revisions from Mitchell's original proposal[3] over the past forty years by Brandt and Trumpower[4], amongst others. The crux of the debate focuses on the Q_o site and the generation of a ubisemiquinone intermediate, which would indicate a stepwise mechanism. The vastly different spectroscopic handles of the 2Fe-2S cluster and heme cofactors make it difficult to monitor their reduction with a single method. To date, only one experiment[5] has been able to monitor the reduction of [2Fe-2S] and heme b_L simultaneously, using ultra-fast freeze quenching of samples detected by EPR at liquid helium temperatures. However, the time resolution was slow compared to the relative equilibration of the total electron transfer system of the enzyme, making inference of relative rates and yield impossible.

A simpler route to monitoring the oxidation state of these and other metal cofactors may lie with histidine, which is often coordinated to metal cofactors like those found in cytochrome bc_1. Cyt *c* coordinates a single histidine to the iron center, while cytochrome *b* and the 2Fe-2S cluster coordinate two histidines but in different geometries. Ultraviolet resonance Raman (UVRR) spectroscopy is not only sensitive to histidine vibrational modes (see chapter 2), it is also likely to discern between histidine vibrational modes while coordinated to different metal environments. The Spiro lab first demonstrated

the possibility of using histidine as a marker of oxidation state using UVRR[6]. In model compounds, histidine's Raman excitation profile was enhanced with UV excitation but was still weak compared to other aromatic residues that would be found in the protein. Spectral overlap in UVRR spectra with the other aromatic residues (phenylalanine, tryptophan, and tyrosine) might cause the histidine vibrational mode to be too weak to measure. Spiro then studied microperoxidase 11 (MP 11)[7], a simple model of cyt *c* which contains eleven amino acids covalently linked to the heme *c*, though none of them besides histidine were aromatic. He reported a spectral signature of iron-bound histidine in deuterium oxide solution in the UVRR spectrum with 229 nm excitation. A 1343 cm^{-1} feature increased in intensity while a 1580 cm^{-1} feature shifted to higher energies upon reduction of MP 11.

Cyt *c* is the subject of this investigation by UVRR. If a similar spectroscopic signature can be determined for the full sized protein in the reduced and oxidized state, then it could yield important information about potentially reporting on the oxidation state of other metal cofactors in cytochrome bc_1. In the course of performing experiments on the oxidation state of cofactors in cytochrome bc_1 as a whole, however, an unanticipated result shifted the focus of this dissertation from electron transfer mechanism of metal cofactors to reporting on structure of membrane proteins using DUVRR.

3.2 Materials and Methods

3.2.1 Materials

L-Tyrosine, L-phenylalanine, L-tryptophan, L-histidine, and equine heart cyt c was purchased from Sigma (St. Louis, MO) and dissolved in phosphate buffered pD=7.4 deuterium oxide (99% purity) from Cambridge Isotope Labs (Andover, MA). Amino acid solutions were made to 200 µM and cyt *c* to 0.5 mg/mL. All solutions were incubated at 4°C overnight to achieve complete deuterium exchange of the amide protons. Stock solutions (1 M) of sodium ferricyanide and sodium ascorbate were used to

oxidize and reduce cyt *c*, respectively. Cytochrome bc_1 was purified from *Rhodobacter capsulatus* according to Valkova-Valchanova[8]. More details about its purification can be found in chapter 4.

3.2.2 Spectral Analysis

The tunable ultraviolet resonance Raman spectrometer is described elsewhere[9] as is as the nitrogen purged flow cell[10]. Briefly, 532 nm laser light from a pumped Nd-YLF was tuned to 880 nm with a Ti-Sapphire crystal. This beam is frequency doubled twice to achieve 220 nm excitation using a barium borate (BBO) and lithium borate (LBO) crystal harmonic generators. The power at the sample was attenuated to no higher than 500 mW. Data was digitally processed with Matlab software (Natick, MA) and an in-house program to remove spectral contributions from gamma rays.

The oxidation state of cyt *c* was assessed by UV-Vis absorbance before and after measuring in the Raman spectrometer by measuring absorbance at 550 nm, the heme *c* Soret band. The same sample was then fully reduced and oxidized to determine total percentage of oxidation of the sample. Only spectra acquired while the sample was at least 90% oxidized/reduced were used.

3.3 Results

3.3.1 UVRR spectra of aromatic amino acids and cyt *c*.

In order to understand the basis contributions to the UVRR spectrum, individual spectra of aromatic amino acids in deuterium oxide were collected and compared to cytochrome c in deuterium oxide. As expected, all peaks in cyt *c* are attributable to an aromatic amino acid with the exception of the amide II' (Figure 3-1). Amide modes only undergo pre-resonance enhancement at 220 nm excitation, but the amide II' is the strongest of these modes and is still apparent in the UVRR spectrum. Histidine is the only amino acid not sufficiently resonance enhanced to observe in the cyt *c* spectrum. The cyt *c* spectrum can even be mostly recreated simply by taking an average of the tyrosine, tryptophan, and

phenylalanine spectra according to their natural abundance in cyt *c* which is 3.8%, 1.0%, and 3.8%, respectively (Figure 3-1).

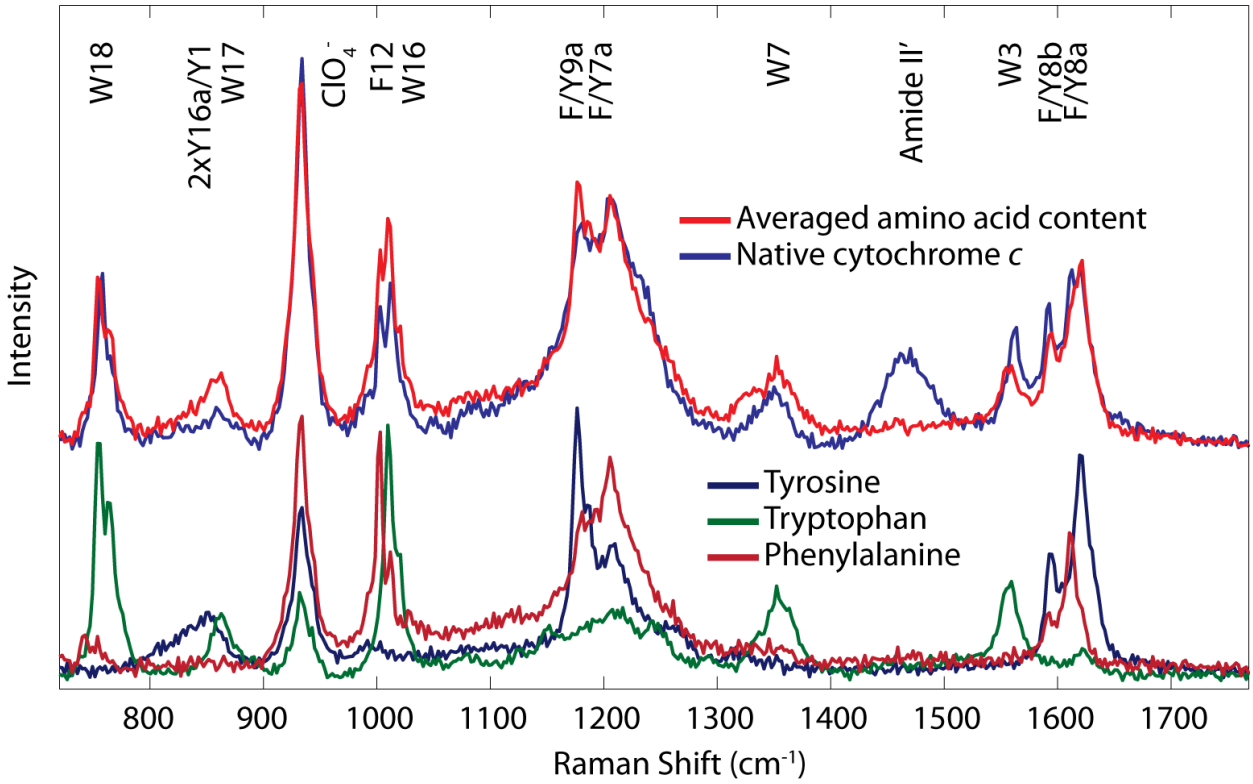

Figure 3-1. UVRR spectrum of cytochrome c compared to its averaged amino acid content. Individual amino acid spectra are shown for comparison. Histidine has no significant contribution to the cyt c spectrum. λ_{ex} = 220 nm.

3.3.2 Reduction and oxidation of cyt *c*

Despite the lack of a resolved feature due to vibrational modes of the histidine residue, UVRR spectra of the oxidized and reduced state of cyt *c* were collected (Figure 3-2). Because oxidation and reduction were chemically induced by potassium ferricyanide and sodium ascorbate, basis spectra for these compounds were collected as well. At the appropriate concentration to induce full oxidation of cyt *c*, ferricyanide has no spectral features above 1200 cm^{-1}. Ascorbate has more discrete features at higher wavenumbers, but their intensity in the reduced cyt c spectrum can be reliably subtracted because perchlorate, an internal intensity standard at 932 cm^{-1}, was present in both samples. A reduced minus oxidized cyt *c* spectrum revealed two features that could be attributed to oxidation/reduction of the

heme iron (Figure 3-2). One was an intensity increase near 1340 cm^{-1}, predicted from the increase in intensity at 1343 cm^{-1} reported by Spiro[7] upon oxidation of MP 11. Spiro's most recent investigation[11] into histidine UVRR spectra identified this as a *v*5a band shifted by metal coordination. The second feature, a shift resulting in a sigmoid-like feature, was also predicted by the MP 11 study. The similarity to UVRR spectral features of reduced/oxidized MP 11 led to the initial conclusion that these features can be also be assigned the reduced/oxidized state of cyt *c*.

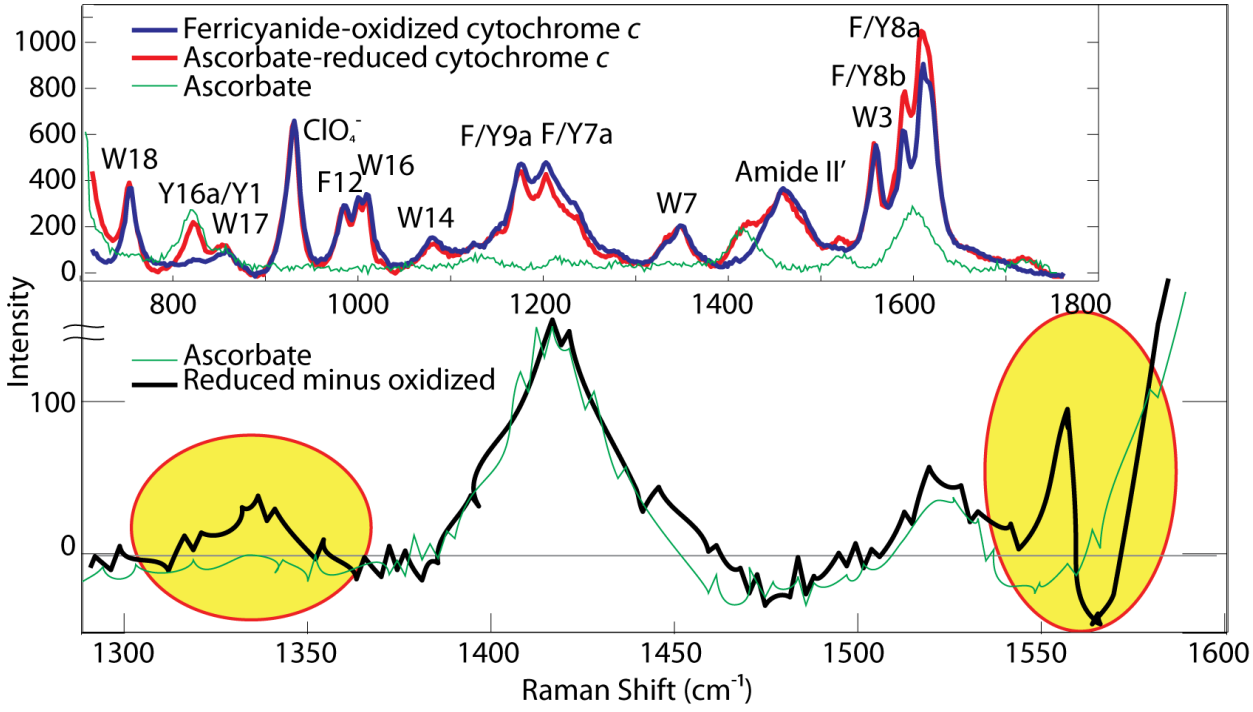

Figure 3-2. UVRR spectra of reduced and oxidized cyt c. Inset: ferricyanide-oxidized and ascorbate-reduced cyt *c* and pure ascorbate. Main: A reduced minus oxidized cyt c spectrum is magnified and overlaid with the ascorbate spectrum. λ_{ex} = 220 nm.

3.3.3 DUVRR spectrum of cytochrome bc_1

In anticipation of characterizing the steady-state spectra of reduced and oxidized cytochrome bc_1, a DUVRR spectrum of the purified air-oxidized sample was collected at 198 nm excitation (Figure 3-3). The choice in excitation wavelength was simply opportunistic given that the instrument is normally tuned to the deep-UV. UVRR spectra were to be collected at 220 nm excitation later, but the results of

the spectrum gave pause. Compared to most soluble protein spectra collected by the Cooley, JiJi[10], Spiro[12], and Asher[13] labs, an unusually large feature at 1670 cm^{-1} was evident and worth pursuing further. The process of assigning this feature unambiguously as the amide I required further effort outlined in chapter 4. Later experiments to acquire DUVRR spectra of reduced cytochrome bc_1 revealed no significant feature like those seen in MP 11 or cyt *c*. If UVRR spectra (at 220 nm or greater excitation) were collected of reduced and oxidized cytochrome bc_1, similar features may be found as those found in cyt *c* or MP 11.

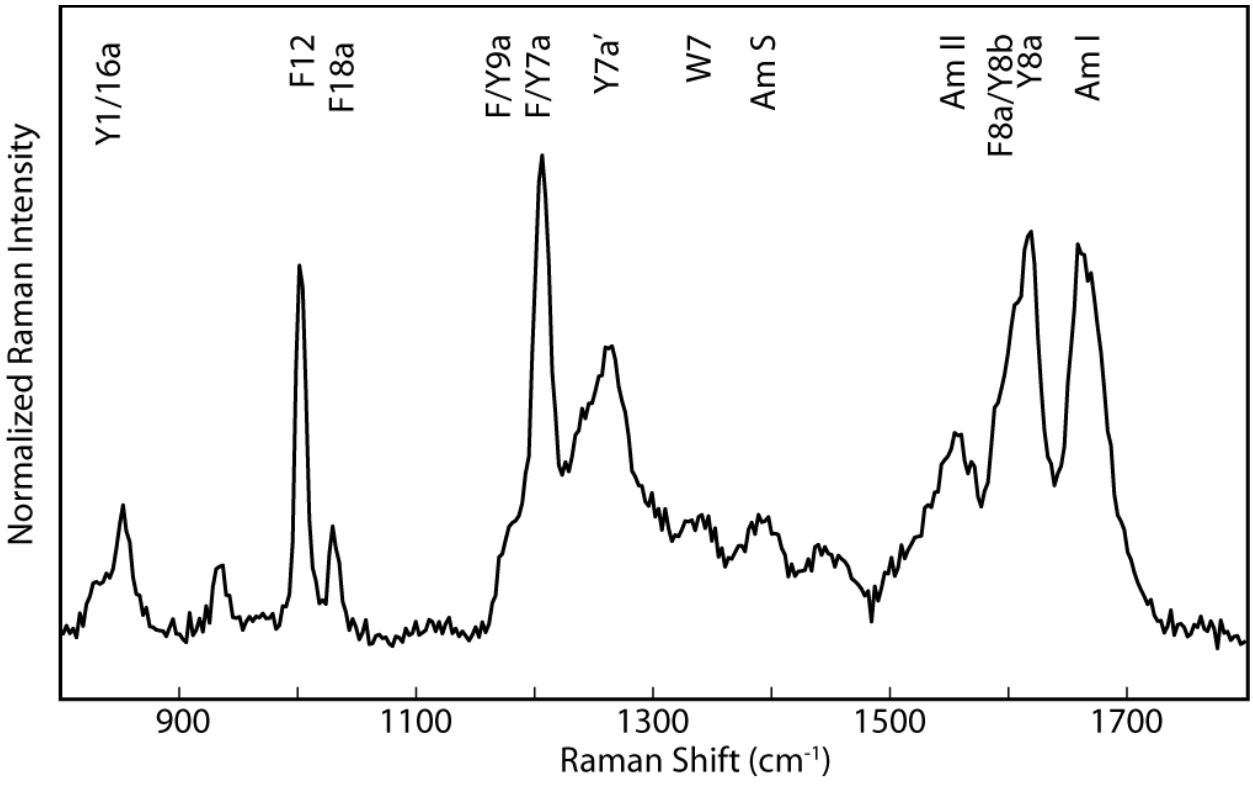

Figure 3-3. DUVRR spectrum of cyt bc_1. λ_{ex} = 198 nm.

3.4 Discussion

3.4.1 Effects of oxidation

Given that MP 11, studied previously by Spiro, is a model of cyt *c* but free of aromatic residues save histidine, it is to be expected that the oxidation state markers persist in the UVRR spectra of cyt *c*.

Histidine is axially coordinated to iron in MP 11 is coordinated in exactly the same manner as cyt *c*. Fortunately, these markers are still evident despite the UVRR spectrum being overwhelmed with aromatic vibrational modes. These bands are not observed in UVRR spectra when taken in aqueous solution and have been assigned to imidazole-*d* modes of histidine residues bound to metal ions[7]. The known enhancement in histidine vibrational modes upon deuteration have been hypothesized by Spiro as a consequence of N-D vibrations from imidazole no longer mixing with the N-H bending mode of the backbone. The mixing of the vibrational modes is apparently non-existent when imidazole is protonated. The enhancement mechanism in metal-bound histidine systems is as of yet unknown.

3.4.2 Determining oxidation state in cyt *c*, *b*, and the Fe-S cluster

Cyt *c* was the subject of initial investigation because it is water soluble and readily purchased in purified form. Analogs for cytochrome *b* and the Fe-S cluster in cytochrome bc_1 are very expensive or require laborious effort to purify, usually requiring detergent. Once purified or purchased, what could we expect from the other histidine-bound metal cofactors in cytochrome bc_1? Aromatic vibrational bands are also to be expected in their UVRR spectra, but this study has shown that histidine-Fe vibrations are still discernible in reduced minus oxidized difference spectra. There is reason to believe that redox spectral markers of cytochrome *b* and Fe-S cluster would not only be observable in UVRR spectra but possibly resolved from one another. A positive correlation of the 1580 cm^{-1} band and histidine-metal bond strength was shown by the Kitagawa lab[14], although only copper, nickel, and zinc coordination compounds were investigated. In the *Rhodobacter capsulatus* cytochrome bc_1 crystal structure (PDB: 1ZRT[2]), the histidine N-Fe distance is 2.126, 1.997, and 2.003 Å for the Fe-S cluster, cyt *c*, and cytochrome *b* cofactors. The distance was the same for the low and high potential heme *b*. These distances are on par with the N-Cu,Zn, and Ni distances in compounds studied in the Kitagawa lab. The differences in bond length are promising for monitoring the oxidized and reduced state of Fe-S cluster.

The bond length in cytochrome *b* is very similar to cyt *c*, but the bis-His coordination might provide some other feature not seen in the single histidine coordination of cyt *c*.

3.4.3 DUVRR of cyt bc_1

The unexpected result from the DUVRR spectrum of cytochrome bc_1 was initially explained by the fact that it is a membrane protein. This particular class of proteins has only recently received indirect attention in DUVRR literature from the spectra of small peptides[15] and a depsipeptide[16]. Only UVRR had been used directly to study membrane proteins, which yielded information such as solvent polarity and hydrophobicity from aromatic vibrational modes, but not secondary structure. Further investigation into DUVRR spectra of cytochrome bc_1, detailed more in chapter 4, contributed to some of the first secondary structure studies of full-sized membrane proteins.

3.5 Bibliography

1. Berry, E. A.; Guergova-Kuras, M.; Huang, L.-s.; Crofts, A. R., Structure and Function of Cytochrome *bc* Complexes. *Annual Review of Biochemistry* **2000,** *69*, 1005-1075.

2. Berry, E. A.; Huang, L.-S.; Saechao, L. K.; Pon, N. G.; Valkova-Valchanova, M. B.; Daldal, F., X-ray Structure of Rhodobacter capsulatus Cytochrome bc1: Comparison With Its Mithochondrial and Chloroplast Counterparts. *Photosynthesis Research* **2004,** *81*, 251-275.

3. Mitchell, P., Protonmotive Redox Mechanism of the Cytochrome bc_1 Complex in the Respiratory Chain: Protonmotive Ubiquinone Cycle. *FEBS Letters* **1975,** *56*, 1-6.

4. Trumpower, B. L., Evidence for a Protonmotive Q Cycle Mechanism of Electron Transfer Through the Cytochrome bc_1 Complex. *Biochemical and Biophysical Research Communications* **1976,** *70*, 73-80.

5. Zhu, J.; Egawa, T.; Yeh, S.-R.; Yu, L.; Yu, C.-A., Simultaneous Reduction of Iron-Sulfur Protein and Cytochrome b_L During Ubiquinol Oxidation in Cytochrome bc_1 Complex. *Proceedings of the Natiocal Academy of Sciences of the United States of America* **2007,** *104*, 4864-4869.

6. Caswell, D. S.; Spiro, T. G., Ultraviolet Resonance Raman Spectroscopy of Imidazole, Histidine, and Cu(imidazole)$_4^{2+}$: Implications for Protein Studies. *Journal of the American Chemical Society* **1986,** *108*, 6470-6477.

7. Zhao, X.; Chen, R.; Deng, Q.; Mabrouk, P. A.; Spiro, T. G., UV Resonance Raman Probe of Heme-Bound Imidazole Established by ^{15}N-Labeling of Hemoglobin. *Israel J Chem* **2000,** *40*, 15-20.

8. Valkova-Valchanova, M. B.; Saribas, A. S.; Gibney, B. R.; Dutton, P. L.; Daldal, F., Isolation and Characterization of a Two-Subunit Cytochrome *b*-c_1 Subcomplex from *Rhodobacter capsulatus* and Reconstitution of Its Ubihydroquinone Oxidation (Q_o) Site with Purified Fe-S Protein Subunit. *Biochemistry* **1998,** *37*, 16242-16251.

9. Balakrishnan, G.; Hu, Y.; Nielsen, S. B.; Spiro, T. G., Tunable kHz Deep Ultraviolet (193-210 nm) Laser for Raman Applications. *Applied Spectroscopy* **2005,** *59*, 776-781.

10. Simpson, J. V.; Balakrishnan, G.; JiJi, R. D., MCR-ALS Analysis of Two-Way UV Resonance Raman Spectra to Resolve Discrete Protein Secondary Structural Motifs. *The Analyst* **2009,** *134*, 138-147.

11. Balakrishnan, G.; Jarzecki, A. A.; Wu, Q.; Kozlowski, P. M.; Wang, D.; Spiro, T. G., Mode Recognition in UV Resonance Raman Spectra of Imidazole: Histidine Monitoring in Proteins. *The Journal of Physical Chemistry B* **2012,** *116*, 9387-9395.

12. Huang, C.-Y.; Balakrishnan, G.; Spiro, T. G., Protein Secondary Structure from Deep-UV Resonance Raman Spectroscopy. *Journal of Raman Spectroscopy* **2006,** *37*, 277-282.

13. Chi, Z.; Chen, X. G.; Holtz, J. S. W.; Asher, S. A., UV Resonance Raman-Selective Amide Vibrational Enhancement: Quantitative Methodology for Determining Protein Secondary Structure. *Biochemistry* **1998,** *37*, 2854-2864.

14. Miura, T.; Satoh, T.; Hori-i, A.; Takeuchi, H., Raman Marker Bands of Metal Coordination Sites of Histidine Side Chains in Peptides and Proteins. *Journal of Raman Spectroscopy* **1998,** *29*, 41-47.

15. (a) Cho, N.; Asher, S. A., UV Resonance Raman and Absorption Studies of Angiotensin II Conformation in Lipid Environments. *Biospectroscopy* **1996,** *2*, 71-82; (b) Shafaat, H. S.; Sanchez, K. M.; Neary, T. J.; Kim, J. E., Ultraviolet Resonance Raman Spectroscopy of a β-Sheet Peptide: A Model for Membrane Protein Folding. *Journal of Raman Spectroscopy* **2009,** *40* (8), 1060-1064.

16. Ozdemir, A.; Lednev, I. K.; Asher, S. A., UVRR Spectroscopic Studies of Valinomycin Complex Formation in Different Solvents. *Spectrochimica Acta, Part A: Molecular and Biomolecular Spectroscopy* **2005,** *61*, 19-26.

Chapter 4: Deep-UV Resonance Raman Analysis of the *Rhodobacter capsulatus* Cytochrome bc_1 Complex Reveals a Potential Marker for the Transmembrane Backbone

Adapted with permission from Halsey, C. M.; Oshokoya, O. O.; JiJi, R. D.; Cooley, J. W., Deep-UV Resonance Raman Analysis of the *Rhodobacter capsulatus* Cytochrome bc_1 Complex Reveals a Potential Marker for the Transmembrane Peptide Backbone. *Biochemistry* 2011, *50* (30), 6531-6538. Copyright 2011 American Chemical Society.

4.1 Abstract

Classical strategies for structure analysis of proteins interacting with a lipid phase typically correlate ensemble secondary structure content measurements with changes in the spectroscopic responses of localized aromatic residues or reporter molecules to map regional solvent environments. Deep-UV resonance Raman (DUVRR) spectroscopy probes the vibrational modes of the peptide backbone itself, is very sensitive the ensemble secondary structures of a protein, and has been shown to be sensitive to the extent of solvent interaction with the peptide backbone[1]. Here we show that a large detergent solubilized membrane protein, the *Rhodobacter capsulatus* cytochrome bc_1 complex, has a distinct DUVRR spectrum versus that of an aqueous soluble protein with similar overall secondary structure content. Cross section calculations of the amide vibrational modes indicate that the peptide backbone carbonyl stretching modes differ dramatically between these two proteins. Deuterium exchange experiments probing solvent accessibility confirm that the contribution of the backbone vibrational mode differences are derived from the lipid solubilized or transmembrane α-helical portion of the protein complex. These findings indicate that DUVRR is sensitive to both the hydration status of a protein's peptide backbone, regardless of primary sequence, and to its secondary structure content. Therefore, DUVRR may be capable of simultaneously measuring protein dynamics and relative water/lipid solvation of the protein.

4.2 Introduction

Trans-membrane (TM) proteins play a role in nearly every facet of cellular homeostasis in all types of organisms, yet, remain the least understood class of proteins at the structural level[2]. Despite well documented difficulties in purifying and crystallizing TM proteins, as well as issues associated with molecular size, detailed structural resolution can and has been obtained through X-ray crystallography or NMR, assuming the protein can be crystallized or is not too large[3]. Potentially, structural information may come from yet to be realized analytical variants of these techniques, i.e. small angle scattering[4], or from newly emerging techniques utilizing neutron scattering[5]. More facile and established techniques can give gross or ensemble secondary structure resolution, such as infrared absorption[6] or circular dichroism spectroscopies[7]. However, these techniques fail in addressing structural fluctuations in membrane proteins as they cannot easily differentiate membrane embedded from solvent accessible portions of a protein without significant sample modification. Fluorescence or electron paramagnetic resonance analyses using aromatic residues[8], or fluorescent[9] or paramagnetic probes chemically attached to proteins, have proven particularly useful locating a region of a protein in relation to the membrane lipid phase, as well as giving information about the transient environment that such residues experience kinetically.

Deep-UV (λ_{ex} < 210 nm) excited resonance Raman (DUVRR) spectroscopy has proven to be a useful tool for elucidating secondary structural content and its changes in soluble proteins[10]. DUVRR has the advantage that various structurally constrained protein regions (those with differing secondary structures) have differing spectral intensities due to variable excitation cross-sections. Additionally, since the intensity of signal relies on the polarizability of the bonding orbitals in the excited versus the ground state, electron withdrawing processes, such as hydrogen bonding from solvent will have a significant impact on the intensity of any or all of the amide I (C=O stretch), II and III (out of phase or in phase N-H bending/C-N stretching, respectively) or S (coupled N-H/C_α-H bending) modes[11].

Furthermore, since the target of investigation is the peptide backbone, which is inherent to all protein sequences, the protein sequence need not be modified in most cases. For these reasons and its amenability to a variety of measurement timescales, DUVRR has proven to be a useful tool for the structural analysis of protein samples that would be commonly classified as problematic for structural analysis, i.e. those that are insoluble or highly dynamic on the measurement scale. In fact, time-resolved events of cooperative allostery in globins, basic tenets of protein unfolding and secondary structure formation and characterization of different secondary structure domains within large protein aggregates have all been resolved by DUVRR analyses[12]. DUVRR has also proven to be sensitive enough to delineate the structure and dynamics of discrete subdomains within the short alanine peptide[13].

Recently, standard, or non-deep UV-excited (λ_{ex} > 220 nm), resonance Raman, sensitive to the aromatic vibrational modes of a protein, have been employed to analyze membrane protein catalytic events in photosystems[14], protein folding and insertion of pore complexes and dynamics of inter-TM strand hydrogen bonding within a membrane interior[15]. However, examination of the structure of membrane-associated proteins has not been realized by DUVRR, presumably due to presuppositions about the complexity of the samples. Specifically, the presence of super-stoichiometric lipid or detergent molecules and the presence of various cofactors could potentially interfere with spectral quality and interpretability by contributing spectral features of their own to the resonance Raman spectra or by absorbing enough incident light to disallow adequate scattering from the protein backbone to allow for DUVRR spectral collection.

The cytochrome (cyt) bc_1 complex from *Rhodobacter capsulatus* (Rcaps) is a good model for testing the feasibility of the analysis of membrane protein structure and solvation by DUVRR, as it can be purified with good yield from Rcaps[16] and is well characterized for its function as well as its detailed atomic structure[17]. Specifically, the cyt bc_1 complex satisfies several sample related potential

spectroscopic pitfalls associated with large transmembrane proteins as it is a large multi-subunit complex, it is very amphiphilic having both significant soluble and membrane embedded domains, it is molecularly complex, containing several non-proteinaceous cofactors and it has significant conformational dynamics within each domain of solubility during catalysis. Specifically, the cyt bc_1 complex from Rcaps contains three TM subunits per monomer of the natively homodimeric protein complex. The three subunits (cyt *b*, FeS and cyt c_1) comprising each monomer contain a total of eight α-helical segments spanning the lipid phase[17d], constituting roughly 45% of the total protein backbone. Detergent solubilized purified cyt bc_1 complex samples also contain three iron containing cofactors in the form of two *b*- and one *c*-type hemes per monomer as well as a "Rieske"-type [2Fe-2S] cluster. Depending upon the extent and stringency of the purification process from Rcaps, various stoichiometries of ubiquinone, bacteriochlorophyll, native lipids[18] and the detergent β-dodecyl maltoside, will also be present. From a catalytic perspective, the cyt bc_1 complex carries out the reduction of two soluble electron carriers (cyt *c*) and one lipophilic carrier (ubiquinone) with reducing equivalents derived from the oxidation of two hydroquinone molecules via a modified and well studied Q-cycle mechanism[19]. The catalysis involves a large-scale domain motion of the FeS subunit soluble domain[20] as well as conformational changes in the TM portion of the protein[21]. Here we present our findings that analysis of TM proteins is not only feasible by DUVRR, but that this technique may represent a novel methodology for the analysis of membrane protein structure in the future.

4.3 Materials and Methods

4.3.1 Cyt bc_1 Purification

Rcaps (pMTS1/MT-RBC1), was grown semiaerobically in the dark at 35 °C in MPYE medium supplemented with 10 μg mL^{-1} kanamycin as described previously[22]. Cells were stored at -80 °C, until such time that chromatophore membranes were prepared and cyt bc_1 was isolated according to

Valkova-Valchanova et al. [16] with the exception that DEAE-sepharose was used for the final anion exchange chromatography step. Cyt *c* and *b* content were verified by redox difference spectroscopy as described previously [23]. A 10 mg mL^{-1} stock was aliquoted and stored at -80°C for DUVRR analysis.

4.3.2 DUVRR Spectroscopy

The DUVRR instrument is similar to those described previously[24]. Briefly, the fourth harmonic of a tunable Ti:sapphire laser (with excitation wavelengths ranging from 197 to 206 nm) was directed onto a thin film of sample flowing between two nitinol wires spaced about 1 mm apart under N_2 gas. Incident laser power at the sample was kept below 500 µW to minimize photodegradation; spectra were also monitored for photodegradation over time. Spectral calibration was carried out using a standard cyclohexane spectrum[25]. Cyt *c* from horse heart (Sigma) and cyt bc_1 solutions were prepared to 0.5 mg mL^{-1} in 20 mM and 120 mM phosphate buffer, respectively, containing the internal standard sodium perchlorate (50 mM and 100 mM, respectively).

4.3.3 Data Analysis

All DUVRR spectral preprocessing was carried out in a MATLAB environment using in house cosmic spike removal and water band removal methods described previously[26]. A non-linear least squares algorithm was carried out by fitting a mixture of Gaussian/Lorentzian peaks to experimental spectra as described previously [27]. Raman cross-sections were calculated on a per amino acid residue basis based upon fitted peak intensities (Equation 1).

$$\sigma_{\lambda,amide} = \frac{\sigma_{ClO_4^-}}{n} \frac{I_{amide}}{I_{ClO_4^-}} \left(\frac{\nu_{exc} - \nu_{ClO_4^-}}{\nu_{exc} - \nu_{amide}} \right)^4 \frac{C_{ClO_4^-}}{C_{amide}} \left(\frac{A_o + A_{amide}}{A_o + A_{ClO_4^-}} \right) \quad \text{(Equation 1)}$$

At a given excitation wavelength, the absolute Raman cross-section (in mbarns $residue^{-1}$ $steradian^{-1}$), σ_{amide}, is derived from σ_{ClO4}^-, the absolute Raman perchlorate cross-section (mbarns $molecule^{-1}$ $steradian^-$

[1]) [24], where *n* is the number of residues in the peptide backbone, *I* is the Raman intensity (peak height) of perchlorate and amide mode, respectively, v_{exc} is the excitation frequency (cm^{-1}), *v* is the Raman shift of perchlorate and the amide mode (Δcm^{-1}), *C* is concentration (on a molar basis), and *A* is the UV absorbance of the sample at the excitation wavelength, A_o, the amide-shifted wavelength, A_{amide}, and the perchlorate-shifted wavelength, A_{ClO4-}.

4.4 Results

4.4.1 DUVRR of membrane and soluble proteins with similar overall secondary structural content.

In order to understand the contribution of the lipid environment of the peptide backbone to DUVRR spectra, two proteins with similar secondary structure and aromatic contents, horse heart cyt *c*, and the TM protein, cyt bc_1 complex (Figure 4-1 upper panel), were analyzed. DUVRR spectra were collected of samples containing 0.5 mg ml^{-1} of either cyt *c* or detergent (β-dodecyl maltoside, β-DM, 1:1 w/w) solubilized cyt bc_1 complex in phosphate buffer (pH 7.0) using an excitation wavelength of 197 nm. Despite the large difference in molecular size, total cofactor content and the presence or absence of lipid, the DUVRR spectra for cyt *c* and the cyt bc_1 complex (Figure 4-1) were similar. Both spectra are dominated by intense features at 1001, 1206, 1266 and 1620 cm^{-1}, which can be assigned to contributions of the aromatic amino acid side chains of tyrosine and phenylalanine residues (Figure 4-1). Peptide backbone amide modes are also clearly visible at 1396 cm^{-1} (amide S), 1555 cm^{-1} (amide II) and 1665 cm^{-1} (amide I). Interestingly, the largest significant difference between the two peptide DUVRR spectra is encountered in the amide I region corresponding to the carbonyl stretching mode. Specifically, the amide I mode in the cyt bc_1 complex sample appears to have a greater intensity vs. the remaining amide modes as compared to the DUVRR spectra of the soluble cyt *c*.

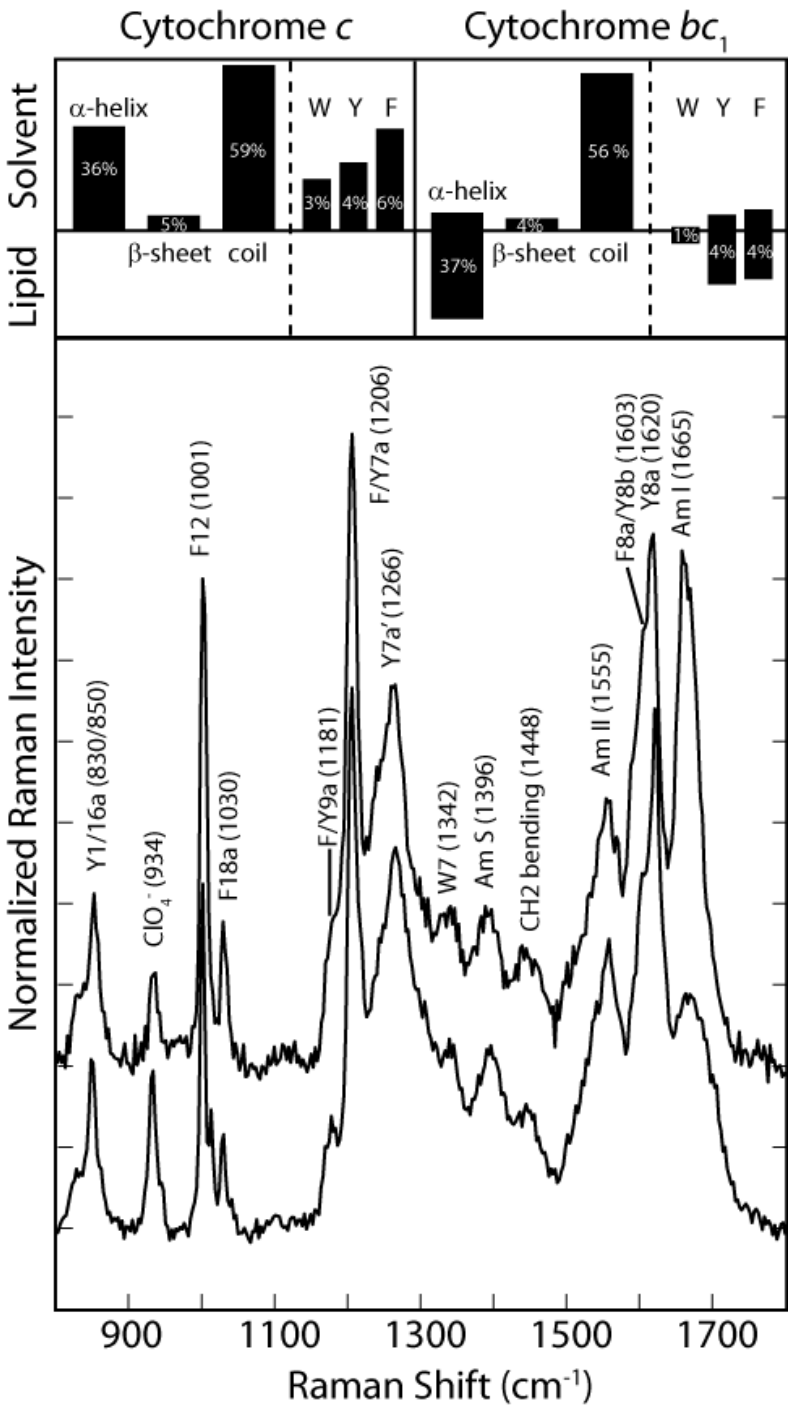

Figure 4-1. DUVRR spectra of aqueous and detergent solubilized proteins with similar secondary structure contents. DUVRR spectra of cyt *c* (lower spectrum) and cyt bc_1 (upper spectrum) excited at 197 nm are shown with vibrational mode assignments, and measured Raman shifts are also indicated for clarity. Spectra were normalized according to the internal standard ClO_4^- intensity and protein concentration. Total secondary structure and aromatic content derived from analysis of the Rcaps structural coordinates (PDB ID: 1ZRT) are shown in the upper panel. Reproduced with permission from Halsey, C. M.; Oshokoya, O. O.; JiJi, R. D.; Cooley, J. W., Deep-UV Resonance Raman Analysis of the *Rhodobacter capsulatus* Cytochrome bc_1 Complex Reveals a Potential Marker for the Transmembrane Peptide Backbone. *Biochemistry* 2011, *50* (30), 6531-6538. Copyright 2011 American Chemical Society.

To identify the molecular origin of the intense feature around 1670 cm^{-1} several non-proteinaceous molecules with carbonyl moieties were examined for their respective DUVRR spectra. DUVRR spectra of 0.5 mg mL^{-1} β-DM or methanol-solubilized bacteriochlorophyll (Bchl, 0.012 mM), two molecules known to be present in the cyt bc_1 complex preparations, indicated no resonantly-enhanced amide modes in the 1600-1700 cm^{-1} region of the spectrum (Figure 4-2). However, similar analysis of highly concentrated, 0.65 mg mL^{-1} (0.75 mM), ubiquinone-10 (UQ) in ethanol revealed a spectral feature at 1670 cm^{-1} similar to the feature seen in the cyt bc_1 complex DUVRR spectra (Figure 4-2, inset).

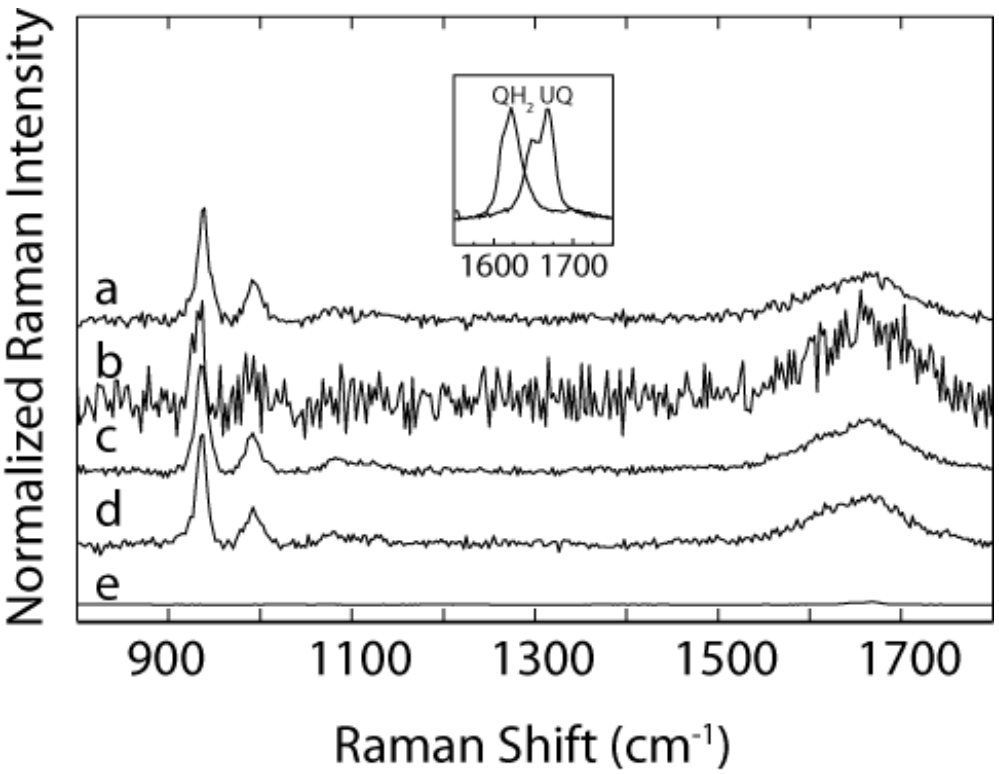

Figure 4-2. DUVRR spectra (λ_{ex} = 198 nm) of non-protein components in detergent solubilized cyt bc_1 complex samples. Spectra of a typical sample buffer (100 mM ClO_4^-, 120 mM phosphate (pH7)) (a), excess bacteriochlorophyll in buffer (12 µM) (b), buffer with 0.5 mg mL^{-1} β-dodecylmaltoside (c), and 2.4 µM QH_2 with β-dodecylmaltoside (d), and with stoichiometric UQ in ethanol (e). Inset: DUVRR spectrum of 2.4 mM QH_2 in sample buffer and 0.75 mM UQ in ethanol. Reproduced with permission from Halsey, C. M.; Oshokoya, O. O.; JiJi, R. D.; Cooley, J. W., Deep-UV Resonance Raman Analysis of the *Rhodobacter capsulatus* Cytochrome bc_1 Complex Reveals a Potential Marker for the Transmembrane Peptide Backbone. *Biochemistry* 2011, *50* (30), 6531-6538. Copyright 2011 American Chemical Society.

Despite the low concentrations of UQ expected to be present in the cyt bc_1 complex samples (~ < 2 per monomer or < 2 µM), two approaches were carried out to diminish the amount of oxidized

quinone in a given sample, thereby determining its potential contribution to the cyt bc_1 complex DUVRR spectrum. The first approach involved diminishing the affinity of the protein sample for UQ by subfractionating the cyt bc_1 complex into the cyt *b* subunit, the cyt *bc* subcomplex, the single transmembrane domain containing FeS and cyt c_1 subunits by size exclusion chromatography. Each of these subcomplexes will have little or no specific affinity for a UQ molecule. As expected, regardless of the subfraction analyzed, the intense amide I band remained in the DUVRR spectrum (Figure 4-3). Secondly, oxidized versus reduced DUVRR spectra of the holoenzyme in pH 9.0 phosphate buffer, where the UQ molecule bound at the higher affinity quinone reduction site (Q_i) in the cyt *b* subunit, should be converted to $QH^{\bullet-}$ or UQH_2, revealed no significant differences in the spectra.

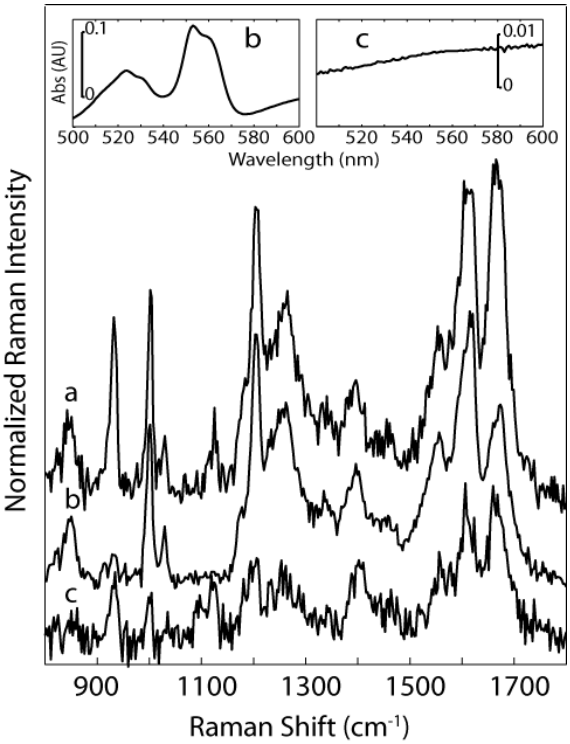

Figure 4-3. DUVRR spectra of (λ_{ex} = 198 nm) of UQ diminished samples. DUVRR spectra of ascorbate-reduced cyt bc_1 at pH 9 (a), the holocomplex subfractionation products the cyt *bc* subcomplex (b), and the Rieske Fe-S cluster (c). Corresponding dithionite-reduced minus ferricyanide-oxidized absorbance spectra of each subfraction sample (b) and (c) are displayed in the inset. DUVRR spectra are scaled for relative comparison of amide mode intensities. Reproduced with permission from Halsey, C. M.; Oshokoya, O. O.; JiJi, R. D.; Cooley, J. W., Deep-UV Resonance Raman Analysis of the *Rhodobacter capsulatus* Cytochrome bc_1 Complex Reveals a Potential Marker for the Transmembrane Peptide Backbone. *Biochemistry* 2011, *50* (30), 6531-6538. Copyright 2011 American Chemical Society.

4.4.2 Identifying the H/D Exchangeable Portions of the Contributing Protein Spectra

The exclusion of detergent, cofactors, Bchl molecules or quinones as the molecular cause of the intense 1665 cm^{-1} spectral feature, prompted further studies into whether the increased amide I mode intensity could be derived from the TM (or region of limited solvent accessibility) portion of the protein backbone. DUVRR spectra (λ_{ex} = 197 nm) of cyt bc_1 complex samples were collected in aqueous phosphate buffer or buffer prepared with deuterium oxide. Immersion of the β-DM solvated cyt bc_1 complex in D_2O resulted in a diminished amide II feature at 1562 cm^{-1} coincident with the emergence of a new spectral feature at 1462 cm^{-1}, known to be the location of the N-D bend derived amide II' mode (Figure 4-4). Much of the amide III mode contribution (1238/1296 cm^{-1}) also disappears from the spectrum, shifting to the amide III' position (970 cm^{-1}) as documented previously[28], which is also an indication of a significant influence of H^+/D^+ exchangeability over the DUVRR response. Interestingly, no significant differences in the amide I position or intensity were observed as a function of deuterium exchange, where the amide I mode would typically be expected to red shift and decrease slightly in intensity as a function of formation of the backbone N-D moiety upon exchange. A residual contribution to the DUVRR spectra at 1562 cm^{-1} can also be seen to remain despite exchange of the sample in D_2O for several days, indicating that at least some portion of the backbone was not solvent accessible.

4.4.3 Response of the Amide Modes to Excitation Wavelength

Despite the increased intensity of the 1665 cm^{-1} mode, other studies using UVRR of membrane proteins have not shown a similar spectral feature. However, all of these studies utilized excitation wavelengths > 207 nm (predominantly > 220 nm). Therefore, we carried out studies to determine if the spectral response of this feature to excitation wavelength was only readily visible in the relatively deep-UV. DUVRR spectra were collected of the cyt bc_1 complex at 197, 198, 200, 202, 204, and 206 nm (Figure 5, left panel). Surprisingly, the enhancement of the 1665 cm^{-1} spectral feature more closely matches that of an aromatic residue than typical soluble protein amide I modes in both deuterium and

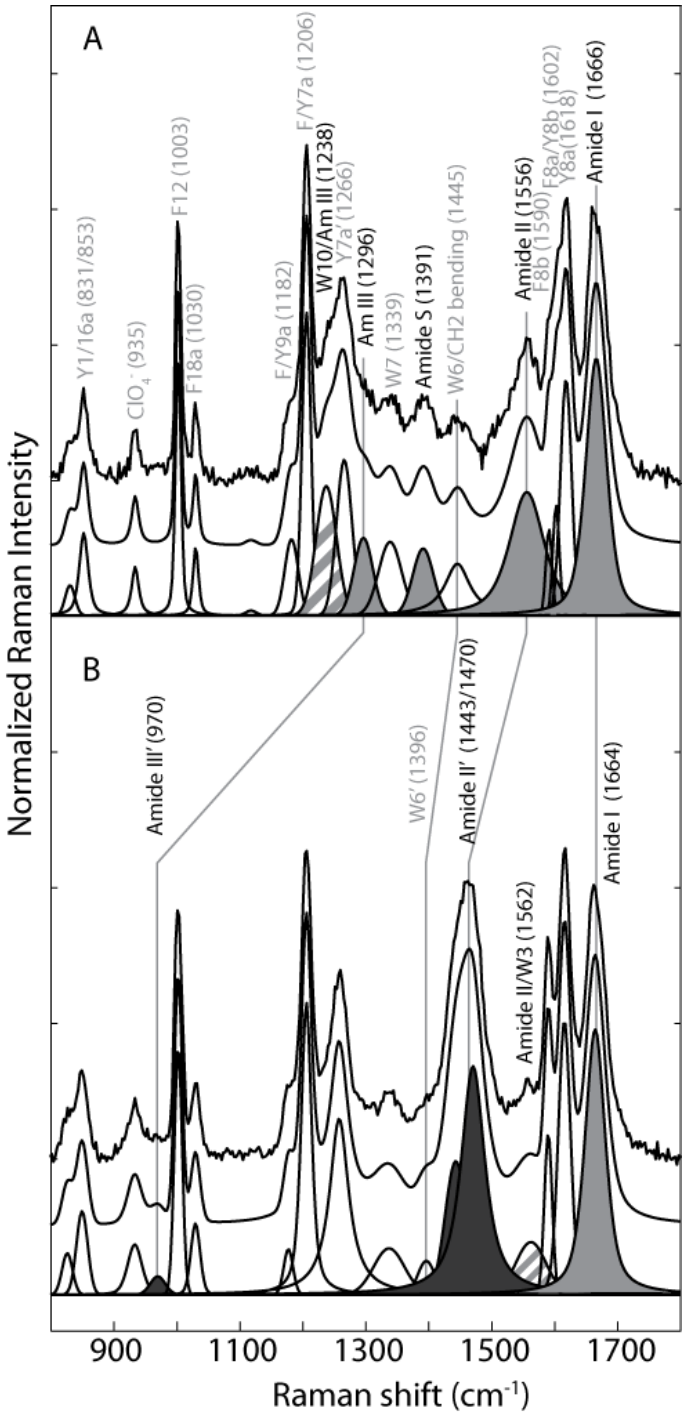

Figure 4-4. Effects of deuterium exchange on the cyt bc_1 complex DUVRR spectrum. Spectra (λ_{ex} = 197 nm) of cyt bc_1 in aqueous (panel A) and deuterated (panel B) buffer with raw spectra after baselining and buffer subtraction (top), a nonlinear least-squares fit (middle), and the individual fitted components (bottom) shown for comparative purposes. The Raman shifts of each assigned band are indicated for panel A and for panel B only if the band has shifted upon deuteration. Components correlative with amide modes are shaded in gray and labeled in black. All other bands are labeled in gray. In cases where amide and aromatic bands are fit the by the same component, the fitted band is striped. Deuterated amide II' and III' modes are shaded a dark gray. The intensities of the spectra have been normalized as in Figure 4-1, and significant shifts due to deuteration are indicated by gray lines. Reproduced with permission from Halsey, C. M.; Oshokoya, O. O.; JiJi, R. D.; Cooley, J. W., Deep-UV Resonance Raman Analysis of the *Rhodobacter capsulatus* Cytochrome bc_1 Complex Reveals a Potential Marker for the Transmembrane Peptide Backbone. *Biochemistry* 2011, *50* (30), 6531-6538. Copyright 2011 American Chemical Society.

non-deuterium exchanged spectra. While the amide I response to excitation energy was dramatically different between the soluble cyt *c* and the cyt bc_1 complex samples, the absolute Raman cross-section of the amide II and amide S modes, normalized for the number of amino acid residues in each protein

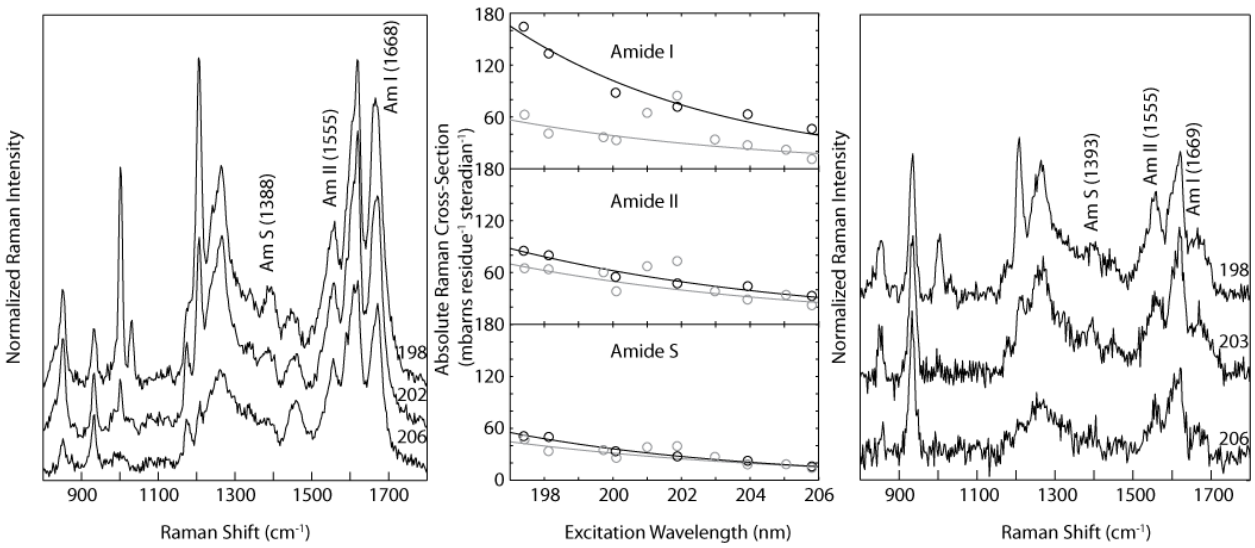

Figure 4-5. Excitation profiles of cyt bc_1 and cyt *c*. The absolute Raman cross sections (middle panel) were calculated based on intensities of the amide I, II, and S bands from 197 to 206 nm excitation. Black circles are calculated cross sections for cyt bc_1 spectra, and gray circles refer to cyt *c* spectra calculated cross sections. Only spectra of cyt bc_1 complex (left panel) collected at 198 nm (top), 202/203 nm (center), and 206 nm (bottom) excitation are shown for clarity; excitation wavelengths (nm) and amide assignments (with Raman shifts in cm^{-1}) are indicated. Reproduced with permission from Halsey, C. M.; Oshokoya, O. O.; JiJi, R. D.; Cooley, J. W., Deep-UV Resonance Raman Analysis of the *Rhodobacter capsulatus* Cytochrome bc_1 Complex Reveals a Potential Marker for the Transmembrane Peptide Backbone. *Biochemistry* 2011, *50* (30), 6531-6538. Copyright 2011 American Chemical Society.

sample (Equation 1), were virtually overlapped (Figure 4-5, middle panel). As expected, if the amide I mode was dominated by the non-exchanging TM region of the protein backbone, this mode's DUVRR Raman cross-section excitation profile was very similar regardless of whether exchange was carried out (Figure 4-6, bottom panel). Additionally, consistent with a small portion of the amide I being derived from > 50% of the protein not embedded in the detergent micelle, the increase in the amide I response with increasing excitation energy is subtly diminished in the deuterium exchanged Raman cross-section excitation profile (Figure 4-6, top panel).

4.5 Discussion

4.5.1 DUVRR Spectra of a Soluble and Partially Lipid-Solvated Protein

The overlapped DUVRR spectra of cyt *c* and cyt bc_1 complex are similar in all DUVRR spectral regions except for the amide I mode (Figure 1). The secondary structure and aromatic content

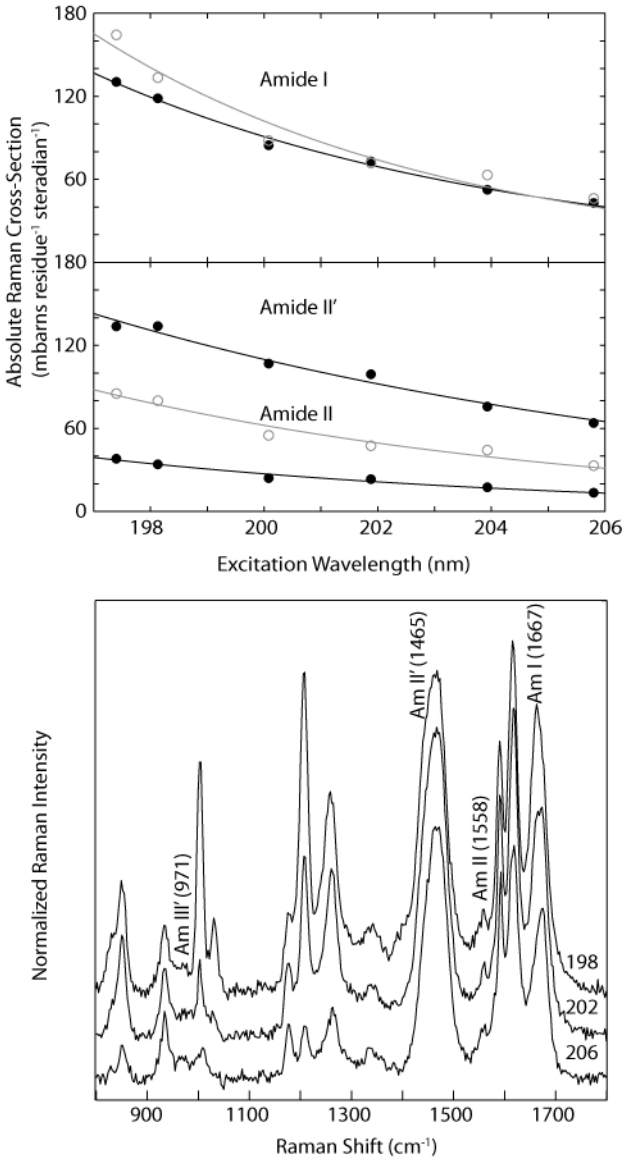

Figure 4-6. Excitation profile of cyt bc_1 in deuterated buffer. The absolute Raman cross sections of deuterated cyt bc_1 (black circles) were calculated based on band intensities from 197 to 206 nm excitation. Gray open circles indicate the absolute Raman cross sections of cyt bc_1 in aqueous buffer. Lines are included to guide the eye. Only spectra collected at 198 nm (top), 202 nm (center), and 206 nm (bottom) excitation are shown in the bottom panel for clarity; excitation wavelengths and amide assignments (with average associated Raman shift in cm^{-1}) are indicated. Reproduced with permission from Halsey, C. M.; Oshokoya, O. O.; JiJi, R. D.; Cooley, J. W., Deep-UV Resonance Raman Analysis of the *Rhodobacter capsulatus* Cytochrome bc_1 Complex Reveals a Potential Marker for the Transmembrane Peptide Backbone. *Biochemistry* 2011, *50* (30), 6531-6538. Copyright 2011 American Chemical Society.

similarities of the two protein samples led us to investigate whether the difference in the intensity of the amide I mode was derived from differences in the non-aqueous solvated peptide backbone content between the aqueous soluble cyt *c* and the surfactant micelle solubilized cyt bc_1 complex. DUVRR spectra of potential spectral contaminants associated with the purification of the cyt bc_1 complex from Rcaps confirmed that these molecules were not the source of the increased vibrational mode intensity at 1665 cm^{-1}. Lack of significant resonantly enhanced modes by these molecules is not surprising as porphyrin-containing cofactors like *c*-type cyt's or Bchl molecules are not typically resonantly enhanced at excitation wavelengths near 197 nm. Therefore the difference in the amide I mode between the two

protein samples must be due to the protein itself and can be postulated to be related to the solvent inaccessible TM domain of the cyt bc_1 complex (or its subfractions).

The peptide TM regions, or more specifically those embedded in the lipid or surfactant regime, are diminished with interaction of the solvent with the peptide backbone carbonyl and amines. Dehydration of the amide backbone has resulted previously in similar enhancements of the amide I mode [11a, 29]. Specifically, the DUVRR spectra of *n*-methylacetamide (NMA) in various solvents have been shown to have changes in the intensities of all of the amide modes, including a very intense amide I versus the remaining amide modes in the more non-polar solvents. Solvent mediated hydrogen bonding perturbs the amide ground state structure predominantly at the amide carbonyl compared to the adjacent amine, presumably because the C=O bond order is significantly altered by the electron withdrawing hydrogen bonds (or their absence in less polar solvents)[11a]. Additional examples of loss of backbone hydration influencing the DUVRR spectrum of a protein backbone, and specifically the anti-correlated intensity changes of the amide I and II modes (increasing and decreasing in intensity, respectively), have also been observed with the depsipeptide valinomycin in various solvents[29c] and in the interior cross β-sheet core of amyloid fibrils[30]. It remains unclear whether the solvent inaccessible regions of the α-helical TM regions of the cyt bc_1 complex exhibit similar diminished intensities of the amide II and III modes as NMA and valinomycin in non-polar solvents.

The cyt bc_1 complex and its resulting DUVRR spectrum are mixtures of lipid-solvated and water-solvated domains. Previously, deuterium exchangeability has been used to delineate the DUVRR spectral signature of the solvent inaccessible interior (cross β-sheet core) from the solvated exterior of amyloid fibrils. Employing a similar strategy with the cyt bc_1 complex resulted in the expected decoupling of vibrational modes eliminating most of the amide II, III, and S modes (Figure 4-4). However, assigning the remaining spectral feature at 1562 cm^{-1} to the amide II mode of the hydrophobic portion of the protein

within a detergent micelle is not straightforward, as the peak position also consistent with a tryptophan mode (W3), even though no other characteristic tryptophan modes are easily distinguished within the spectrum. The amide I, by contrast, is almost completely unaffected by deuteration, where classically backbone deuteration would result in a small red shift and loss of intensity[28, 31]. Lack of change in the amide I intensity and position as a function of H/D exchange implies that the bulk of the intensity of this mode is derived from the detergent-solvated region of the protein complex. Evidence of contribution of the exchangeable region of the protein to the amide I mode can be inferred from differences in the Raman cross-sections between the pre- and post-deuterium exchanged samples (Figure 4-6). Using the amide I cross-sections of NMA at 200 nm excitation reported previously[11a], in water and in acetonitrile, the water-solvated amide I can be estimated to be one tenth of the area of the amide I from a lipid-solvated environment. Given that 45% of the backbone lies in the membrane, the difference in the aqueous and D_2O immersed cyt bc_1 samples indicate that roughly 10% of the total amide I mode intensity is derived from the water-solvated portion (~55%) of the cyt bc_1 complex protein backbone, or that the amide I mode response is 10 times more intense for the lipophilic portion of the protein backbone than its equivalent solvent exposed portions. Lipid-solvated contributions to the amide III and S are not well resolved from overlapped aromatics and cannot be compared with these analyses.

4.5.2 Lipid Solvated α-Helical DUVRR Spectrum and Raman Cross Section

The excitation profile of all amide modes of NMA have been reported in both water and acetonitrile [11a, 32]. The non-polar environment resulted in significant enhancement of the amide I mode compared to the amide II mode, a trend opposite to what is expected in water. This observation allows one to compare the amide I/amide II ratios as a means to probe the degree to which water has been excluded from the α-helical peptide backbone. The wavelength dependence of cyt bc_1 DUVRR spectra, for example, reveals a marked departure from cyt *c* (Figure 4-5). Most noticeably at 197 nm excitation, the amide I is always more intense than the amide II. Excitation profiles of soluble proteins have been

shown to be unique to specific secondary structure types[27]. The lipid-solvated region is entirely □-helical and our estimation of the amide I intensity and position could serve as the basis for the first documented lipid-solvated α-helical UVRR spectrum. In addition to being much more intense, the maxima of the amide I mode is also significantly blue shifted versus those previously assigned to α-helical secondary structures in solvated protein and peptides. However, it remains unclear to what extent other factors like helical packing might contribute to the amide I mode enhancement in this proteins DUVRR spectra versus other lipid solubilized regions in other proteins.

A small number of previously published studies have used excitation wavelengths less than 210 nm to collect resonant Raman spectra of lipid or surfactant solvated proteins, however, none reported any remarkable feature associated with the amide I mode[30, 33]. The clearest example can be seen in the works of Shafaat et al.[33a] where the authors reported increased Raman cross-sections for amide as well as tryptophan vibrational modes for a model β-strand hexapeptide consistent with the increased per residue amide I mode cross-sections of cyt bc_1. The lack of a significant change in the Raman enhancement, especially of the amide I mode, reported in these studies using excitation wavelengths 207.5, is consistent with excitation profiles of the cyt bc_1 complex presented here (Figure 4-5), where the amide I mode Raman cross-section compared to the amide II mode decreases dramatically with decreasing excitation energies.

Interestingly, based upon previously assigned DUVRR amide signatures of aqueous solvated proteins and peptides[10a, b], the cyt bc_1 lipid solvated region DUVRR spectral features described herein would have led to the erroneous assignment of the regions structure as a predominantly □-sheet or random coil dominated region of the protein merely as a function of its blue shifted spectral position following H/D exchange experiments. However, it is clear from crystal structures the membrane-embedded TM portion of the protein is α-helical. Therefore, future efforts will need to concentrate on

obtaining classical secondary structure signatures within the lipid phase before confident secondary structural content assignments can be made for membrane vs. soluble domains of proteins using DUVRR.

4.6 Conclusion

Collection of resonance Raman spectra of lipid or surfactant solubilized proteins is feasible in the far deep-UV (< 205 nm) despite the substantial absorbance of the sample at the excitation wavelengths used. The consequent resonant Raman enhancement of the peptide backbone associated with the desolvated regions of the protein have the potential to be a unique structural marker for membrane or lipid solvation of proteins and their structures. In fact, the ability of DUVRR spectroscopy to report on the peptide backbones solvation and structural constraints, while still gleaning site-specific information from naturally occurring aromatic residues make this technique a potentially valuable tool for analysis of the structural consequences of lipid-protein interactions.

4.7 Bibliography

1. Wang, Y.; Purrello, R.; Georgiou, S.; Spiro, T. G., UVRR Spectroscopy of the Peptide Bond. 2. Carbonyl H-Bond Effects on the Ground and Excited-State Structures of *N*-Methylacetamide. *Journal of the American Chemical Society* **1991,** *113* (17), 6368-6377.

2. White, S. H., The progress of membrane protein structure determination. *Protein Science* **2004,** *13*, 1948-1949.

3. Arora, A.; Tamm, L. K., Biophysical approaches to membrane protein structure determination. *Curr. Opin. Struct. Biol.* **2001,** *11*, 540-547.

4. Putnam, C. D.; Hammel, M.; Hura, G. L.; Tainer, J. A., X-ray solution scattering (SAXS) combined with crystallography and computation: defining accurate macromolecular structures, conformations and assemblies in solution. *Quarterly Reviews of Biophysics* **2007,** *40*, 191-285.

5. (a) Han, X.; Mihailescu, M.; Hristova, K., Neutron diffraction studies of fluid bilayers with transmembrane proteins: structural consequences of the achondroplasia mutation. *Biophysical Journal* **2006,** *91*, 3736-3747; (b) Skar-Gislinge, N.; Simonsen, J. B.; Mortensen, K.; Feidenhans'l, R.; Sligar, S. G.; Møller, B. L.; Bjørnholm, T.; Arleth, L., Elliptical structure of phospholipid bilayer nanodiscs encapsulated by scaffold proteins: casting the roles of the lipids and the protein. *Journal of the American Chemical Society* **2010,** *132*, 13713-13722.

6. Arrondo, J. L. R.; Goñi, F. M., Structure and dynamics of membrane proteins as studied by infrared spectroscopy. *Progress in Biophysics & Molecular Biology* **1999,** *72*, 367-405.

7. (a) Wallace, B. A., Protein characterisation by synchrotron radiation circular dichroism spectroscopy. *Quarterly Reviews of Biophysics* **2009,** *42*, 317-370; (b) Wallace, B. A.; Lees, J. G.; Orry, A. J. W.; Lobley, A.; Janes, R. W., Analyses of circular dichroism spectra of membrane proteins. *Protein Science* **2003,** *12*, 875-884.

8. Kim, J. E.; Arjara, G.; Richards, J. H.; Gray, H. B.; Winkler, J. R., Probing folded and unfolded states of outer membrane protein A with steady-state and time-resolved tryptophan fluorescence *Journal of Physical Chemistry B* **2006,** *110*, 17656-17662.

9. (a) Joo, C.; Balci, H.; Ishitzuka, Y.; Buranachai, C.; Ha, T., Advances in single molecule fluorescence methods for molecular biology. *Annual Review of Biochemistry* **2008,** *77*, 51-76; (b) Matos, P. M.; Franquelim, H. G.; Castanho, M. A. R. B.; Santos, N. C., Quantitative assessment of peptide-lipid interactions. Ubiquitous fluorescence methodologies. *Biochimica et Biophysica Acta* **2010,** *1798*, 1999-2012.

10. (a) Chi, Z.; Chen, X. G.; Holtz, J. S. W.; Asher, S. A., UV resonance Raman-selective amide vibrational enhancement: quantitative methodology for determining protein secondary structure. *Biochemistry* **1998,** *37*, 2854-2864; (b) Huang, C.-Y.; Balakrishnan, G.; Spiro, T. G., Protein secondary structure from deep-UV resonance Raman spectroscopy. *Journal of Raman Spectroscopy* **2006,** *37*, 277-282; (c) Shashilov, V.; Sikirzhytski, V.; Popova, L. A.; Lednev, I. K., Quantitative methods for structural characterization of proteins based on deep UV resonance Raman spectroscopy. *Methods* **2010,** *52*, 23-37.

11. (a) Wang, Y.; Purrello, R.; Georgiou, S.; Spiro, T. G., UVRR spectroscopy of the peptide bond. 2. Carbonyl H-bond effects on the ground- and excited-state structures of N-methylacetamide. *Journal of the American Chemical Society* **1991,** *113*, 6368-6377; (b) Triggs, N. E.; Valentini, J. J., An investigation of hydrogen bonding in amides using Raman spectroscopy. *Journal of Physical Chemistry* **1992,** *96*, 6922-6931; (c) Mikhonin, A. V.; Bykov, S. V.; Myshakina, N. S.; Asher, S. A., Peptide secondary structure folding reaction coordinate: correlation between UV Raman amide III frequency, Ψ Ramachandran angle, and hydrogen bonding. *Journal of Physical Chemistry B* **2006,** *110*, 1928-1943; (d) Myshakina, N. S.; Ahmed, Z.; Asher, S. A., Dependence of amide vibrations on hydrogen bonding. *Journal of Physical Chemistry B* **2008,** *112*, 11873-11877.

12. Huang, C.-Y.; Balakrishnan, G.; Spiro, T. G., Early events in apomyoglobin unfolding probed by laser T-jump/UV resonance Raman spectroscopy. *Biochemistry* **2005,** *44*, 15734-15742.

13. Asher, S. A.; Ianoul, A.; Mix, G.; Boyden, M. N.; Karnoup, A.; Diem, M.; Schweitzer-Stenner, R., Dihedral ψ angle dependence of the amide III vibration: a uniquely sensitive UV resonance Raman secondary structural probe. *J. Am. Chem. Soc.* **2001,** *123*, 11775-11781.

14. (a) Chen, J.; Barry, B. A., Ultraviolet resonance Raman microprobe spectroscopy of photosystem II. *Photochemistry and Photobiology* **2008,** *84*, 815-818; (b) Chen, J.; Bender, S. L.; Keough, J. M.; Barry, B. A., Tryptophan as a probe of photosystem I electron transfer reactions: a UV resonance Raman study. *Journal of Physical Chemistry B* **2009,** *113*, 11367-11370.

15. Sanchez, K. M.; Neary, T. J.; Kim, J. E., Ultraviolet resonance Raman spectroscopy of folded and unfolded states of an integral membrane protein. *Journal of Physical Chemistry B* **2008,** *112*, 9507-9511.

16. Valkova-Valchanova, M. B.; Saribas, A. S.; Gibney, B. R.; Dutton, P. L.; Daldal, F., Isolation and characterization of a two-subunit cytochrome b-c_1 subcomplex from *Rhodobacter capsulatus* and reconstitution of its ubihydroquinone oxidation (Q_o) site with purified Fe-S protein subunit. *Biochemistry* **1998,** *37*, 16242-16251.

17. (a) Hunte, C.; Palsdottir, H.; Trumpower, B. L., Protonmotive pathways and mechanisms in the cytochrome bc_1 complex. *FEBS Letters* **2003,** *545*, 39-46; (b) Xia, D.; Yu, C.-A.; Kim, H.; Xia, J.-Z.; Kachurin, A. M.; Zhang, L.; Yu, L.; Deisenhofer, J., Crystal structure of the cytochrome bc_1 complex from bovine heart mitochondria. *Science* **1997,** *277*, 60-66; (c) Berry, E. A.; Guergova-Kuras, M.; Huang, L.-s.; Crofts, A. R., Structure and function of cytochrome *bc* complexes. *Annu. Rev. Biochem.* **2000,** *69*, 1005-1075; (d) Berry, E. A.; Huang, L.-s.; Saechao, L. K.; Pon, N. G.; Valkova-Valchanova, M. B.; Daldal, F., X-ray structure of *Rhodobacter capsulatus* cytochrome bc_1: comparison with its mitochondrial and chloroplast counterparts. *Photosynthesis Research* **2004,** *81*, 251-275.

18. Lange, C.; Nett, J. H.; Trumpower, B. L.; Hunte, C., Specific roles of protein-phospholipid interactions in the yeast cytochrome bc_1 complex structure. *EMBO Journal* **2001,** *20*, 6591-6600.

19. (a) Crofts, A. R., The mechanism of the ubiquinol:cytochrome *c* oxidoreductases of mitochondria and of *Rhodopseudomonas sphaeroides*. In *The Enzymes of Biological Membranes*, Martonosi, A. N., Ed. Plenum Publ. Corp.: New York, 1985; Vol. 4, pp 347-382; (b) Trumpower, B. L.; Gennis, R. B., Energy transduction by cytochrome complexes in mitochondrial and bacterial respiration: the enzymology of coupling electron transfer reactions to transmembrane proton translocation. *Annual Review of Biochemistry* **1994,** *63*, 675-716; (c) Darrouzet, E.; Cooley, J. W.; Daldal, F., The cytochrome bc_1 complex and its homologue the b_6f complex: similarities and differences. *Photosynthesis Research* **2004,** *79*, 25-44; (d) Kramer, D. M.; Nitschke, W.; Cooley, J. W., The Cytochrome bc_1 and Related *bc* Complexes: The Rieske/Cytochrome *b* Complex as the Functional Core of a Central Electron/Proton Transfer Complex. In *The Purple Phototrophic Bacteria*, Hunter, C. N.; Daldal, F.; Thurnauer, M. C.; Beatty, J. T., Eds. Springer: New York, 2009; pp 451-473.

20. (a) Darrouzet, E.; Valkova-Valchanova, M. B.; Moser, C. C.; Dutton, P. L.; Daldal, F., Uncovering the [2Fe2S] domain movement in cytochrome bc_1 and its implications for energy conversion. *Proceedings of the National Academy of Sciences of the United States of America* **2000,** *97*, 4567-4572; (b) Xiao, K.; Yu, L.; Yu, C.-A., Confirmation of the involvement of protein domain movement during the catalytic cycle of the cytochrome bc_1 complex by the formation of and intersubunit disulfide bond between cytochrome *b* and the iron-sulfur protein. *Journal of Biological Chemistry* **2000,** *275*, 38597-38604; (c) Darrouzet, E.; Daldal, F., Movement of the iron-sulfur subunit beyond the *ef* loop of cytochrome *b* is required for multiple turnovers of the bc_1 complex but not for single turnover Q_o site catalysis. *Journal of Biological Chemistry* **2002,** *277*, 3471-3476.

21. (a) Cooley, J. W.; Ohnishi, T.; Daldal, F., Binding dynamics at the quinone reduction (Q_i) site influence the equilibrium interactions of the iron sulfur protein and hydroquinone oxidation (Q_o) site of the cytochrome bc_1 complex. *Biochemistry* **2005,** *44*, 10520-10532; (b) Cooley, J. W.; Lee, D.-W.; Daldal, F., Across membrane communication between the Q_o and Q_i active sites of cytochrome bc_1. *Biochemistry* **2009,** *48*, 1888-1899; (c) Cooley, J. W., A structural model for across membrane coupling

between the Q_o and Q_i active sites of cytochrome bc_1. *Biochimica et Biophysica Acta* **2010,** *1797*, 1842-1848.

22. Gray, K. A.; Dutton, P. L.; Daldal, F., Requirement of histidine 217 for ubiquinone reductase activity (Q_i site) in the cytochrome bc_1 complex *Biochemistry* **1994,** *33*, 723-733.

23. van Gelder, B. F., Optical properties of cytochromes from beef heart mitochondria, submitochondrial vesicles, and derived preparations. *Methods in Enzymology* **1978,** *53*, 125-128.

24. Balakrishnan, G.; Hu, Y.; Nielsen, S. B.; Spiro, T. G., Tunable kHz deep ultraviolet (193-210 nm) laser for Raman applications. *Appl. Spectrosc.* **2005,** *59*, 776-781.

25. Ferraro, J. R.; Nakamoto, K., *Introductory Raman Spectroscopy*. Academic Press: Boston, 1994.

26. Simpson, J. V.; Oshokoya, O.; Wagner, N.; Liu, J.; JiJi, R. D., Pre-processing of ultraviolet resonance Raman spectra. *Analyst* **2011,** *136*, 1239-1247.

27. Simpson, J. V.; Balakrishnan, G.; JiJi, R. D., MCR-ALS analysis of two-way UV resonance Raman spectra to resolve discrete protein secondary structural motifs. *Analyst* **2009,** *134*, 138-147.

28. Sugawara, Y.; Kirakawa, A. Y.; Tsuboi, M., In-plane force constants of the peptide group: Least squares adjustment starting from *ab initio* values of *N*-methylacetamide. *Journal of Molecular Spectroscopy* **1984,** *108*, 206-214.

29. (a) Torii, H.; Tatsumi, T.; Tasumi, M., Effects of hydration on the structure, vibrational wavenumbers, vibrational force field and resonance Raman intensities of *N*-methylacetamide. *J. Raman Spectrosc.* **1998,** *29*, 537-546; (b) Markham, L. M.; Hudson, B. S., *Ab initio* analysis of the effects of aqueous solvation on the resonance Raman intensities of *N*-methylacetamide. *J. Phys. Chem.* **1996,** *100*, 2731-2737; (c) Ozdemir, A.; Lednev, I. K.; Asher, S. A., UVRR spectroscopic studies of valinomycin complex formation in different solvents. *Spectrochim. Acta, Part A* **2005,** *61*, 19-26.

30. (a) Xu, M.; Shashilov, V.; Lednev, I. K., Probing the cross-β core structure of amyloid fibrils by hydrogen-deuterium exchange deep ultraviolet resonance Raman spectroscopy *J. Am. Chem. Soc.* **2007,** *129*, 11002-11003; (b) Popova, L. A.; Kodali, R.; Wetzel, R.; Lednev, I. K., Structural variations in the cross-β core of amyloid β fibrils revealed by deep UV resonance Raman spectroscopy. *J. Am. Chem. Soc.* **2010,** *132*, 6324-6328.

31. Mayne, L. C.; Ziegler, L. D.; Hudson, B., Ultraviolet resonance Raman studies of *N*-methylacetamide. *Journal of Physical Chemistry* **1985,** *89*, 3395-3398.

32. Chen, X. G.; Asher, S. A.; Schweitzer-Stenner, R.; Mirkin, N. G.; Krimm, S., UV Raman determination of the $\pi\pi^*$ excited state geometry of *N*-methylacetamide: vibrational enhancement pattern. *J. Am. Chem. Soc.* **1995,** *117*, 2884-2895.

33. (a) Shafaat, H. S.; Sanchez, K. M.; Neary, T. J.; Kim, J. E., Ultraviolet resonance Raman spectroscopy of a β-sheet peptide: a model for membrane protein folding. *Journal of Raman Spectroscopy* **2009,** *40*, 1060-1064; (b) Cho, N.; Asher, S. A., UV resonance Raman and absorption studies of angiotensin II conformation in lipid environments. *Biospectroscopy* **1996,** *2*, 71-82; (c) Holtz, J. S. W.;

Lednev, I. K.; Asher, S. A., UV resonance Raman study of angiotensin II conformation in nonaqueous environments: lipid micelles and acetonitrile. *Biopolymers (Biospectroscopy)* **2000,** *57*, 55-63.

Chapter 5: Simultaneous Observation of a Peptide Backbone Lipid Solvation and α-Helical DUVRR Spectrum and Raman Cross Section

Adapted with permission from Halsey, C. M.; Xiong, J.; Oshokoya, O. O.; Johnson, J. A.; Shinde, S.; Beatty, J. T.; Ghirlanda, G.; JiJi, R. D.; Cooley, J. W., Simultaneous Observation of Peptide Backbone Lipid Solvation and α-Helical Structure by Deep-UV Resonance Raman Spectroscopy. *ChemBioChem* **2011,** *12* (14), 2125-2128. Copyright 2011 John Wiley and Sons.

5.1 Abstract

Despite a variety of methodologies aimed at improving membrane protein structure analysis, information about membrane proteins in their native membrane environments remains scarce[1]. Currently no structurally sensitive spectroscopic techniques are capable of co-determining ensemble structural content and localized lipid vs. aqueous solvation information. Here, we describe the first deep-UV (λ_{ex} < 210 nm) resonance Raman (DUVRR) spectra of a model α-helical peptide embedded in a membrane-mimetic environment, confirming sensitivity to secondary structure content and revealing sensitivity of DUVRR to the lipid solvation of the peptide backbone.

5.2 Introduction

Analyses of membrane protein structural dynamics are hampered by the experimental difficulties associated with elucidating structural changes and correlating those changes to their respective solvation by the non-polar lipid or surfactant versus the aqueous phases. No kinetically amenable spectroscopic techniques are capable of delineating subtle changes in protein structure while simultaneously reporting on that structure's solvation without protein modification by deuterium exchange, isotope labeling, mutagenesis or post-translational spin/fluorophore label attachment. Glimpses of the dynamics and stabilizing forces involved with protein folding and

insertion into membranes have recently been gleaned by UV excited resonance Raman spectroscopy focused on excitation wavelengths (λ_{ex} > 220 nm) specific for aromatic residues. Deep-UV (λ_{ex} < 210 nm) excitation, which has been a valuable tool for analysing the structure of soluble proteins by accessing the $\pi \rightarrow \pi^*$ transition of the peptide backbone vibrational modes and their dynamics, has not been previously explored successfully for this class of hydrophobic proteins.[2] The DUVRR protein spectral response consists of four peptide backbone related Amide (Am) responses, I (C=O stretching), II (in phase C-H/N-H stretching/bending), III (out of phase C-H/N-H stretching/bending) and S (coupled C-H/N-H bending; alternately referred to as C_αHb)[2a]. The combinations of Am mode positions and intensities are strongly correlated to the constraints imparted by particular secondary structures with soluble proteins[3]. Solvent interaction and its extent with the peptide backbone can also influence the Am mode spectral positions in DUVRR and IR and intensities in DUVRR alone[4]. Theoretical calculations with *N*-methylacetamide (NMA) in different solvent polarities have revealed that the solvent dependent Am I intensity differences seen in the DUVRR spectra, but not the IR spectra are derived from the sensititivity of the former technique to the polarizability term of the C=O bond. Herein, we present evidence that a surfactant-solubilized protein region also has altered Am mode intensities, especially in the C=O stretching region.

5.3 Experimental

Sodium perchlorate, sodium phosphate, equine heart myoglobin, and hexafluoroisopropanol were purchased from Sigma (St. Louis, MO). Dodecyl phosphocholine (DPC) and dimyristoyl phosphatidylcholine (DMPC) were purchased from Avanti Polar Lipids (Alabaster, AL). β-dodecyl maltoside (DDM) was purchased from Biosynth (Itasca, IL). DPC micelle solubilized ME1 dUVRR samples were prepared as described in sodium perchlorate (200 mM) and phosphate buffer (20 mM) (micellar incorporation was monitored by appearance of helical structure in CD spectra, see supplemental information). Myoglobin (0.5 mg mL^{-1}) was solubilized in phosphate buffer (20 mM, pH 7.0) and sodium

perchlorate (50 mM). "Chromatophore" membranes (1.0 mg mL^{-1}) and purified cytochrome bc_1 complex (0.5 mg mL^{-1}) were prepared from *Rhodobacter capsulatus* as in Valkova-Valchanova.[5] Light harvesting complex/reaction center/pufX supercomplex was purified from *Rhodobacter sphaeroides* according to a modification of the procedure described by Abresch et al.[6] in which the complex was solubilized using a mixture of sodium cholate (0.5% w/v) and n-octyl-β-D-glucopyranoside (4% w/v), the detergents exchanged for sodium cholate (0.2%) and DDM (0.06%) while the protein was bound to a Ni^{2+}-NTA column, and the dimer was separated from the monomer by banding on a 15 to 35% sucrose gradient containing sodium cholate (0.2%) and DDM (0.06%). The supercomplex was then diluted (0.5 mg mL^{-1}) in sodium perchlorate (50 mM), Tris (10 mM, pH 8.0), NaCl (25 mM), DDM (0.06% w/v), and sodium cholate (0.2% w/v).

The tuneable deep UV excitation source, collection optics and sampling apparatus are described elsewhere[7]. Spectral calibration was done by cyclohexane spectra correction[8]. All data was processed in a MATLAB environment to remove interferences from gamma rays and contributions from buffer.

5.4 Results and Discussion

As a model for the common α-helical membrane embedded protein domain we have examined the *de novo* designed ME1 peptide, which contains a single hydrophobic α-helical segment encompassing roughly 75% of the total peptide backbone. Like its parent protein, it is extremely insoluble in aqueous solvents and only forms stable α-helical homodimers within a micellar environment[9]. The DUVRR spectrum using an excitation source of 197 nm of a dodecylphosphocholine (DPC) solubilized ME1 sample contains aromatic side chain derived modes (1180-1210 and 1580-1620 cm^{-1}) arising from the single tyrosine and phenylalanine residues within the peptide sequence (Figure 5-1)[10]. Peptide backbone contributions can also be assigned for the Am I (1658 cm^{-1}), II (1546 cm^{-1}) and III (1260-1340 cm^{-1}) modes and a smaller feature where the Am S (1400 cm^{-1}) mode would be expected.

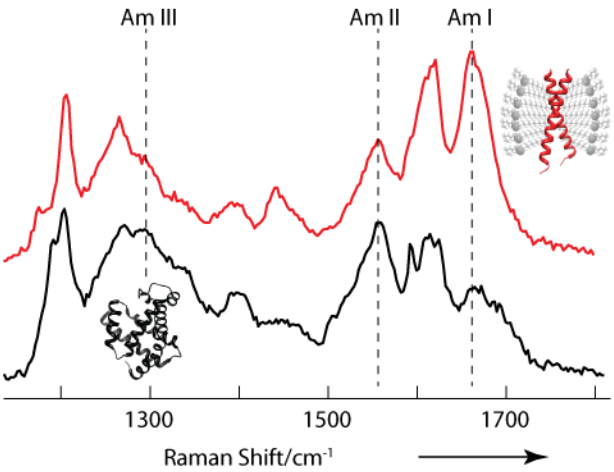

Figure 5-1. Deep-UV resonance Raman spectra of a detergent-solubilized ME1 (red) and aqueous-solvated myoglobin (black), both α-helical proteins. All spectra were collected using 197 nm excitation and have been normalized to the intensity of the ClO4- internal standard peak at 935 cm-1. Reprinted with permission from Halsey, C. M.; Xiong, J.; Oshokoya, O. O.; Johnson, J. A.; Shinde, S.; Beatty, J. T.; Ghirlanda, G.; JiJi, R. D.; Cooley, J. W., Simultaneous Observation of Peptide Backbone Lipid Solvation and α-Helical Structure by Deep-UV Resonance Raman Spectroscopy. *ChemBioChem* 2011, *12* (14), 2125-2128. Copyright 2011 John Wiley and Sons.

The Am III mode's position coupled to the limited extent of Am S contribution is consistent with the preponderance of the peptide being α-helical[3b, 11] and in good agreement with CD spectra collected of the same sample. All features of a DPC containing sample without peptide were consistent with a typical buffer blank, which have been subtracted based upon perchlorate (ClO_4^-) internal standard intensities.

Comparison of the ME1 DUVRR spectra to that of an aqueous soluble, similarly structured (~ 74% α-helical) protein, myoglobin, reveals similar positions and intensities for the Am II, III and S modes. In fact, the positions and intensities of the Am II, the Am III_1 (1339 cm^{-1}), Am III_2 (1294 cm^{-1}), Am III_3 (1264 cm^{-1}), and the relatively weak Am S mode are all very characteristic of a predominantly helical protein.[12] It could be argued that myoglobin with its stable tertiary structure is not the obvious choice for a water solvated α-helical peptide backbone as there is naturally a heterogeneity to the extent of solvent accessibility to the backbone overall. However, the stability of the helical regions in physiological buffer environments and the similar percent content of helical and coiled regions in the myoglobin and the ME1 peptide make it a convenient choice for comparative purposes. The contribution to the DUVRR spectra from non-helical peptide backbone regions, specifically the Am III_3 (1264 cm^{-1}) and Am S (1390-1400 cm^{-1}) modes, are very similar between the two protein samples. The Am I mode DUVRR spectral position also is similar for each protein and consistent with previously published helical DUVRR spectra, however, the feature is much more intense in the micelle solvated ME1 sample. Intensity changes have

been observed previously with the Am I mode as a function of solvent polarity with the model amide moiety *N*-methylacetamide (NMA) or the depsipeptide valinomycin.[4a-d] Most recently, Asher and coworkers have documented the influence on Cl^- on the intensity of the water band which lies directly beneath the Am I mode.[13] However, the salt content is consistent between the myoglobin, ME1, and in the DPC containing blank spectra indicating this is likely not the cause of the strong spectral feature. In fact, the DPC solvated ME1 DUVRR spectrum has a more similar spectral profile to the DUVRR spectrum of the core of an amyloid fibril than it has to a typical water soluble α-helical protein spectrum like that of myoglobin.[4e] The DUVRR spectrum of the amyloid fibril core was elucidated from difference spectra of the solvent accessible and solvent inaccessible regions of these ordered aggregates.[14] It is not surprising that the DUVRR spectra of the solvent inaccessible fibril interior, or β-sheet core, and that of a surfactant solubilized protein domain are similar as both represent instances where the peptide backbone has limited interactions with bulk aqueous solvent. Therefore, it is likely that the increased Am I mode intensity in each case results from loss of hydrogen bonding of the peptide backbone with the solvent water similar to NMA in non-polar solvent.

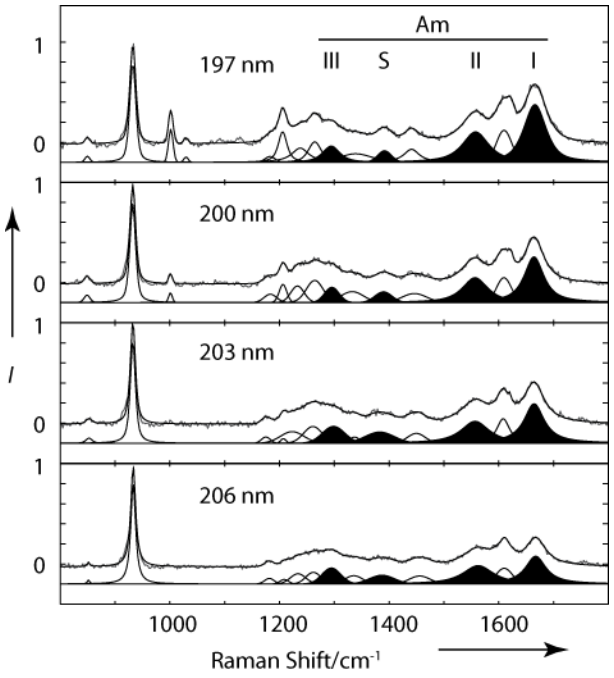

Figure 5-2. Deep-UV resonance Raman spectra of the helical ME1 peptide collected at varying excitation wavelengths. DUVRR spectra at four excitation wavelengths are shown with the fits for the amide (filled black) and aromatic modes (open peaks). All spectral intensities, *I*, have been normalized the ClO_4^- feature intensity at 935 cm^{-1}. Reprinted with permission from Halsey, C. M.; Xiong, J.; Oshokoya, O. O.; Johnson, J. A.; Shinde, S.; Beatty, J. T.; Ghirlanda, G.; JiJi, R. D.; Cooley, J. W., Simultaneous Observation of Peptide Backbone Lipid Solvation and α-Helical Structure by Deep-UV Resonance Raman Spectroscopy. *ChemBioChem* 2011, *12* (14), 2125-2128. Copyright 2011 John Wiley and Sons.

Selective DUVRR response of vibrational modes, imparted by the excitation energy, has previously allowed for the resolution of discrete contributors to a given spectra.[11b, 15] It appears visually that the intensity of the fit Am I mode does not change co-linearly with that of the Am II, III and S modes (Figure 5-2). However, discrepancies in the molecular size of the ME1 and myoglobin proteins preclude significant interpretation of the differences in resonant enhancement of each vibrational mode on a per molecule basis because of the varied chromophore content.[3b]

Yet, by taking the number of amino acid residues in the protein into account in the formal calculation of the absolute Raman cross-sections via Equation 5-1, a per residue cross section can be calculated. The cross section, σ, is normalized to the ratios of the Am mode to internal standard intensities, *I*, the differences in excitation frequency (cm^{-1}), v_o, and Raman shifts (Δcm^{-1}), *v*, self-absorption correction factors, A_o+*A*, and relative concentrations, *C*, and finally normalized to the number of amino acid residues per molecule, r. The ME1 per amino acid residue Am I mode intensity increases with increased incident excitation energy in a non-linear manner with respect to the amide II response, while the Am II mode excitation profiles for the aqueous and lipid soluble helical proteins are roughly overlapped (Figure 5-3). Interestingly, while the Am I mode is known to be the most sensitive to solvent polarity amongst the four backbone vibrational modes, the Am I mode intensity may also be indicative of differing intra-helical hydrogen bonding strength(s) in membrane vs. aqueous solvated protein regimes. [1, 4a, 4d, 16]

$$\sigma_{amide} = \frac{\sigma_{ClO_4^-}}{r}\frac{I_{amide}}{I_{ClO_4^-}}\left(\frac{\nu_{ClO_4^-}}{\nu_{amide}}\right)^4\frac{C_{ClO_4^-}}{C_{amide}}\left(\frac{A_0+A_{amide}}{A_0+A_{ClO_4^-}}\right) \qquad \text{Equation 5-1}$$

In order to establish that an increased Am I mode intensity is a general phenomenon of DUVRR spectra of proteins with lipid solvated helical regimes, we have examined proteins of various sizes, means of solubilization, and hydrophobic or “transmembrane” content. Specifically, we have examined three samples, derived from purple bacterial sources: detergent-solubilized cytochrome bc_1 complex,

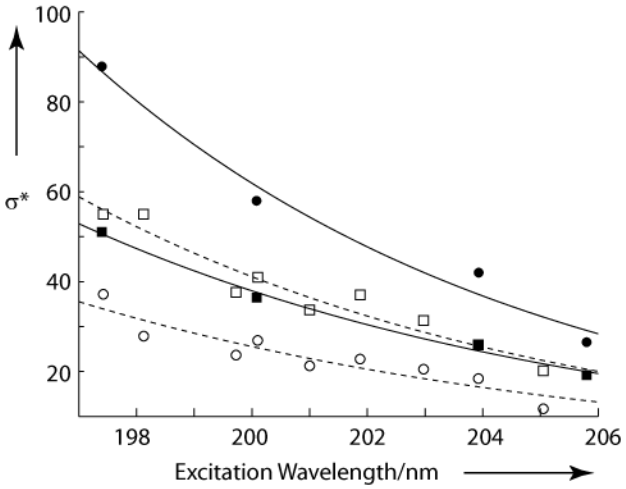

Figure 5-3. Excitation profiles of individual amide modes. Am I (circles) and Am II (squares) per residue cross sections, σ (*units of mbarns amino acid residue^{-1} steradian^{-1}), are plotted versus excitation wavelength for DPC-solubilized ME1 (closed symbols; solid fits) and myoglobin (open symbols; dashed fits). Reprinted with permission from Halsey, C. M.; Xiong, J.; Oshokoya, O. O.; Johnson, J. A.; Shinde, S.; Beatty, J. T.; Ghirlanda, G.; JiJi, R. D.; Cooley, J. W., Simultaneous Observation of Peptide Backbone Lipid Solvation and α-Helical Structure by Deep-UV Resonance Raman Spectroscopy. *ChemBioChem* 2011, *12* (14), 2125-2128. Copyright 2011 John Wiley and Sons.

the light harvesting complex/reaction center/pufX supercomplex, and “chromatophore" native lipid membranesubfractions from lysed bacterial cells. Despite subtle differences in the positions and intensities of the Am I and II modes, owing to the varied structural and transmembrane contents of the varied membrane protein samples, the intense Am I mode is a ubiquitous DUVRR marker for all of the protein samples with lipid solvated helical regions (Figure 5-4).

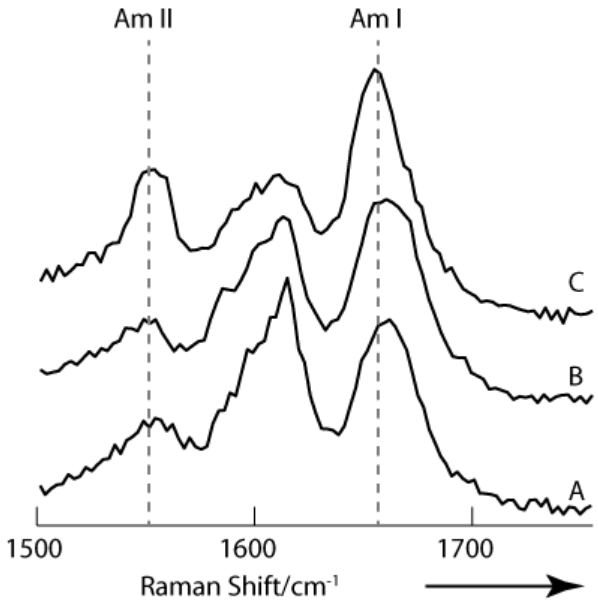

Figure 5-4. Deep-UV resonance Raman spectra of various membrane protein samples. DUVRR spectra of *Rhodobacter* derived A) purified cytochrome bc1 complex, B) light harvesting comple/reaction center/Puf X supercomplexes, and C) chromatophore membranes. Protein, detergent, and buffer concentrations are listed in the experimental section. Spectra were collected and processed as in Figure 5-1. Reproduced with permission from Halsey, C. M.; Xiong, J.; Oshokoya, O. O.; Johnson, J. A.; Shinde, S.; Beatty, J. T.; Ghirlanda, G.; JiJi, R. D.; Cooley, J. W., Simultaneous Observation of Peptide Backbone Lipid Solvation and α-Helical Structure by Deep-UV Resonance Raman Spectroscopy. *ChemBioChem* 2011, *12* (14), 2125-2128. Copyright 2011 John Wiley and Sons.

5.5 Conclusion

This work illustrates for the first time that DUVRR spectroscopic analysis of protein secondary structural content can be feasibly extended to membrane-associated peptides. The Am I mode of ME1 appears to be dominated by the "de-solvated" region of the protein, making it a potentially valuable marker for membrane embedded protein structure. Thus, DUVRR spectroscopy may provide a unique spectral avenue by which to selectively distinguish between lipid and aqueous solvated portions of the ensemble secondary structure, thereby providing a valuable tool for the structural study of the lipid solvated portion of any number of amphiphilic peptides in a time-resolved manner.

5.6 Bibliography

1. White, S. H., Biophysical dissection of membrane proteins. *Nature (London, U. K.)* **2009,** *459*, 344-346.

2. (a) Austin, J. C.; Jordan, T.; Spiro, T. G., Ultraviolet Resonance Raman Studies of Proteins and Related Model Compounds. In *Biomolecular Spectroscopy, Part A*, Clark, R. J. H.; Hester, R. E., Eds. John Wiley & Sons: Chichester, 1993; pp 55-127; (b) Asher, S. A.; Mikhonin, A. V.; Bykov, S., UV Raman Demonstrates that α-Helical Polyalanine Peptides Melt to Polyproline II Conformations. *Journal of the American Chemical Society* **2004,** *126*, 8433-8440; (c) Shashilov, V. A.; Lednev, I. K., 2D Correlation Deep UV Resonance Spectroscopy of Early Events of Lysozyme Fibrillation: Kinetic Mechanism and Potential Interpretation Pitfalls. *J. Am. Chem. Soc.* **2008,** *130*, 309-317; (d) Shashilov, V. A.; Lednev, I. K., Advanced Statistical and Numerical Methods for Spectroscopic Characterization of Protein Structural Evolution. *Chem. Rev. (Washington, DC, U. S.)* **2010,** *110*, 5692-5713.

3. (a) Chi, Z.; Chen, X. G.; Holtz, J. S. W.; Asher, S. A., UV resonance Raman-selective amide vibrational enhancement: quantitative methodology for determining protein secondary structure. *Biochemistry* **1998,** *37*, 2854-2864; (b) Huang, C.-Y.; Balakrishnan, G.; Spiro, T. G., Protein secondary structure from deep-UV resonance Raman spectroscopy. *Journal of Raman Spectroscopy* **2006,** *37*, 277-282; (c) Shashilov, V.; Sikirzhytski, V.; Popova, L. A.; Lednev, I. K., Quantitative methods for structural characterization of proteins based on deep UV resonance Raman spectroscopy. *Methods* **2010,** *52*, 23-37.

4. (a) Wang, Y.; Purrello, R.; Georgiou, S.; Spiro, T. G., UVRR spectroscopy of the peptide bond. 2. Carbonyl H-bond effects on the ground- and excited-state structures of N-methylacetamide. *Journal of the American Chemical Society* **1991,** *113*, 6368-6377; (b) Markham, L. M.; Hudson, B. S., *Ab Initio* Analysis of the Effects of Aqueous Solvation on the Resonance Raman Intensities of *N*-Methylacetamide. *J. Phys. Chem.* **1996,** *100*, 2731-2737; (c) Torii, H.; Tatsumi, T.; Tasumi, M., Effects of Hydration on the Structure, Vibrational Wavenumbers, Vibrational Force Field and Resonance Raman Intensities of *N*-Methylacetamide. *J. Raman Spectrosc.* **1998,** *29*, 537-546; (d) Ozdemir, A.; Lednev, I. K.; Asher, S. A.,

UVRR spectroscopic studies of valinomycin complex formation in different solvents. *Spectrochim. Acta, Part A* **2005,** *61*, 19-26; (e) Popova, L. A.; Kodali, R.; Wetzel, R.; Lednev, I. K., Structural variations in the cross-β core of amyloid β fibrils revealed by deep UV resonance Raman spectroscopy. *J. Am. Chem. Soc.* **2010,** *132*, 6324-6328; (f) Hayashi, T.; Mukamel, S., Electrostatic DFT Map for the Complete Vibrational Amide Band of NMA. *J. Phys. Chem. A* **2005,** *109*, 9747-9759; (g) Mukherjee, S.; Chowdhury, P.; Gai, F., Infrared Study of the Effect of Hydration on the Amide I Band and Aggregation Properties of Helical Peptides. *J. Phys. Chem. B* **2007,** *111*, 4596-4602.

5. Valkova-Valchanova, M. B.; Saribas, A. S.; Gibney, B. R.; Dutton, P. L.; Daldal, F., Isolation and characterization of a two-subunit cytochrome b-c_1 subcomplex from *Rhodobacter capsulatus* and reconstitution of its ubihydroquinone oxidation (Q_o) site with purified Fe-S protein subunit. *Biochemistry* **1998,** *37*, 16242-16251.

6. Abresch, E. C.; Axelrod, H. L. A.; Beatty, J. T.; Johnson, J. A.; Nechushtai, R.; Paddock, M. L., Characterization of a highly purified, fully active, crystallizable RC-LH1-PufX core complex from *Rhodobacter sphaeroides Photosynth. Res.* **2005,** *86*, 61-70.

7. Balakrishnan, G.; Hu, Y.; Nielsen, S. B.; Spiro, T. G., Tunable kHz deep ultraviolet (193-210 nm) laser for Raman applications. *Appl. Spectrosc.* **2005,** *59*, 776-781.

8. Ferraro, J. R.; Nakamoto, K., *Introductory Raman Spectroscopy*. Academic Press: Boston, 1994.

9. Cordova, J. M.; Noack, P. L.; Hilcove, S. A.; Lear, J. D.; Ghirlanda, G., Design of a functional membrane protein by engineering a heme-binding site in glycophorin A. *Journal of the American Chemical Society* **2007,** *129*, 512-518.

10. Fodor, S. P. A.; Copeland, R. A.; Grygon, C. A.; Spiro, T. G., Deep-Ultraviolet Raman Excitation Profiles and Vibronic Scattering Mechanisms of Phenylalanine, Tyrosine, and Tryptophan. *J. Am. Chem. Soc.* **1989,** *111*, 5509-5518.

11. (a) JiJi, R. D.; Balakrishnan, G.; Hu, Y.; Spiro, T. G., Intermediacy of Poly(L-Proline) II and β-Strand Conformations in Poly(L-Lysine) β-Sheet Formation Probed by Temperature-Jump/UV Resonance Raman Spectroscopy. *Biochemistry* **2006,** *45*, 34-41; (b) Simpson, J. V.; Balakrishnan, G.; JiJi, R. D., MCR-ALS analysis of two-way UV resonance Raman spectra to resolve discrete protein secondary structural motifs. *Analyst* **2009,** *134*, 138-147.

12. Mikhonin, A. V.; Ahmed, Z.; Ianoul, A.; Asher, S. A., Assignments and Conformational Dependencies of the Amide III Peptide Backbone UV Resonance Raman Bands. *Journal of Physical Chemistry B* **2004,** *108*, 19020-19028.

13. Xiong, K.; Asher, S. A., Lowest Energy Electronic Transition in Aqueous Cl^- Salts: $Cl^- \rightarrow (H_2O)_6$ Charge Transfer Transition. *J. Phys. Chem. A* **2011**.

14. Song, S.; Asher, S. A., UV resonance Raman studies of peptide conformation in poly(L-lysine), poly(L-glutamic acid), and model complexes: the basis for protein secondary structure determinations. *J. Am. Chem. Soc.* **1989,** *111*, 4295-4305.

15. Simpson, J. V.; Oshokoya, O.; Wagner, N.; Liu, J.; JiJi, R. D., Pre-processing of ultraviolet resonance Raman spectra. *Analyst* **2011,** *136*, 1239-1247.

16. (a) White, S. H.; von Heijne, G., Transmembrane helices before, during, and after insertion. *Curr. Opin. Struct. Biol.* **2005,** *15*, 378-386; (b) White, S. H., Membrane Protein Insertion: The Biology-Physics Nexus. *J. Gen. Physiol.* **2007,** *129*, 363-369.

Chapter 6: Influence of the Lipid Environment on Valinomycin Structure and Cation Complex Formation

Adapted with permission from Halsey, C. M.; Benham, D. A.; JiJi, R. D.; Cooley, J. W., Influence of the Lipid Environment on Valinomycin Structure and Cation Complex Formation. *Spectrochimica Acta Part A: Molecular and Biomolecular Spectroscopy* **2012,** *96*, 200-206.

6.1 Abstract

Carrier-type molecular ionophores, such as the cyclic dodecadepsipeptide valinomycin, often must undergo structural changes during the binding and transport of a cation across the lipid membrane. Observing the structural fluctuations that occur during this process experimentally has proven extremely difficult due to the complexities of spectroscopic analysis of protein structure/dynamics in native lipid bilayer environments. Currently, our understanding of how valinomycin selectively transports ions across membranes is derived from atomic structures solved of the cyclic macromolecule solvated in various organic solvents and complimentary *in silico* dynamics experiments. We have shown recently that deep-UV excited resonance Raman spectroscopy (DUVRR) has a unique ability to characterize secondary structure content and simultaneously provide information about the relative solvation of the probed peptide backbone[1]. Interpretation of DUVRR spectra of valinomycin in swelled lipid and unilamellar lipid bilayer environments indicate that the uncomplexed valinomycin molecule dynamically samples both the open and closed conformations as described for the structures derived from polar and non-polar organic solvents, respectively. Upon introduction of potassium, the structure of valinomycin in swelled lipid environments resembles more closely that of the open conformation. The shift in structure upon complexation is accompanied by a significant decrease in the valinomycin DUVRR spectral amide I intensity, indicating that the open conformation is more water solubilized and is seemingly “trapped” or predominantly located close to the lipid-water interface. The trapping of the valinomycin in the act of complex of potassium at the bilayer-solvent

interface and its analysis by DUVRR represents the first spectroscopic description of this state. Conversely, an opposite trend is observed in the amide I intensity upon potassium complexation in unilamellar (or extruded) vesicles, implying the predominant conformation upon potassium binding in native bilayers is one where the peptide backbone of valinomycin is desolvated as would be expected if the molecule were more readily able to traverse a bilayer interior. Interpretation of the DUVRR spectral features is also consistent with the loss or formation of hydrogen bonds observed in the open and closed structures, respectively. Valinomycin must then sample several conformations in the absence of appropriate ions depending upon its locale in the lipid bilayer until potassium causes a greater degree of closure of the open conformer and an increased residency within the more non-polar interior. The potassium induced decreased solubility enables diffusion across the membrane where potassium release can occur by equilibration at the opposite lipid water interface.

6.2 Introduction

The ionophore valinomycin (Val) belongs to a broad class of antimicrobial peptides that alter the function and integrity of lipid bilayers. Val itself is a potent K^+ ion transporter, which has been used extensively in a variety of studies to collapse membrane potentials (⍰ψ) during investigations of membrane trafficking and enzyme catalysis[2]. The simplicity of Val's molecular architecture has facilitated its use as a model for how selective membrane transport is achieved by antimicrobial peptides. Val is a dodecadepsipeptide comprised of a repeating, cyclic trimer of alternating peptide and ester bonds whose formula can be written as cyclo-(D-valine-L-Lac-L-valine-D-Hyv)$_3$ where Lac is lactic acid and Hyv is hydroxyvaleric acid. The valine residues alternate between the D and L conformations and, thus, the stereochemistry lends itself to a general tennis ball seam appearance, moderated by breaking and forming hydrogen bonds intramolecularly or with polar solvent (Figure 6-1). The six amide

carbonyls are all oriented towards the metal cation forming a near ideal octahedral environment for complexation, selective for potassium based on ionic radius[3].

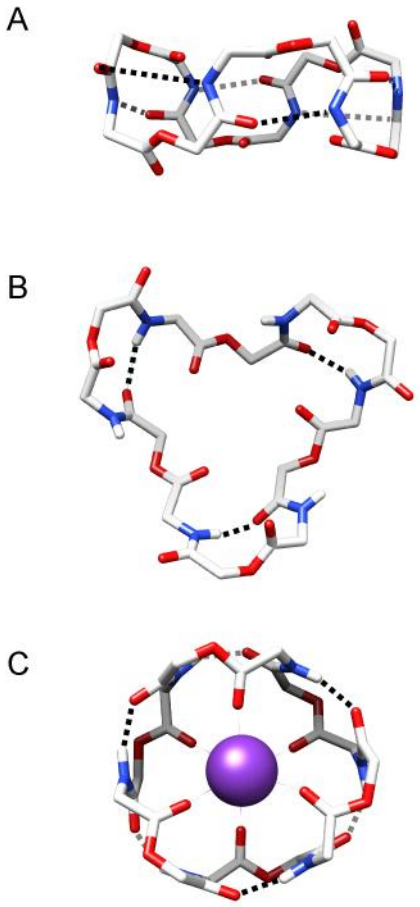

Figure 6-1. Various structural forms of Val. Representations of the crystal structures derived from (A) non-polar (Cambridge Database ID: VALINM30), (B) polar solvent (GEYHOH), and (C) complexed to potassium (purple) (VALINK). Dashed lines represent hydrogen bonds, with the two planes of bonds indicated as black or gray. Structure are taken from references 30-32. Reprinted with permission from Halsey, C. M.; Benham, D. A.; JiJi, R. D.; Cooley, J. W., Influence of the Lipid Environment on Valinomycin Structure and Cation Complex Formation. *Spectrochimica Acta Part A: Molecular and Biomolecular Spectroscopy* 2012, *96*, 200-206. Copyright 2012 Elsevier.

The mechanism of the potassium-selective ionophore has been a target of biophysical spectroscopic efforts dating back to its initial isolation from *Streptomyces fulvissimus* in 1955 and total synthesis in 1963[4]. Historically Val was the first ionophore whose structure was derived from spectroscopic methods prior to obtaining an atomic structure[5]. The uncomplexed state is highly sensitive to solvent polarity while the complexed state is only weakly so. Three conformations of the uncomplexed state vary from fully hydrogen bonded valine residues to no intramolecular hydrogen bonding. In general, Val adopts a relatively rigid structure in non-polar medium and a more flexible structures in more polar organic media[6]. Of these conformations, previously[7] named the A, B, and C

states, the structures solved in non-polar (*n*-octane) (Figure 6-1A) and medium polarity (dimethyl sulfoxide) (Figure 6-1B) are thought to represent the most biologically relevant. Of particular note when examining the structure of the solved structures is differing hydrogen bonding of the amide backbone. Specifically, conformation A features six 4→1 type intramolecular hydrogen bonds between an amide (Am) N-H and carbonyl oxygen (Figure 6-1A). In the more flexible conformation B, only three intramolecular hydrogen bonds remain and are formed by the D-valine NH group to the Am carbonyl (Figure 6-1B). The consequence is an open conformation on one side of the ring. Upon complexation, the ester carbonyls coordinate a central potassium atom while maintaining the hydrogen bonding motif similar to that of conformation A (Figure 6-1C), regardless of solvent polarity. All that is known about the structure of Val and its changes with K^+ binding are presently derived from studies carried out in organic solvent environments, which lack the amphiphilic and ordered phase geometries of a lipid bilayer or membrane.

Determination of biomolecular conformation within lipid membranes has improved dramatically in terms of the complexity and size of the structures capable of being solved[8]. X-ray diffraction or NMR methods have not generally been amenable to samples of Val solubilized in lipid bilayers due to its rapid structural dynamics and the atomic complexity associated with the lipid milieu. However, lower resolution techniques like CD, IR, and Raman spectroscopy have been invaluable for the structural characterization of Val, especially in solution. To date, no single technique has been successful in interrogating Val's structure while it is present in dilute concentrations in the native lipid membrane. In the few cases where structural information has been accomplished in native membranes, the techniques have required laborious sample modification, usually via selective isotopic labeling. Deep-UV resonance Raman spectroscopy (DUVRR) takes advantage of the sensitivity of resonance Raman spectroscopy to backbone conformation while selectively enhancing the Am backbone vibrational signals[9]. This is accomplished by using excitation energies near the peptide's electronic transitions below

210 nm. Neither water nor lipid scattering is enhanced in this region and therefore contributions from the membrane are negligible in the DUVRR spectrum. Additionally, while deuteration can be informative, it is not required to produce spectra whose interpretation can provide valuable insight. DUVRR spectroscopy has proven to be a powerful technique for the determination of secondary structure of soluble, globular proteins[10] , even quantifying β-turns[11], and has been extended only recently to the structural characterization of membrane proteins. In doing so, a unique sensitivity of the technique has been established for peptide backbone solvation allowing for simultaneous solvation and structural characterizations of peptides and proteins[1, 12].

Contributions from the non-classical D amino acids and ester linkages of the depsipeptides backbone are not altogether understood, however, DUVRR spectra are a sum of the vibrational influences of the ϕ and ψ torsion angles of the backbone, which should not be significantly affected by D amino acids [13]. Therefore, we present here the first study of the structural transitions of Val as a function of cation binding and lipid environment phase, revealing significant insights into the mechanistic steps of cation binding and transmembrane transport.

6.3 Materials and Methods

6.3.1 Preparation of non-extruded lipid and unilamellar liposome solutions

Val (MP Biomedicals) was dissolved in methanol to a 10 mg/mL solution. For non-extruded (NE) lipid samples, aliquots of Val were mixed with dimyristoyl phosphatidylcholine (DMPC) in chloroform (Avanti Polar Lipids) and dried under a stream of argon, followed by at least one hour under vacuum to remove residual solvent. Hydration in 18.2 MΩ· cm water (Barnstead) or sodium phosphate buffer (pH 7) was followed by tip sonication for 2 minutes. Unilamellar liposomes were prepared by extrusion after rehydration through a 50 nm radius filter (Liposofast). Val was titrated into liposome solutions from

methanol stock solutions. DMPC concentration was determined via phosphate assay[14]. Stocks of potassium chloride in water and methanol were used for potassium complexation experiments.

6.3.2 DUVRR

Sodium perchlorate (Sigma) was added as an internal intensity standard for DUVRR measurements after suitable spectra had been collected without sodium present. Val samples measured in excess sodium had sodium perchlorate and sodium phosphate present. Final concentrations of samples analyzed by DUVRR were 0.5 mg mL^{-1} valinomycin and 3.1 mM DMPC. The DUVRR instrument has been described previously[15] and laser power at the sample was attenuated to 500 μW or less to avoid damage to the sample.

6.4 Results

6.4.1 DUVRR spectra of valinomycin in NE and extruded lipid environments

DUVRR spectra were acquired of Val in NE and extruded DMPC at 197 nm excitation (Figure 6-2). Despite the fact that the cyclic depsipeptide is not a true polypeptide chain, the DUVRR spectra is dominated by the vibrational modes derived from the Am related vibrational modes as observed previously in organic solvents [16]. Examination of the swelled lipid, NE, solubilized Val samples reveals peak maxima characteristic of the Am I (1673 cm^{-1}), II (1547 cm^{-1}), III (1244/1290 cm^{-1}) and an Am S (a $C_{\alpha}H$ bending coupled mode, 1389 cm^{-1}) bands (Figure 6-2 and Table 6-1). The relative peak positions are consistent with peak maxima observed previously in the organic solvents, implying that the structure of the molecule may be similar between the two conditions of solubilization. Closer examination reveals that the Am I and II DUVRR spectral features of Val solubilized in NE DMPC lipids are intermediate in position and intensity between spectra obtained in polar or non-polar solvents. This result is not entirely consistent with previous studies indicating that the structure of Val in the lipid phase is most similar to

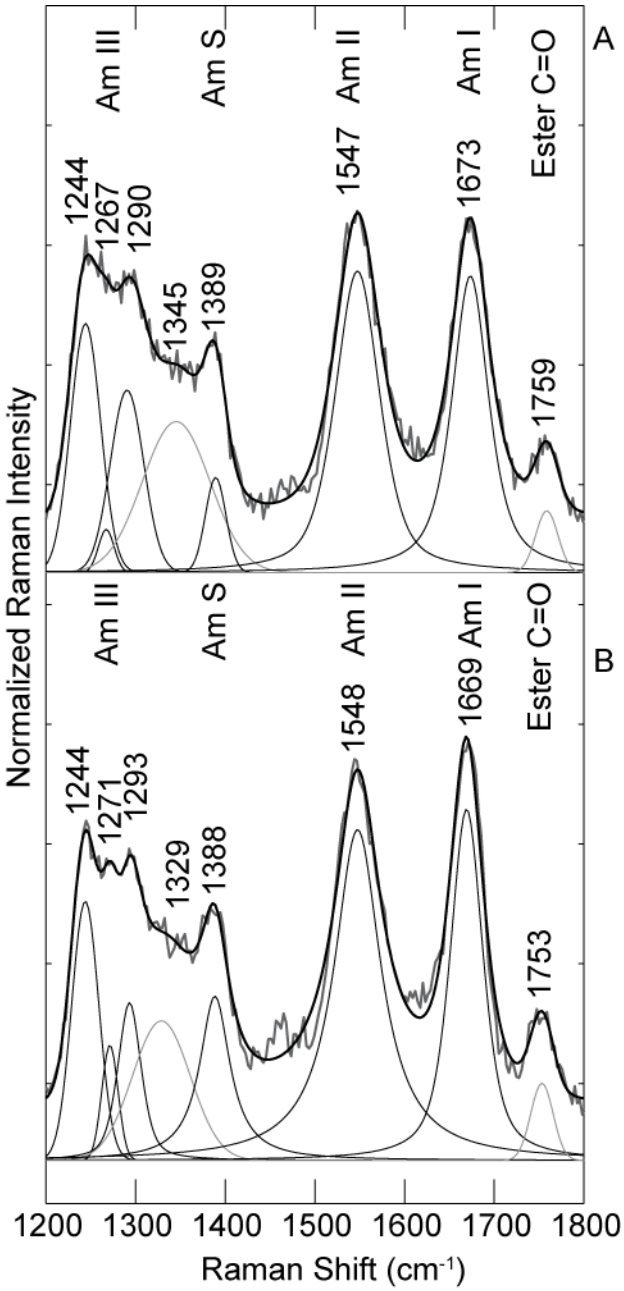

Figure 6-2. DUVRR spectra of Val in different lipid environments. DUVRR spectra of Val (0.5 mg/mL) solubilized in NE lipids (top panel) and SUV's (bottom panel) using a 197 nm excitation source. Non-linear least square fits are included for each spectrum to more accurately determine the associated vibrational frequencies (in wavenumbers) as indicated. Reprinted with permission from Halsey, C. M.; Benham, D. A.; JiJi, R. D.; Cooley, J. W., Influence of the Lipid Environment on Valinomycin Structure and Cation Complex Formation. *Spectrochimica Acta Part A: Molecular and Biomolecular Spectroscopy* 2012, *96*, 200-206. Copyright 2012 Elsevier.

structures determined in non-polar chloroform phases[17]. As it is clear that the solvent environment can significantly alter the equilibrium structural interconversion between a closed and open form, the nature of the lipid environment might also have an influence towards the Val structure or structural equilibrium. To investigate this possibility, we have also examined by DUVRR the structure of Val solubilized by in NE and extruded (SUV's) DMPC lipid environments. DUVRR spectra of Val solubilized in monodisperse DMPC SUV's display Am mode positions that are very similar to those of Val found in

swelled lipid environments. A small red shift (4 cm^{-1}) in the Am I mode and a similar shift in the hydrogen bond free ester carbonyl stretching mode 1759 cm^{-1} to 1753 cm^{-1} is observed for Val going from NE lipid to SUV lipid samples (Figure 6-2). While this small spectral change is consistent with a shift towards the proposed closed structures observed with bound metal cations, the spectral change is small and more likely represent a subtle shift in the equilibrium Val structure rather than a rigid snapping into place of one conformation or the other. These observations, which imply that the Val molecules are still structurally flexible even after lipid solubilization, led us to examine to what extent the introduction of metal cations would influence this conformational flexibility in the lipid environment.

6.4.2 Effects of potassium complexation on lipid solubilized valinomycin

While there is a great deal understood about how Val binds a cationic metal in various organic solvents, it remains unclear what specific events lead to metal binding and transport within and across a membrane. For instance, what the structure of Val looks like before and after binding the metal is unclear as solvents cannot effectively mimic the membrane surface-water interface. In an effort to understand how metal complexation influences the structure of Val in a lipid environment, DUVRR were collected with the uncomplexed ionophore pre-equilibrated within a lipid regime. Any conclusions about Val metal binding and ion transport function must also take into account the nature of the lipid regime within which the ionophore is equilibrated as each will have differing solvent interactions as the lipid head group surface. In the NE lipid environment, a upon KCl addition a decrease in intensity is observed in the Am I, II, and in portions of the Am III modes (near 1670, 1548 and 1244 cm^{-1}, respectively), which was accompanied by a blue shift of the Am II mode from 1548 to 1554 cm^{-1} (Figure 6-3A and Table 2). The addition of equimolar potassium to Val pre-equilibrated into a DMPC lipid bilayer (SUV's) similarly caused the Am II mode to blue shift from 1548 to 1551 cm^{-1} for the metal ligated complex (Val-K), while also decreasing this modes intensity. However, an opposite effect on the Val DUVRR Am I and II mode intensities is observed when extruded and NE Val-K samples are compared. Specifically, the Am I mode

decreased or increased in intensity upon introduction of potassium to Val solubilized in NE lipid and SUV lipids, respectively. The changes in the intensity of the Am I mode are characteristic of changes in the extent of hydration of the amide carbonyl moiety, indicating that potassium addition may change the equilibrium location of the Val molecule within the membrane. Perhaps most interesting with respect to the mechanism of ion transport by Val is that the disparate changes in the Am mode intensities and spectral positions following introduction of potassium between NE lipids and SUV's implies that the Val structure is in an intermediate ensemble form, between a solvated and lipid solubilized form, prior to metal binding.

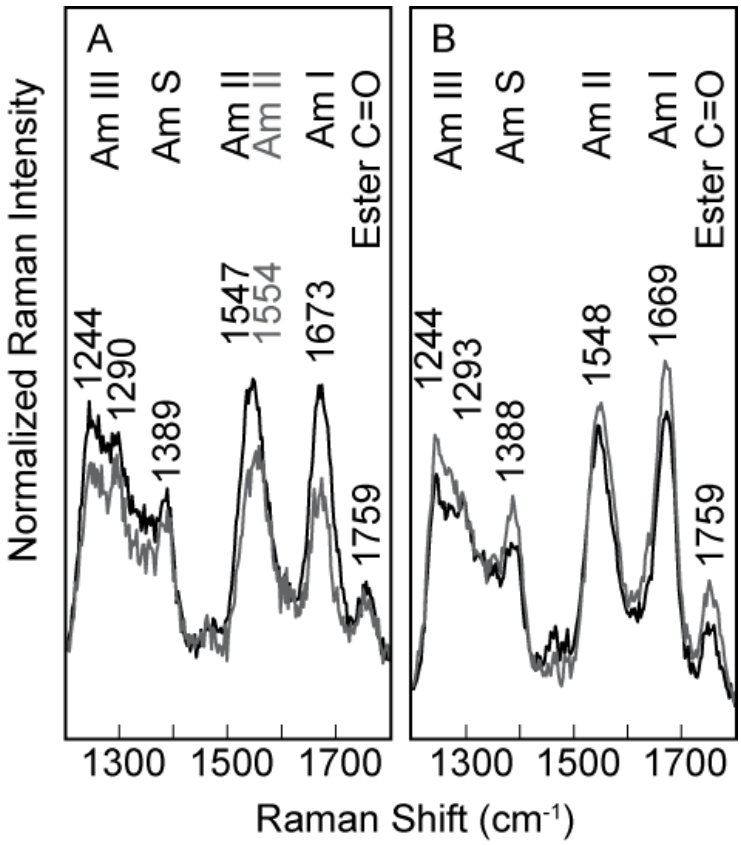

Figure 6-3. DUVRR spectra of post-equilibrated Val-K complexes. Potassium was titrated into valinomycin solubilized in NE lipids (panel A) and SUV's (panel B). Val in lipid (black line) was mixed with potassium chloride at a 1:1 mole ratio (gray line). Vibrational frequencies for each assigned mode are indicated as well as any significant shifts. Reprinted with permission from Halsey, C. M.; Benham, D. A.; JiJi, R. D.; Cooley, J. W., Influence of the Lipid Environment on Valinomycin Structure and Cation Complex Formation. *Spectrochimica Acta Part A: Molecular and Biomolecular Spectroscopy* 2012, *96*, 200-206. Copyright 2012 Elsevier.

6.4.3 Pre-equilibrium of valinomycin with potassium in NE lipids and SUV's

In light of the differences in the Val-K DUVRR spectra in NE lipids and SUV's, we sought to test whether the interaction of Val with potassium is altered as a function of the molecules structure when pre-equilibrated in the lipid environment. Therefore, DUVRR spectra were collected of Val equilibrated with potassium prior to the subsequent interaction with a lipid phase. In both lipid phase cases, a clear trend is seen in the DUVRR spectra of pre-equilibrated Val-K upon lipid solvation (Figure 6-4), which both include increases in the intensities of the Am I, II and portions of the Am III mode. Additionally, both NE lipid and SUV pre-equilibrated Val-K DUVRR spectra display similar Am I (1672/1671 cm^{-1}) and Am II (1545/1540 cm^{-1}) spectral positions as well as the appearance of a strong Am III (1290 cm^{-1}) feature (Table 6-2). DUVRR spectra of the post-equilibrated Val-K between the NE lipid and SUV environments must be attributable to differences of the environment of Val while at the membrane surface.

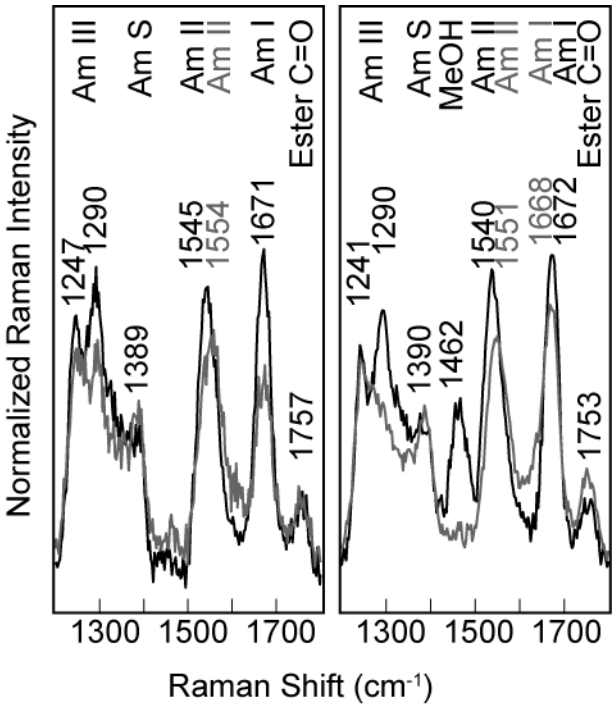

Figure 6-4. DUVRR spectra of pre- and post-equilibration of Val-K. Val was equilibrated with potassium before or after incorporation into NE lipids (panel A) and SUV's (panel B). Pre- (black spectrum) and post- (gray spectrum) equilibration were prepared as described in the materials and methods section. Reprinted with permission from Halsey, C. M.; Benham, D. A.; JiJi, R. D.; Cooley, J. W., Influence of the Lipid Environment on Valinomycin Structure and Cation Complex Formation. *Spectrochimica Acta Part A: Molecular and Biomolecular Spectroscopy* 2012, *96*, 200-206. Copyright 2012 Elsevier.

6.4.4 Potassium complexation by lipid solubilized valinomycin in the presence of competing cations

In the presence of superstoichiometric concentrations of sodium ions in NE lipid and SUV solubilized Val solutions, the DUVRR spectrum of Val closely resembles that of the pre-equilibrated Val-K spectra. Specifically, the spectra are characterized by the Am I mode being more intense than the Am II, the presence of a clear 1290 cm^{-1} Am III mode, and peak maxima at 1669/1673 cm^{-1} and 1547/1548 cm^{-1} for the Am I and II, respectively. However, despite a well-documented greater affinity of valinomycin for potassium than for sodium ions, valinomycin DUVRR spectra display no noticeable changes upon addition of stoichiometric potassium (Figure 6-5 and Table 3). This observation implies that the sodium-Val complex and Val-K structures are similar within the lipid environment, which is in line with previous observations from organic solvent solubilized Val.

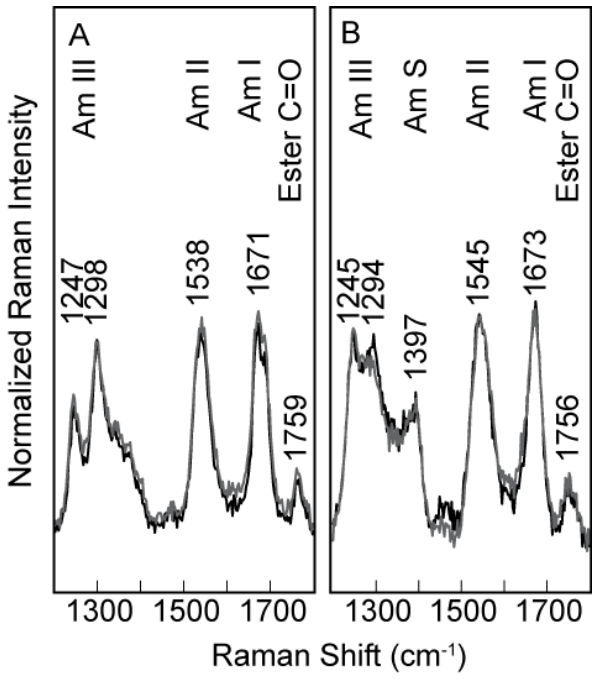

Figure 6-5. DUVRR spectra of Val-K as a function of NaCl concentration. Potassium was titrated in Val in NE lipids (panel A) and SUV's (panel B) in the presence and absence of sodium. Sodium perchlorate (100 mM) and monobasic sodium phosphate (120 mM) was present in a 450 µM Val solution (black line), when potassium chloride was added at a 1:1 mole ratio (gray line). Reprinted with permission from Halsey, C. M.; Benham, D. A.; JiJi, R. D.; Cooley, J. W., Influence of the Lipid Environment on Valinomycin Structure and Cation Complex Formation. *Spectrochimica Acta Part A: Molecular and Biomolecular Spectroscopy* 2012, *96*, 200-206. Copyright 2012 Elsevier.

Table 6-1. Raman Shifts (cm^{-1}) of Amide Modes of Valinomycin Without Na^+/K^+ in DUVRR Spectra

	Amide Modes								
Environment	III_c	III_b	III_a	S	II	I	Ester C=O	λ_{ex}[b]	Source
Methanol	1245	NF[a]	1298	1389	1555	1639/1680	1758	206	[16]
Cyclohexane	1241	NF[a]	1298	1370	1532	1667	1758	206	[16]
NE lipids	1244	1267	1290	1389	1547	1673	1759	197	This study
SUV	1244	1271	1293	1388	1548	1669	1753	197	This study

a. NF, not fit
b. Excitation wavelength in nm, and also in Table 2 and 3.

Table 6-2. Raman Shifts (cm^{-1}) of Amide Modes of Valinomycin with KCl in DUVRR Spectra

	Amide Modes								
Environment[a]	III_c	III_b	III_a	S	II	I	Ester C=O	λ_{ex}	Source
Methanol	1245	NF	1298	1389	1542	1640/1673	1758	206	[16]
NE lipids, pre	1246	1269	1294	1388	1545	1671	1758	197	This study
NE lipids, post	1246	1269	1294	1388	1554	1671	1758	197	This study
SUV, pre	1245	1271	1290	1390	1540	1672	1755	197	This study
SUV, post	1245	1271	1290	1390	1551	1668	1755	197	This study

a. Pre and post refer to exposure of valinomycin to K^+ prior to or after hydration in buffer.

Table 6-3. Raman Shifts (cm^{-1}) of Amide Modes of Valinomycin with $NaClO_4$ in DUVRR Spectra

	Amide Modes							
Environment	III_c	III_b	III_a	S	II	I	Ester C=O	λ_{ex}
NE lipids	1240	1266	1290	1393	1538	1670	1747	197
Liposomes	1245	1270	1293	1389	1551	1671	1753	197

6.5 Discussion

6.5.1 Influence of lipid solvation and membrane locale on valinomycin structural ensembles

Extensive analyses of Val conformation(s) have been reported for solubilization in organic solvents of varying polarities [18]. Surprisingly, despite the breadth in technique and age of intensive studies of Val structure and function, very few studies have been carried out in the environment where

Val carries out its ion transport function, lipid bilayers. In fact, there have only been three previous reports of Val structural analysis in an intact lipid membrane [17, 19]. These studies utilized either changes in chemical shifts of ^{1}H NMR or amide I' carbonyl stretching frequencies in FTIR spectra and all three studies came to the conclusion that the ensemble structure of the complexed and uncomplexed Val resided within the lipid bilayer in the closed form. Additionally, findings by FTIR went on to state that the Val structure in NE lipids and liposomes was determined to be essentially identical with molecules probed in non-polar organic solvents. Our findings here using a sensitive DUVRR technique corroborate at face value that the ensemble structure of the uncomplexed Val is similar to what has been described previously in organic solvents. However, despite the initial similarities between the two lipid phases and to previous organic solvent analyses, it is clear that the spectra are intermediate between the fully complexed (Na^{+} or K^{+}) and uncomplexed forms of Val and in SUV's and Val-K in NE lipids. In fact, the observation that the uncomplexed form resides in an intermediate configuration is indicated by both a ensemble structural intermediate and an intermediate locale in the membrane as the DUVRR spectra Am II position is intermediate between the two post-equilibrated Val-K DUVRR spectra (indicative of intermediate ensemble structure and intramolecular hydrogen bonding) and a middle ground for Am I mode intensity (indicative of a mixed content of carbonyl hydration). In fact, if one takes into consideration that the intensity of the Am I mode likely directly reflects the extent of the solvation of the carbonyl modes, independent of their hydrogen bonding with the macromolecule, the molecule in the uncomplexed form is likely dynamically associated with the interior and surface of the lipid bilayer in both NE and SUV lipids.

It is important to note that the conclusions made in this work are made using the single spectroscopic technique DUVRR and samples are devoid of isotopic, paramagnetic, or primary structure manipulations, yet the interpretations are in perfect agreement with higher resolution NMR based assays, which argued that the uncomplexed form of Val must transiently "visit" the surface of the lipid

bilayer to acquire potassium ions. This transient visitation was based upon very subtle differences in NMR Val chemical shifts borne from interactions with a variety of paramagnetic shift reagents bound to the membrane surface [17a]. Interestingly, UV (206 and 229 nm excitation) resonance Raman spectra of Val have also been reported [16] in methanol and cyclohexane showing a similar trend with respect to the Am II position and Am I intensity going from polar to non-polar environments. Specifically, similar Am I and II maxima are observed, while the intensity of the Am I mode is also seen to increase in the more non-polar cyclohexane environment. Despite the similarities between DUVRR spectra collected previously in non-polar solvents and in lipids environs here, significant differences in the Am III region are clear. Therefore, the equilibrium structure in the more native lipid environment represents an ensemble of structures previously unseen in solvent. While, the established phenomenology for the response of the Am III region in polypeptides is not wholly applicable to a depsipeptide backbone, it should be noted that the feature that grows in at 1290 cm^{-1} with potassium complexation is also prominent in □-helical dominated spectra where strong intramolecular hydrogen bonding and structural rigidity are the dominant features. Furthermore, this interpretation of stronger equilibrium hydrogen bonding and reduced phi/psi angle sampling is consistent with what should be a more static Val structure upon tight complexation of the alkali-cation.

6.5.2 Implications for potassium binding and transport

The influence of potassium binding on the Val DUVRR spectrum is very informative for understanding how potassium is transported across a membrane. DUVRR spectra indicate that uncomplexed Val samples differing environments and different ensembles of structure prior to the addition of potassium. Specifically, the uncomplexed form of Val samples the water/lipid interface in both lipid forms as evidenced by the substantial spectral changes upon addition of potassium. Conversely, the intensity of the Am I mode is either increased or decreased following potassium binding in lipid bilayers or NE lipids, respectively, implying that the carbonyls are more or less shielded from

forming hydrogen bonds with water molecules. Interestingly, in the post-equilibrated Val-K both Am II modes are shifted in the same manner that the DUVRR of the Am II is shifted when Val goes from non-polar to polar solvents. Since the previous studies should correlate directly to the states from which the atomic structures are derived, the changed Am II mode upon complexation likely indicates a subtle decrease in the intramolecular hydrogen bonding. Thus, in both cases the ensemble internal hydrogen bonded content is diminished, while in the hydrated NE swelled lipid environment the carbonyl mode is indicating a more aqueous environment. One explanation for this difference and for the difference between the pre- and post-equilibrated Val-K DUVRR spectra is that the "locking" of the closed form is less stable when potassium is in dynamic equilibrium with the aqueous environment. The differences between the NE lipid and SUV post-equilibrated cases can be rationalized as a function of the extent of water penetration into the membrane surface in each case. Therefore, Val closes upon coordination of the alkali-cation as long as there is not too much water penetration present at the lipid membrane surface, but the dynamics are such that the latter set of internal 4$\rightarrow$1 hydrogen bonding is less static than in non-polar organic solvents. In essence, this implies that the Val-K is trapped in a partially open conformation less hydrophobic state in the more hydrated NE lipids. This will hold interest for future investigators using *in silico* means by which to describe the dynamics and thermodynamic forces necessary for ion transport as it is an experimental benchmark for a distinct transient state of the process. It is logical to assume that in a native membrane bilayer, like the SUV's used here, that Val-K is free to more readily sample the internal hydrophobic core of the membrane as long as there is an intact barrier to water penetration at the membrane surface (Figure 6-6), but still readily samples the surface (open and closed states) as evidenced by the Am II mode shifts.

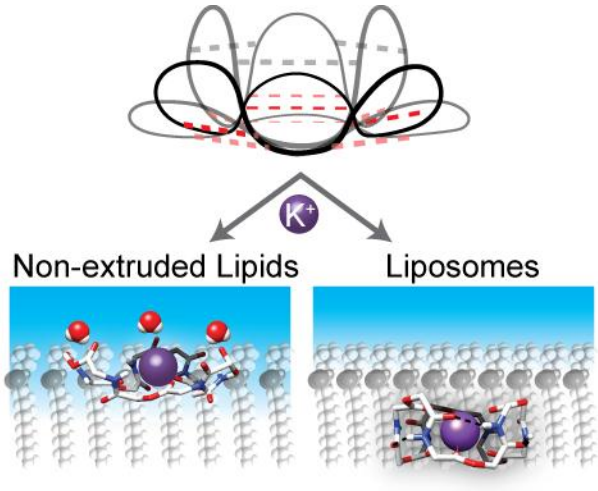

Figure 6-6. Model of Val structure during potassium binding in differing lipid environments. Representation of proposed valinomycin conformation in equilibrium without potassium present (intramolecular hydrogen bonds shown in dashed lines) and degree of backbone hydration when complexed to potassium in NE lipids and liposomes. Reprinted with permission from Halsey, C. M.; Benham, D. A.; JiJi, R. D.; Cooley, J. W., Influence of the Lipid Environment on Valinomycin Structure and Cation Complex Formation. *Spectrochimica Acta Part A: Molecular and Biomolecular Spectroscopy* 2012, *96*, 200-206. Copyright 2012 Elsevier.

6.6 Conclusions

Using a novel approach of DUVRR analysis in native membrane, we have demonstrated that Val has a significant structural dependence derived from both the binding of a cation as well as the nature of the lipid environment within which it is found. The first spectroscopic evidence of the structure of the antimicrobial ionophore at the time of actual potassium binding is presented and represents a unique new structural form not fully observed in solvent based experiments. We have proposed a model in which Val goes from sampling the surface and membrane interior varying its structure wildly from a very open to fully closed state, to a state where Val is now in a predominantly more closed environment, but is still retains structural dynamics in its internal hydrogen bonding necessary to maintain the equilibration of the alkali-metal with the bulk solvent.

6.7 Bibliography

1. Halsey, C. M.; Xiong, J.; Oshokoya, O.; Johnson, J. A.; Shinde, S.; Beatty, J. T.; Ghirlanda, G.; JiJi, R. D.; Cooley, J. W., Simultaneous observation of peptide backbone lipid solvation and α-helical structure by deep-UV resonance Raman spectroscopy. *ChemBioChem* **2011,** *12*, 2125-2128.

2. (a) Tedeschi, H., Old and new data, new issues: the mitochondrial $\Delta\Psi$. *Biochimica et Biophysica Acta* **2005,** *1709*, 195-202; (b) Rottenberg, H.; Covian, R.; Trumpower, B. L., Membrane potential greatly enhances superoxide generation by the cytochrome bc_1 complex reconstituted into phospholipid vesicles. *The Journal of Biological Chemistry* **2009,** *284*, 19203-19210.

3. Grell, E.; Funck, T.; Eggers, F., In *Molecular Mechanisms of Antibiotic Action on Protein Biosynthesis and Membranes*, Muñoz, E.; García-Ferrándiz, F.; Vazquez, D., Eds. Elsevier: Amsterdam, 1972; p 646.

4. (a) Ovchinnikov, Y. A.; Ivanov, V. T.; Shkrob, A. M., *Membrane-Active Complexones*. Elsevier Scientific Publishing Company: Amsterdam, 1974; Vol. 12, p 464; (b) Brockmann, H.; Schmidt-Kastner, G., Valinomycin I, XXVII. Mitteil. über antibiotica aus actinomyceten. *Chemische Berichte* **1955,** *88*, 57-61; (c) Shemyakin, M. M.; Aldanova, N. A.; Vinogradova, E. I.; Feigina, M. Y., The structure and total synthesis of valinomycin. *Tetrahedron Letters* **1963,** *4* (28), 1921-1925.

5. Ovchinnikov, Y. A.; Ivanov, V. T., Conformational states and biological activity of cyclic peptides. *Tetrahedron* **1975,** *31*, 2177-2209.

6. Shemyakin, M. M.; Ovchinnikov, Y. A.; Ivanov, V. T.; Antonov, V. K.; Vinogradova, E. I.; Shkrob, A. M.; Malenkov, G. G.; Evstratov, A. V.; Laine, I. A.; Melnik, E. I.; Ryabova, I. D., Cylodepsipeptides as chemical tools for studying ionic transport through membranes. *Journal of Membrane Biology* **1969,** *1*, 402-430.

7. Ovchinnikov, Y. A.; Ivanov, V. T., Integrated conformational studies of cyclopeptides. *Tetrahedron* **1974,** *30*, 1871-1890.

8. Bill, R. M.; Henderson, P. J. F.; Iwata, S.; Kunji, E. R. S.; Michel, H.; Neutze, R.; Newstead, S.; Poolman, B.; Tate, C. G.; Vogel, H., Overcoming barriers to membrane protein structure determination. *Nature Biotechnology* **2011,** *29*, 335-340.

9. (a) Austin, J. C.; Jordan, T.; Spiro, T. G., Ultraviolet Resonance Raman Studies of Proteins and Related Model Compounds. In *Biomolecular Spectroscopy, Part A*, Clark, R. J. H.; Hester, R. E., Eds. John Wiley & Sons: Chichester, 1993; pp 55-127; (b) Asher, S. A., Ultraviolet Raman Spectroscopy. In *Handbook of Vibrational Spectroscopy*, Chalmers, J. M.; Griffiths, P. R., Eds. John Wiley & Sons Ltd: Chichester, 2002; Vol. 1, pp 557-571.

10. Chi, Z.; Chen, G.; Holtz, J. S. W.; Asher, S. A., UV resonance Raman-selective amide vibrational enhancement: quantitative methodology for determing protein secondary structure. *Biochemistry* **1998,** *37*, 2854-2864.

11. Huang, C.-Y.; Balakrishnan, G.; Spiro, T. G., Protein secondary structure from deep-UV resonance Raman spectroscopy. *J. Raman Spectrosc.* **2006,** *37*, 277-282.

12. (a) Halsey, C. M.; Oshokoya, O.; JiJi, R. D.; Cooley, J. W., Deep-UV resonance Raman analysis of the *Rhodobacter capsulatus* cytochrome bc_1 complex reveals a potential marker for the transmembrane peptide backbone. *Biochemistry* **2011,** *50*, 6531-6538; (b) Shafaat, H. S.; Sanchez, K. M.; Neary, T. J.; Kim, J. E., Ultraviolet resonance Raman spectroscopy of a β-sheet peptide: a model for membrane protein folding. *Journal of Raman Spectroscopy* **2009,** *40*, 1060-1064; (c) Holtz, J. S. W.; Lednev, I. K.; Asher, S. A.,

UV resonance Raman study of angiotensis II conformation in nonaqueous environments: lipid micelles and acetonitrile. *Biopolymers* **2000,** *57*, 55-63.

13. Frushour, B. G.; Koenig, J. L., Raman spectra of D and L amino acid copolymers. Poly-DL-alanine, poly-DL-leucine, and poly-DL-lysine. *Biopolymers* **1975,** *14*, 363-377.

14. Rouser, G.; Fleischer, S.; Yamamoto, A., Two dimensional thin layer chromatographic separation of polar lipids and determination of phospholipids by phosphorus analysis of spots. *Lipids* **1970,** *5*, 494-496.

15. Balakrishnan, G.; Hu, Y.; Nielsen, S. B.; Spiro, T. G., Tunable kHz Deep Ultraviolet (193-210 nm) Laser for Raman Applications. *Applied Spectroscopy* **2005,** *59*, 776-781.

16. Ozdemir, A.; Lednev, I. K.; Asher, S. A., UVRR Spectroscopic Studies of Valinomycin Complex Formation in Different Solvents. *Spectrochimica Acta, Part A: Molecular and Biomolecular Spectroscopy* **2005,** *61*, 19-26.

17. (a) Meers, P.; Feigenson, G. W., Location and ion-binding of membrane-associated valinomycin, a proton nuclear magnetic resonance study. *Biochimica et Biophysica Acta* **1988,** *938*, 469-482; (b) Jackson, M.; Mantsch, H. H., Valinomycin and its interaction with ions in organic solvents, detergents, and lipids studied by Fourier transform IR spectroscopy. *Biopolymers* **1991,** *31*, 1205-1212.

18. (a) Rothschild, K. J.; Asher, I. M.; Stanley, H. E.; Anastassakis, E., Raman spectroscopy of uncomplexed valinomycin. 2. Nonpolar and polar solution. *Journal of the American Chemical Society* **1977,** *99*, 2032-2039; (b) Asher, I. M.; Rothschild, K. J.; Stanley, H. E., Raman spectroscopic study of the valinomycin-KSCN complex. *Journal of Molecular Biology* **1974,** *89*, 205-222; (c) Yamamoto, S.; Watarai, H.; Bouř, P., Monitoring the backbone conformation of valinomycin by Raman optical activity. *ChemPhysChem* **2011,** *12*, 1509-1518; (d) Yamamoto, S.; Straka, M.; Watarai, H.; Bouř, P., Formation and structure of the potassium complex of valinomycin in solution studied by Raman optical activity. *Physical Chemistry Chemical Physics* **2010,** *12*, 11021-11032; (e) Neupert-Laves, K.; Dobler, M., The crystal structure of a K^+ complex of valinomycin. *Helvetica Chimica Acta* **1975,** *58*, 432-442; (f) Karle, I. L.; Flippen-Anderson, J. L., A new conformation exhibiting near-threefold symmetry for uncomplexed valinomycin in crystals from dimethyl sulfoxide. *Journal of the American Chemical Society* **1988,** *110*, 3253-3257; (g) Smith, G. D.; Duax, W. L.; Langs, D. A.; DeTitta, G. T.; Edmonds, J. W.; Rohrer, D. C.; Weeks, C. M., The crystal and molecular structure of the triclinic and monoclinic forms of valinomycin, $C_{54}H_{90}N_6O_{18}$. *Journal of the American Chemical Society* **1975,** *97*, 7242-7247.

19. Feigenson, G. W.; Meers, P. R., ^{1}H NMR study of valinomycin conformation in a phospholipid bilayer. *Nature* **1980,** *283*, 313-314.

Chapter 7: Conclusions

While structure determination of membrane proteins occurs mostly through the use of NMR or X-ray crystallography, deep-UV resonance Raman spectroscopy (DUVRR) fulfills a need to rapidly and cheaply determine secondary structure content. Vibrational modes from aromatic amino acid residues even describe the polarity of their localized environment. From our findings, DUVRR also comments on the solvent accessibility of the protein backbone embedded in the lipid membrane.

DUVRR spectra of cytochrome bc_1 and cytochrome *c* give a strong argument that desolvating the protein backbone within the lipid bilayer results in an intense carbonyl-stretching mode called the amide I. The intensity of this mode appears to be proportional to the relative amount of desolvation of the protein. The model membrane protein ME1 was investigated to confirm that known relationships for aqueous proteins between vibrational mode frequencies and secondary structure content were conserved in membrane proteins. For α-helical proteins, we can confirm that these relationships are conserved. Future characterization efforts will need to confirm other known frequency-structure relationships like beta-sheet proteins, the other predominant secondary structure in the membrane. Ultimately these results will be essential for describing secondary structure changes in the membrane, i.e. folding and unfolding.

In essence, DUVRR is an invaluable technique for any system that contains a repeating amide group. The conformation of the depsipeptide valinomycin was interrogated directly in the lipid bilayer for the first time. The ability to distinguish conformations of protein-like structures in the membrane will be beneficial for studying the mechanism of other ionophoric depsipeptides.

As these conclusions are some of the first made in the application of DUVRR to describing structure of membrane proteins and depsipeptides, further research is warranted to get a full spectral

survey of membrane protein structure motifs. This is a direction which is already being pursued in the Cooley lab.

VITA

Christopher Matthew Halsey was born November 26, 1984 in Springfield, MO and grew up in Liberty, MO. He graduated from Liberty High School in 2003. He pursued a Bachelor of Science degree in chemistry at Truman State University in Kirksville, MO and graduated magna cum laude with general honors in 2007. He went on immediately to the PhD program in chemistry at the University of Missouri, the first to join the lab of Dr. Jason Cooley. He will receive his doctorate in chemistry in November of 2012 and will join the faculty of Westminster College in Fulton, MO as an assistant professor of chemistry.